


5-2018

FUNCTIONAL HETEROGENEITY OF FIBROBLASTS IN DERMAL WOUND HEALING

Ehsan Ehsanipour

Follow this and additional works at: https://digitalcommons.library.tmc.edu/utgsbs_dissertations

 Part of the [Cell Biology Commons](#), and the [Medicine and Health Sciences Commons](#)

Recommended Citation

Ehsanipour, Ehsan, "FUNCTIONAL HETEROGENEITY OF FIBROBLASTS IN DERMAL WOUND HEALING" (2018). *UT GSBS Dissertations and Theses (Open Access)*. 855.

https://digitalcommons.library.tmc.edu/utgsbs_dissertations/855

This Dissertation (PhD) is brought to you for free and open access by the Graduate School of Biomedical Sciences at DigitalCommons@TMC. It has been accepted for inclusion in UT GSBS Dissertations and Theses (Open Access) by an authorized administrator of DigitalCommons@TMC. For more information, please contact laurel.sanders@library.tmc.edu.

**FUNCTIONAL HETEROGENEITY OF FIBROBLASTS IN DERMAL WOUND
HEALING**

By

Ehsan Ali Ehsanipour, M.S.

APPROVED:

Raghu Kalluri, M.D., Ph.D.
Advisory Professor

Menashe Bar-Eli., Ph.D.

Valerie LeBleu, Ph.D.

Mikhail Kolonin, Ph.D.

Samuel Mok, Ph.D.

APPROVED:

Dean, The University of Texas
MD Anderson Cancer Center UTHealth Graduate School of Biomedical
Sciences

FUNCTIONAL HETEROGENEITY OF FIBROBLASTS IN DERMAL WOUND
HEALING

A

DISSERTATION

Presented to the Faculty of

The University of Texas

MD Anderson Cancer Center UTHealth

Graduate School of Biomedical Sciences

in Partial Fulfillment

of the Requirements

for the Degree of

DOCTOR OF PHILOSOPHY

by

Ehsan Ali Ehsanipour, M.S.
Houston, Texas

May, 2018

Dedication

In loving memory of Dr. Toru Miyake

Acknowledgements

First and foremost, I give my gratitude to my PhD advisor, Dr. Raghu Kalluri. The major concerns when looking for a lab is to find one with a reputation for productivity, good funding, exciting projects, and experience mentoring students. In the Kalluri lab I found all of these facets, but I also found an advisor and lab environment that was willing to be supportive both scientifically and personally. A PhD, especially in a large and competitive lab, can be highly stressful. Thankfully, Dr. Kalluri's leadership has built an environment that I can honestly consider a second family. Moreover, his obsessive dedication to both his science and his trainees is inarguably the reason why our laboratory has managed to succeed in a world that has become more and more competitive. I will always look back on my experience in this laboratory to guide my future level of commitment and how to build the level of comradery and teamwork of the Kalluri Lab.

I give special thanks to Dr. Valerie LeBleu for all of her help putting together my thesis and organizing my work. Dr. Kalluri once remarked that I have an "activation energy" problem, and without siphoning off some of Dr. LeBleu's tremendous enthusiasm I know I would not have reached the finish line in the time I did. I additionally thank Dr. Olga Volpert, who in addition to providing support through the drudgeries of lab life also put in an inordinate amount of her own time to help me complete my manuscript for submission.

My colleagues in the Kalluri Lab over the years, all hundred of them, deserve mention for their willingness to provide help at every turn. It is easy to feel lost in a

large lab, but the students, post-docs, and technicians have shown an incredible willingness to help, guide, and mentor me of the years.

FUNCTIONAL HETEROGENEITY OF FIBROBLASTS IN DERMAL WOUND HEALING

Ehsan A. Ehsanipour, M.S.

Advisory Professor: Raghu Kalluri, M.D., Ph.D.

Impaired wound healing can lead to excessive scarring, dehiscence, chronic ulcers, and infection, which have adverse impact on the quality of life and pose a significant economic burden on the health care system. Thus, new therapeutic approaches are critically important. Dermal fibroblasts are critical players in cutaneous wound healing, possibly lending their contractile properties and extracellular matrix (ECM) remodeling functions to promote effective tissue repair. Dermal fibroblasts are also postulated to orchestrate tissue repair by interacting with and controlling other cell types in the wound microenvironment. It has become increasingly clear that the generic term “fibroblast” encompasses a diverse cell population with distinct origins and heterogeneous functions. Fibroblast heterogeneity is in part exemplified by the numerous expression markers used to distinguish them. The overarching goal of this study is to precisely define the heterogeneity of dermal fibroblasts and unravel their functional roles during cutaneous wound healing process.

In order to decipher the dynamics of fibroblast marker composition during the wound repair process we utilized multiplexed immunolabeling platforms in order to

quantify the expression of multiple fibroblast markers within a single tissue. Using this approach, along with lineage tracing studies, we observed that a population of resident dermal fibroblasts in normal skin, labeled with FSP1/S100A4, acquire the myofibroblast phenotype associated with acquisition of α SMA expression. Importantly, not all α SMA⁺ cells arose from FSP1/S100A4⁺ progenitors, indicating that there exist at least two populations of fibroblasts which contribute to the pool of activated myofibroblasts during tissue repair.

Further experimentation was carried using transgenic mouse models which allow selective depletion based on expression of fibroblast markers such as α SMA, FSP1/S100A4, FAP, and Collagen1 α 1. Using these models, we were able to identify unique phenotypes associated with depletion of these populations in the context of wound repair. While depletion of α SMA⁺ cells resulted in a complete inability to re-epithelialize, results from other depletion models were more nuanced, affecting collagen deposition, revascularization, and dermal thickness.

The work presented here offers novel insights on the dynamic nature of wound healing fibroblasts and proposes new avenues for the treatment of chronic wounds.

Table of Contents

Approval Sheet.....	<i>i</i>
Title page.....	<i>ii</i>
Copyright.....	<i>iii</i>
Dedication.....	<i>iv</i>
Acknowledgements.....	<i>v</i>
Abstract.....	<i>vi</i>
Table of Contents.....	<i>viii</i>
List of Illustrations.....	<i>ix</i>
List of Tables.....	<i>x</i>
Chapter 1. Introduction.....	1
Chapter 2. Heterogeneity of dermal wound fibroblasts.....	16
Chapter 3. Functional role of fibroblasts in dermal wound healing.....	36
Chapter 4. Origin and role of α SMA ⁺ fibroblasts in dermal wound repair.....	54
Chapter 5. Materials and Methods.....	80
Chapter 6. Discussion.....	87
Bibliography.....	96
Vita.....	108

List of Illustrations

Figure 1. Layers of the skin and constituent parts.....	3
Figure 2. The three phases of wound repair.....	5
Figure 3. Overview of the full-thickness skin (FTS) wound healing process.....	17
Figure 4. α SMA expression during cutaneous wound repair	19
Figure 5. FSP1/S100A4 expression during cutaneous wound repair.....	20
Figure 6. Vimentin expression during cutaneous wound repair	21
Figure 7. Differential expression of genes associated with fibroblasts and fibroblast activation during cutaneous wound repair.....	22
Figure 8. Schematic of multispectral imaging platform procedure	24
Figure 9. Definition of tissue segmentation of cutaneous wounds to restrict analysis to defined areas	26
Figure 10. Dynamic changes in expression of putative fibroblast markers during cutaneous wound repair.....	27
Figure 11. Co-expression of markers during wound repair.....	31
Figure 12 Lineage tracing of FSP1/S100A4+ cells immunolabeled with α SMA.....	33
Figure 13. Spatial distribution of fibroblast subpopulations in cutaneous wounds....	34
Figure 14. Schematic of thymidine-kinase mediated depletion	37
Figure 15. In vitro confirmation of cellular ablation of ear fibroblasts in generated mouse models	39
Figure 16. Functional contribution of α SMA+ fibroblasts in wound closure	41

Figure 17. Functional contribution of FSP1/S100A4+ fibroblasts in cutaneous wound closure.....	42
Figure 18. Functional contribution of FAP+ fibroblasts in wound closure.....	43
Figure 19. Functional contribution of Col1 α 1+ fibroblasts in cutaneous wound closure	45
Figure 20. Functional contribution of DDR2+ fibroblasts in cutaneous	46
Figure 21. Col1 α 1+ fibroblasts contribute to granulation tissue thickness in cutaneous wound healing	48
Figure 22. Differential expression of collagen-1 in wounds with distinct depletion of fibroblast subpopulations	49
Figure 23. Differential angiogenic response in wounds with distinct depletion of fibroblast subpopulations	50
Figure 24. Depletion of α SMA+ fibroblasts promotes an hypoxic wound microenvironment	51
Figure 25. Depletion of α SMA+ fibroblasts prevents wound closure	55
Figure 26. Impaired re-epithelialization in α SMA+ fibroblasts-depleted wounds	56
Figure 27. Reduced stiffness in α SMA+ fibroblasts-depleted wounds	58
Figure 28. Impact of α SMA+ fibroblasts depletion on wound closure is reversible...59	
Figure 29. Visualization of α SMA-RFP+ fibroblasts in cutaneous wounds.....	61
Figure 30. α SMA+ cells in the cutaneous wound co-express lower dermal lineage marker Sca1.....	62
Figure 31. α SMA+ fibroblasts accumulating in the cutaneous wound are not recruited from the bone marrow.	63

Figure 32. Wild type bone marrow transplantation in α SMA-TK mice did not rescue wound closure	65
Figure 33. TGF β family cytokine gene expression in the cutaneous wound repair process.	67
Figure 34. TGF β family receptor gene expression in the cutaneous wound repair process.	68
Figure 35. The functional contribution of α SMA+ fibroblasts in wound healing do not rely on persistent TGF β signaling.....	69
Figure 36. Global gene expression profiling of wound tissue with and without α SMA+ fibroblasts depletion	71
Figure 37. Immunotyping analyses of wounds with and without α SMA+ fibroblasts depletion	73
Figure 38. Gr-1+ cells are significantly increased in α SMA+ fibroblasts-depleted wounds	74
Figure 39. Depletion of GR-1+ cells did not rescue the impaired wound closure in α SMA+ fibroblasts-depleted wounds	75
Figure 40. Confirmation of successful depletion of GR-1+ cells using anti-GR-1 antibody	77
Figure 41. IL-6 production is critical for wound healing and is elevated as compensatory mechanism in α SMA+ fibroblasts-depleted wounds.....	78

List of Tables

Table 1. Putative Fibroblast Markers	12
Table 2. Table 2. Summary of findings on the functional contribution of distinct fibroblast subpopulations in cutaneous wound healing.....	53

Chapter 1. Introduction

1.A. Dermal wound and repair process

Over 6 million people in the United States alone suffer from chronic wounds, with estimated annual treatment costs reaching \$25 billion (1-3). Chronic wounds may ensue due to continuous injurious stimuli, and/or result from impairment in the normal wound repair process. Impaired wound healing negatively impacts the affected tissue, and can lead to excessive scarring, dehiscence, chronic ulcers, and infection (4). By definition, chronic wounds are wounds that fail to progress through the normal phases of wound healing, either persisting longer than six weeks or recurring frequently (5). Although there are many potential origins for non-healing wounds presented in the clinic, most ulcers are caused by ischemia due to diabetes, venous stasis, or pressure (6-8). Regardless of their varying etiology, chronic wounds share the common features of a prolonged and exaggerated inflammatory response, persistent infection, increased reactive oxygen species (ROS), and the inability of dermal and epidermal cells to respond to reparative stimuli (9, 10). Dermal wounds, in particular chronic dermal wounds, not only pose a significant economic burden, but severely reduce quality of life and continue to present as a clinical challenge with a need for more effective therapeutic approaches.

The clinical challenge of dermal wound healing, such as in malignancies as well as in aesthetic reconstruction, motivated a growing body of research aimed to gain better control over the responses involved in the wound healing process. A burgeoning field in cosmetic and regenerative medicine has made use of cellular and

acellular grafts to aid the repair of damaged tissues in patients whose normal healing response is impaired as well as in the treatment of acute wounds (11-14). Various dermal substitutes have been developed for the reconstruction of human skin, but the results in the clinic have remained elusive, resulting in issues such as scarring, insufficient vascularization, host rejection, absence of adnexal structures in the skin, lack of long term integration, and variable response rates (11, 13). A plausible explanation proposed for the inconsistencies observed between the promising pre-clinical findings and the poor outcomes in patients lies in the crude nature of cell extracts used for skin replacements. These biological skin substitutes often consist of a mixture of a matrix proteins and either keratinocytes, fibroblasts, or both. Allogenic cells are collected from cadaver or neonatal foreskin, expanded in culture, and cryopreserved prior to the preparation of skin equivalents (12). However, these approaches show limited success in the transplant of cells that participate in wound repair and regeneration; and it underscores the need for a more precise cellular and molecular knowledge of the functional components of dermal wound repair.

Dermal wounds result from the injury of the soft covering of animals or skin. The skin is composed of two layers: the epidermis and the dermis (**Figure 1**). The epidermis comprises the outermost layer of the skin, providing the protective barrier against UV radiation, outside pathogens, excessive water loss, as well as physical and chemical insults. This layer consists of a stratified squamous epithelium composed primarily of keratinocytes, which act to produce protective keratins and maintain the structural integrity of the skin in response to insults. The dermis is itself composed of the papillary and reticular dermis, and this layer houses the hair follicles,

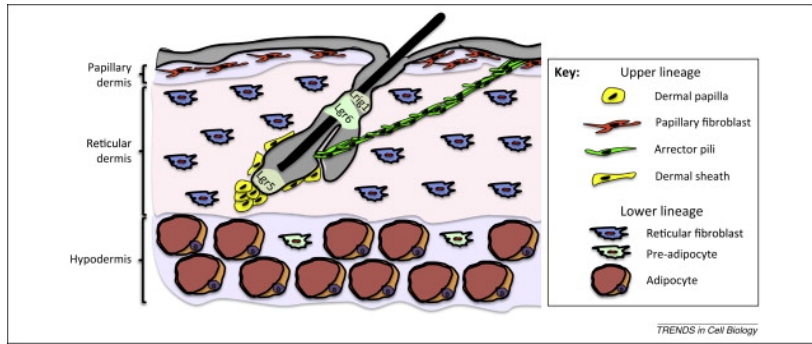


Figure 1. Layers of the skin and constituent parts

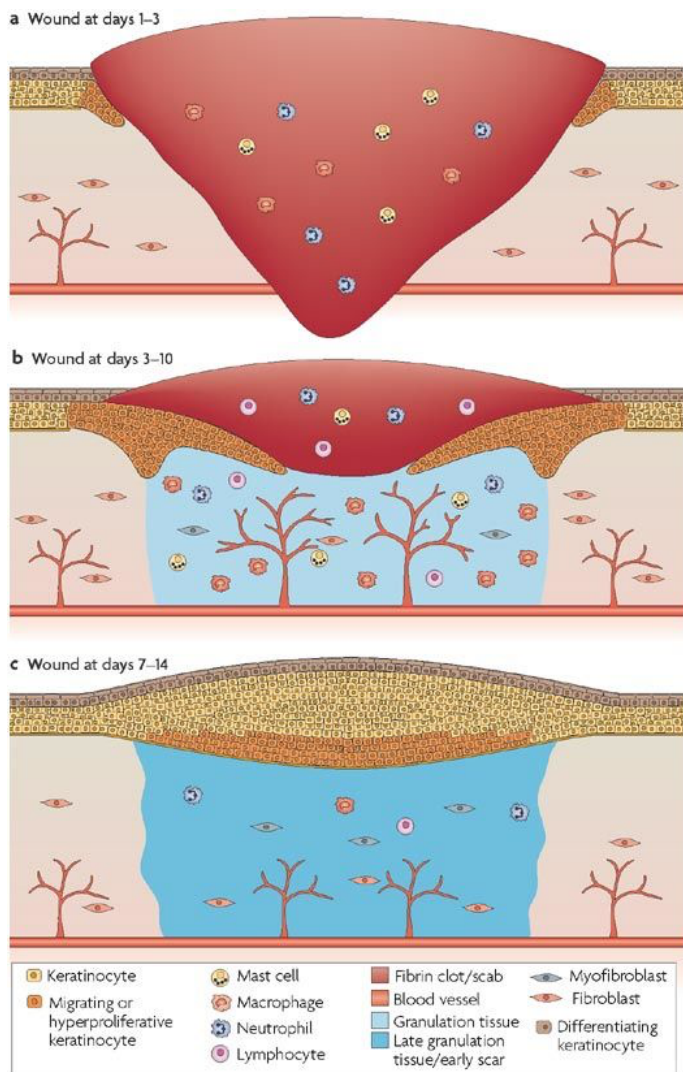
The skin is composed of the epidermis and dermis. The dermis itself can be further subdivided into the papillary dermis, reticular dermis, and an underlying hypodermis composed of fat and connective tissue. Each of these compartments contains specialized cells for their function and maintenance. (Driskell RR and Watt FM, Understanding fibroblast heterogeneity in the skin, Trends in Cell Biology 2015). Copyright Clearance 11699634

sebaceous glands, and sweat glands.

The dermal wound healing process is described as the succession of three phases, defined on the basis of specific histomorphological changes (**Figure 2**). These phases include 1) the inflammatory phase, 2) the proliferative phase (development of granulation tissue), and 3) the regeneration phase (including maturation and scar formation) (15). In humans, the final remodeling phase can span years until the regenerated tissue resembles the uninjured skin, and even then, the strength of the dermis and collagen buildup may remain impaired. Critically, the three phases of dermal wound repair are largely arbitrary, with considerable overlap with regards to functional changes and the cell populations involved (5). Within these phases, hallmarks of dermal wound healing include the recruitment and accumulation of immune and mesenchymal cells, remodeling of the extracellular matrix in the wound bed, and an angiogenic response. These distinct components operate in a complex and highly-coordinated network to ensure wound closure and repair.

1) The inflammatory phase

The initial disruption of dermal tissue is immediately followed by the formation of a blood clot, reestablishing hemostasis and providing extracellular matrix for cell migration (5). Minutes following injury, blood vessels are constricted to prevent blood and fluid loss. Activated platelets aggregate at the sites of vessel injury, forming a temporary seal that covers the fractured vessel wall. These aggregated platelets form a fibrin clot and provide a matrix scaffold for neutrophils and monocytes. The platelets



Nature Reviews | Molecular Cell Biology

Figure 2. The three phases of wound repair

- The inflammatory phase. In the first three days after injury neutrophils, macrophages and lymphocytes are attracted to the wound site
- The proliferation phase. Three to ten days after wounding new blood vessels are formed, fibroblasts proliferate and lay down extracellular matrix components, and keratinocytes begin to migrate along the injured dermis to re-epithelialize the wound
- The resolution phase. Begins in earnest after re-epithelialization is completed. The cellular density of the granulation tissue is reduced and the extracellular matrix is remodelled

(Schafer M and Werner S, Cancer as an overhealing wound: an old hypothesis revisited, Nature Reviews Molecular Cell Biology) Copyright Clearance 11699635

trapped in the clot function as a barrier not only to encourage hemostasis but also to stimulate immune cell recruitment and activation to the wound. Platelets contain specialized organelles referred to as alpha granules containing both clotting factors and growth factors, including platelet-derived growth factor (PDGF), insulin-like growth factor-1 (IGF-1), epidermal growth factor (EGF), and transforming growth factor-beta ($TGF\beta$). Together these factors function to attract and activate fibroblasts, endothelial cells, and macrophages, initiating the wound healing cascade.

Granulocytes (or polymorphonuclear leukocytes, PMN) are possibly the first immune cells, recruited by platelet-derived cytokines, to infiltrate the wound, adhering to endothelial cells in the blood vessels adjacent to the wound. Once at the wound site, these cells phagocytose bacteria and foreign particles, eliminating them via the release of degrading enzymes and oxygen-derived free radicals. During normal wound healing in mice, PMN accumulation is maximal two days following wounding, and these cells gradually decrease in number via apoptosis or phagocytic clearance prior to complete re-epithelialization (16). However, in the case of chronic wounds, neutrophils remain abundant (17).

The initial PMN influx is followed by the migration of monocytes recruited from the bone marrow and systemic circulation to the wound site, where they differentiate locally into macrophages (18). This infiltration peaks two days following dermal wound, and gradually decreases with time during the maturation phase. Macrophages release additional cytokines and growth factors into the wound, facilitating the recruitment of fibroblasts, keratinocytes, and endothelial cells. Macrophages are presumably associated with the resolution of local inflammation, as well as setting up for the

subsequent phases of wound healing, including angiogenesis, granulation tissue formation, fibroblast recruitment and extracellular matrix remodeling (19). Macrophage-derived growth factors, such as PDGF and vascular endothelial growth factor (VEGF), initiate granulation tissue formation.

2) The proliferative phase (development of granulation tissue)

The proliferative phase of wound healing involves neo-angiogenesis, the proliferation of fibroblasts, and re-epithelialization of the wound site. During this phase, the dead space resulting from injury is replaced by new tissue. This phase is often referred to as the granulation stage of wound repair due to the formation of granulation tissue, referring to the pink granular appearance of invading capillaries within the wound. Granulation tissue is made up primarily of proliferating fibroblasts, capillaries, and tissue macrophages within in a matrix of collagen and the glycoproteins fibronectin and tenascin.

During this stage epithelial cells at the wound margins, and any surviving dermal epithelial appendages within the wound bed, begin their proliferation and migration beneath the hardened scab formed during the early inflammatory phase. The epidermis adjacent to the wound edge begins to thicken and keratinocytes weaken their attachment to the underlying dermis in order to facilitate their migration towards the wound center. When the advancing epithelial cells meet, further movement is halted by contact inhibition.

Within the wound bed, fibroblasts are attracted to the wound site by the

signaling molecules, including PDGF and TGF β . Fibroblasts are stimulated to proliferate and produce a provisional matrix of fibronectin and hyaluron (HA). In the granulation tissue, activated fibroblasts are in part defined by their acquired expression of alpha-smooth muscle actin (α SMA), and often referred to as myofibroblasts. The expression of α SMA in microfilament bundles or stress fibers endows myofibroblasts with contractile properties. The accumulation of α SMA⁺ fibroblasts plays a major role in the contraction, formation, and maturation of the granulation tissue (20). Fibroblasts, as detailed below, are however a complex population of cells with likely distinct roles and functions in the maturation of the granulation tissue (21). They presumably synthesize and deposit a stronger matrix of collagen and proteoglycans that eventually replace the provisional matrix. This newly constructed extracellular matrix (ECM) provides support for the expansion of other cells within the wound.

Apart from fibroblasts accumulation and ECM remodeling, angiogenesis and vasculogenesis form a vital component of the wound healing cascade. This process not only results in the replacement of damaged or excised vessels, but also provides a source of nutrients for the increased cell density in wounds during repair. Modulating wound angiogenesis in itself has been considered as a potential therapeutic target, as delayed or defective angiogenesis is implicated in healing impairment (22-25).

3) The resolution phase (including maturation and scar formation)

The final stage of wound repair is the resolution, or remodeling, phase. This

step overlaps with the development of granulation tissue and may continue over a period of years before the wound site again resembles its uninjured form. During this phase the provisional matrix matures as fibronectin and HA are broken down, and collagen bundles thicken (26). Type III collagen, a principal component of the immature granulation tissue, is gradually replaced by type I collagen. Lastly, elastin, which is responsible for skin elasticity, re-emerges. However, the repaired dermis never regains the original strength or plasticity of normal, unwounded skin (27). In the resolution phase of healing the cell number is dramatically reduced, presumably due to apoptosis of myofibroblast and vascular cells (28). As the ECM is continually remodeled, there is ongoing collagen synthesis and breakdown.

1. B. Fibroblast biology and functions

Fibroblasts are cells of mesenchymal origin and are present in many tissues in the body. Despite, or perhaps due to, their pervasiveness within the body, a precise definition of fibroblasts function has remained elusive (21, 29). Morphologically, fibroblasts are defined as elongated cells exhibiting a spindle-like shape which adhere to tissue culture substrates (30). Resident fibroblasts are normally in a quiescent state and are primarily considered to be responsible for the establishment and maintenance of connective tissue stroma. However, their functional definition has been further expanded to describe cells capable of secreting both structural and non-structural ECM molecules, reorganizing and remodeling the ECM through matrix metalloproteinases, regulation of the inflammatory response, and participation in both

autocrine and paracrine signaling with other cell types (29, 31).

In injured tissues, fibroblasts have been found to transition to an activated, or myofibroblast, state and take part in many aspects of the tissue remodeling cascade (32-35). Myofibroblasts were originally identified on the basis of ultrastructural morphology. Myofibroblasts could be distinguished from normal, quiescent tissue, fibroblasts on the basis of their prominent microfilament bundles and shared characteristics with smooth muscle cells (36) (37). Morphologically, the myofibroblasts contain contractile apparatus analogous to the stress fibers present in cultured fibroblasts. Myofibroblasts have been identified in many pathological conditions including keloid scars in the skin, renal fibrosis, fibrotic liver, and idiopathic pulmonary fibrosis (38-42). Cells with features of myofibroblasts have also been described in tumors, where they have been termed cancer-associated fibroblasts (43, 44).

The transition between normal fibroblast and myofibroblasts is considered to be controlled primarily through TGF β signaling. TGF β is first produced by phagocytic cells and subsequently by fibroblasts, initiating a self-perpetuating cycle leading to the appearance of myofibroblasts. TGF β is a well-studied growth factor that exerts many biological actions during development and tissue repair (45-48). In fibroblasts, TGF β induces the expression of α SMA and stimulates the production of collagen type I.

Despite their roles in wound healing, fibrosis, and cancer, a reliable definition of activated fibroblasts remains elusive due to their heterogeneous nature (29, 44). The filament protein alpha-smooth muscle actin (α SMA) is currently the predominant cellular marker for myofibroblasts. However, other fibroblast-associated proteins such

as intermediate filament associated proteins, transmembrane proteins, and ECM molecules, have also been associated with fibroblasts involved in tissue repair (**Table 1**). Even with a growing list of cellular markers used to delineate fibroblasts, no consensus marker or group of markers have been able to capture the entirety of fibroblast populations (32, 49). This issue is further compounded by findings indicating considerable, but not complete, overlap in the expression of putative fibroblast markers (50, 51). The molecular marker-based definition of fibroblasts thus also includes exclusion criteria, such as lack of expression of immune (e.g. CD45) or endothelial markers (e.g. CD31) (further detailed below). The functional heterogeneity of fibroblasts, in development and tissue repair/remodeling, remains an active area of investigation (11, 21, 49, 52).

Table 1. Putative Fibroblast Markers

Fibroblast Marker	Function	Also Expressed In	Reference
α -Smooth Muscle Actin (α SMA)	Intermediate-filament associated protein	Pericytes, smooth muscle cells	(53)
Vimentin	Intermediate-filament associated protein	Endothelial cells, neurons	(50)
Fibroblast Specific Protein 1(FSP1) / S100 Calcium-Binding Protein A4 (S100A4)	Intermediate-filament associated protein	Macrophages	(54)
Fibroblast Activation Protein (FAP)- α	Serine Protease	Activated melanocytes, macrophages	(55)
Collagen 1	Collagen biosynthesis	Osteoblasts	(56)
Platelet Derived Growth Factor α (PDGFR α)	Growth factor receptor	Mesenchymal stromal cells	(57)
Discoidin Domain Receptor 2 (DDR2)	Receptor tyrosine kinase	Smooth muscle cells, adipose tissue	(58)

1.C. Dermal wound fibroblasts in tissue repair

Fibroblasts, a dominant cell type in dermal wound healing, are considered functional contributors to the wound healing process. Long considered to primarily function to establish and remodel the ECM, fibroblasts have now been demonstrated to interact closely with a multitude of cell types including immune cells (59), endothelial cells (23, 24), keratinocytes (60), and adipocytes (61-63). Additionally, dysregulation of fibroblast proliferation and function has been associated with the two major types of wound related ailments: excessive scarring/fibrosis and incomplete wound healing (34). Therefore, studies of fibroblast functions and dysfunction during wound healing would offer important new insights with potential advancements in wound therapeutics.

The first wave of fibroblasts recruitment emerges together with the sprouting vasculature in wound healing. In addition to their role in the production of basement membrane proteins, fibroblasts engage in paracrine and autocrine interactions in the skin (64-68). Fibroblasts release growth factors/cytokines that play a significant role in wound repair through their signaling with keratinocytes to stimulate re-epithelialization. Myofibroblasts disappear from the wound site, presumably via apoptosis, following which a distinct fibroblast population accumulate to form a collagenous matrix (69). However, impaired remodeling of the collagenous matrix results in the formation of scar tissue (15, 70, 71). Persistence of myofibroblasts in a closed wound is a characteristic of hypertrophic scars, often found in burn injuries (28, 53).

As described above, both positive selection (α SMA⁺, Col1a1⁺, FSP1⁺, etc) or negative selection (CD31⁻, desmin⁻, CD45⁻) have been used to study fibroblasts in

wound healing. Although a clearer distinction between fibroblasts in normal and diseased tissues/organs (e.g. fibrosis and cancer (29, 44) is emerging; the cutaneous fibroblasts in intact skin and the healing wound are both heterogeneous and diverse. Studies have focused on distinguishing between fibroblasts from the papillary (upper) and reticular (lower) dermis, which were shown to differ in their *in vitro* proliferation rates, capacity for matrix generation, and production/response to cytokines (72-75). These studies relied on the mechanical separation of the skin layers and *ex vivo* expansion. However, this strategy lacks the capacity to recapitulate interactions with other cell populations which occur in homeostatic tissues and during tissue remodeling. More recently, extensive immunolabeling and lineage tracing experiments (57) have indicated that proliferative and matrix-synthesizing reticular fibroblasts were most robustly captured by the transmembrane protein Dlk1, while the papillary dermis fibroblasts were found to be Dpp4 positive. The growth factor receptor PDGFR α was found to be an early marker of both lineages (57). However, this study focused on the acquisition of markers during the course of development, rather than in the repair process.

Subpopulations of fibroblasts reside in distinct anatomical locations within the skin. At least three subpopulations have been identified in the dermis: superficial (or papillary) fibroblasts, reticular fibroblasts, and fibroblasts associated with hair follicles. These cell subpopulations can be isolated and exhibit distinct phenotypic and gene expression differences when cultured (72, 74, 76, 77). Dermal papilla fibroblasts have been described in the dermal sheath that surrounds the outside of the hair follicle. They are involved in the regeneration of the dermal papilla and can also become

wound healing myofibroblasts after a lesion or injury (78-80). Fibrocytes, defined as hematopoietic derived cells expressing leukocyte markers and capable of synthesizing collagen. These cells may be recruited to the injured skin with inflammatory cells during the early stages of wound repair and subsequently acquire a myofibroblastic phenotype (81-83).

Papillary fibroblasts, as their name indicate, reside in the papillary dermis, a ~300-400um thin layer of poorly organized collagen fiber bundles, in contrast with the thicker and well-organized fiber bundles of the reticular dermis (77). The depth of the papillary dermis is variable depending upon age, anatomical location, and other factors. The papillary dermis contains more type III collagen than the type I collagen rich reticular dermis (84). The separation of the papillary and reticular layers of the skin allows establishment of explant cultures of cells from each layer. Papillary fibroblasts are more proliferative than reticular fibroblasts (72, 76, 77, 85, 86). When seeded into layers of type I collagen, reticular fibroblasts produce greater contractions than do papillary fibroblasts (85, 86). Studies have indicated that the initial phase of cutaneous wound repair is mediated by the reticular fibroblasts (57). By contrast, upper dermal fibroblasts are recruited during subsequent phases of wound repair, during re-epithelialization and hair follicle formation.

Despite ongoing studies and recent advances (11, 21, 87), the functional characterization of dermal fibroblast in wound repair has been hampered by an inability to identify and target such a heterogenous cell population. In this thesis, novel approaches were developed, which, coupled with powerful mouse genetic engineering, enabled the capture of the dynamic changes in fibroblasts composition

during cutaneous wound repair and functionally tease out their contribution to wound closure. The novel immunolabeling techniques detailed therein, and the use of genetic fate mapping for fibroblasts with genetically engineered mouse models (GEMMs), allowed for the visualization of multiple markers during the wound repair process. Further, additional GEMMs allowing for the targeted depletion of defined cell populations during cutaneous wound repair offered novel insights into the functional contribution of distinct fibroblasts subpopulations. Critically, our studies have employed the most common *in vivo* model of wound healing, namely the full thickness skin (FTS) dermal punch model. This model involves the surgical excision of the epidermis and dermis to the depth of the fascial planes or subcutaneous fat (88). The model follows the standard process of inflammatory, proliferative, and resolution phases detailed above.

Chapter 2. Heterogeneity of dermal wound fibroblasts

2. A. Fibroblast marker expression in dermal wound injury

To ascertain the fibroblast heterogeneity in dermal wound repair, the full thickness skin (FTS) dermal punch model was established. In this model, the epidermis and dermis layers of the skin are excised surgically. Adult mice ranging from 8-12 weeks of age were wounded bilaterally on their dorsal side using a sterile dermal 8mm biopsy punch (**Figure 3A**). The wound repair process was evaluated, and distinct time points were chosen to represent the various stages of the wound healing process, from inflammation (Day 3-6), to granulation (Days 9-12), and remodeling/resolution (Days 14-32). Visual inspections of the wound diameter enabled the measure of rate of wound closure (**Figure 3B**). Representative H&E imaging of the wounds and normal skin allowed for further characterization of the stages of wound repair, and the definition of wound margins and skin tissue layers for subsequent immunohistochemical analyses (**Figure 3C**).

Initial characterization of the putative dermal fibroblasts markers, namely type I collagen, α SMA, FSP-1/S100A4 and Vimentin, revealed both compositional and spatial distinctions during dermal wound healing (**Figures 3-6**). In normal skin, type I Collagen is densely concentrated at the dermis (**Figure 3D**). At three days following wounding, collagen staining was limited to the margins. By day 9, collagen positive area was visible throughout the forming granulation tissue, but it was not until day 30 post-wounding that collagen density approached pre-wound levels. In contrast,

immunostaining for α SMA positive fibroblasts revealed low expression in normal skin,

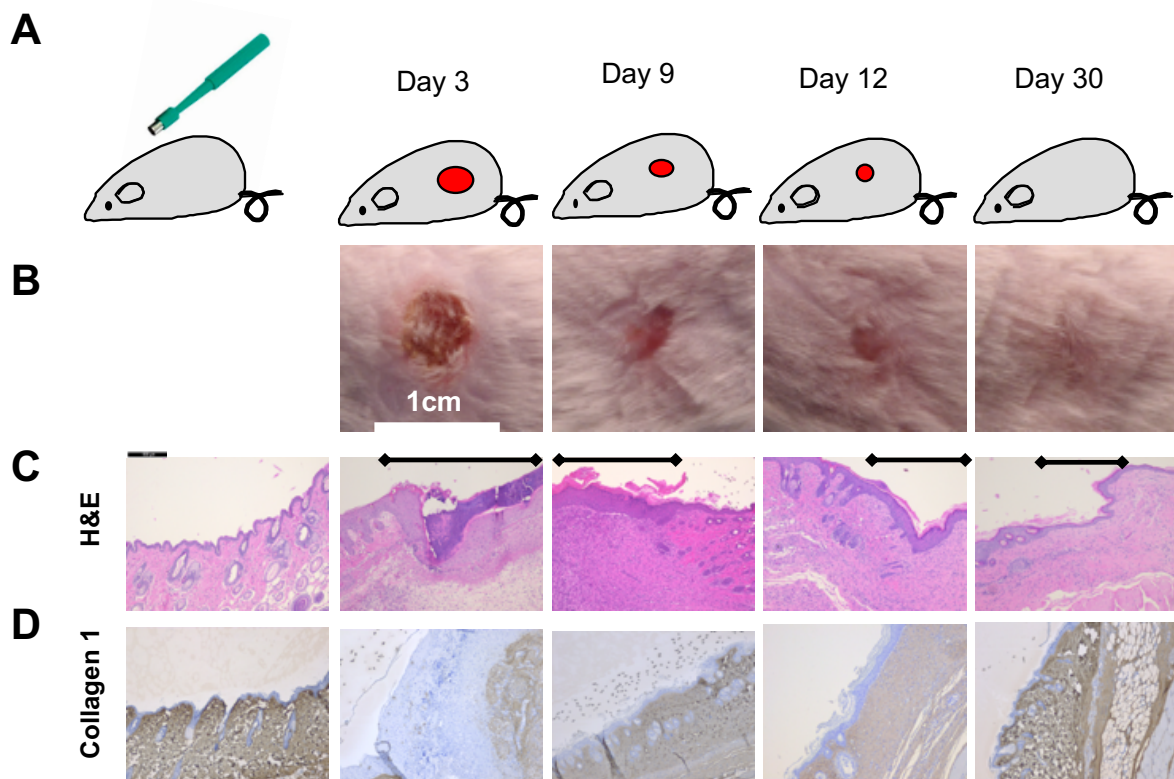


Figure 3. Overview of the full-thickness skin (FTS) wound healing process
 (A) Schematic cartoon of wound generation and closure in the full thickness wound model
 (B) Representative macroscopic images of mouse wounds at days 3 through 30 post-wounding
 (C) Representative histological sections of normal skin and wounds at days 3 through 30 post-wounding (H&E), black bars indicate wound region
 (D) Representative immunohistological sections of normal and wounded skin stained for Collagen 1

isolated primarily to cells associated with blood vessels and hair follicles (**Figure 4A**). At day 6 post wounding, α SMA positive cells were most prevalent in the expanding lower dermal regions at the margins of the wound site (**Figure 4B**). By day 9, α SMA positive cells were found at the innermost areas of the granulation tissue and showed a precipitous fall in positive cell number following (**Figures 4D**). In contrast to α SMA, immunolabeling for FSP1/S100A4 was prevalent in normal skin, especially at the interface between the dermis and epidermis (**Figure 5A**). At day 6, positive cells were already visible throughout the developing granulation tissue (**Figure 5B**), but there did not appear to be any increase in positive cell number at later time-points (**Figures 5C-D**). Interestingly, Vimentin positive immunolabeling was low in both normal skin and early wound timepoints, isolated primarily to blood vessels (**Figures 6A and B**). Wound tissue at day 9 and 14 however, showed an increase in vimentin positive staining (**Figures 6C and D**).

Further, transcriptomic analyses of the skin for the above listed makers as well as Fibroblast Activation Protein (FAP, another fibroblast marker subject to further study below) showed expression of FSP-1/S100A4 (*S100A4*), and to a lesser extent Vimentin (*Vim*), rise and peak as early as day 3 post wounding, whereas α SMA (*Acta2*) and *Fap* expression rise and peak and day 6 post wounding (**Figure 7**). Transcript levels of *Col1a1* showed no specific upregulation throughout wound repair (**Figure 7**). Collectively, these results indicate that the expression of the fibroblast markers evaluated is dynamic during the wound repair process (time) and in their pattern of expression (heterogeneous spatial distribution), and that transcript and protein levels are distinctly coupled. These findings underscored the heterogeneity of

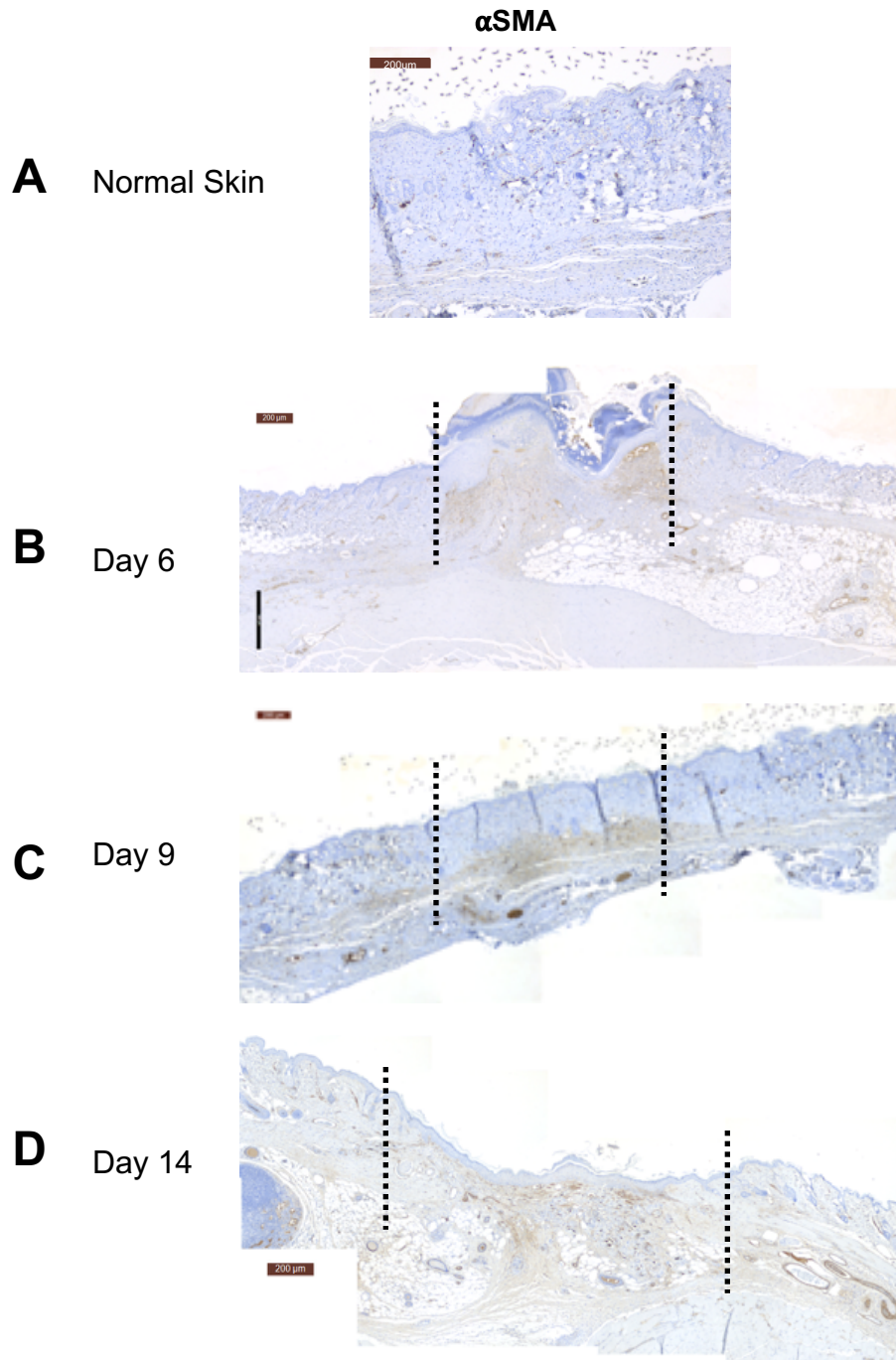


Figure 4. α SMA expression during cutaneous wound repair
 Representative immunohistological sections of normal skin and wounds at days 6 through 14 post-wounding (α SMA). Wound margins are labeled with dashed black lines

- (A) Representative image of α SMA immunolabeling in normal skin
- (B) Representative image of α SMA immunolabeling in Day 6 wounds
- (C) Representative image of α SMA immunolabeling in Day 9 wounds
- (D) Representative image of α SMA immunolabeling in Day 14 wounds

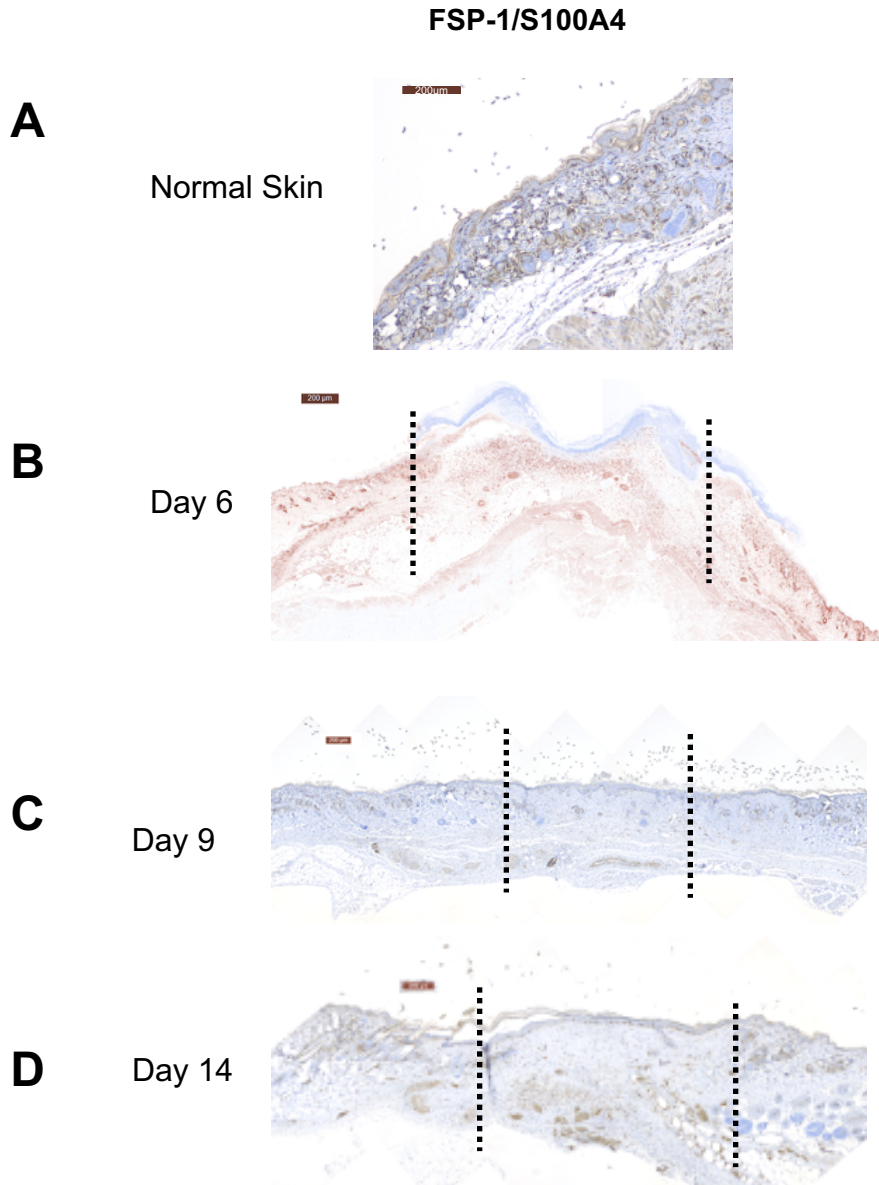


Figure 5. FSP1/S100A4 expression during cutaneous wound repair
 Representative immunohistological sections of normal skin and wounds at days 6 through 14 post-wounding (FSP-1). Dashed black bars indicate wound margins
 (A) Representative image of FSP1/S100A4 immunolabeling in normal skin
 (B) Representative image of FSP1/S100A4 immunolabeling in Day 6 wounds
 (C) Representative image of FSP1/S100A4 immunolabeling in Day 9 wounds
 (D) Representative image of FSP1/S100A4 immunolabeling in Day 14 wounds

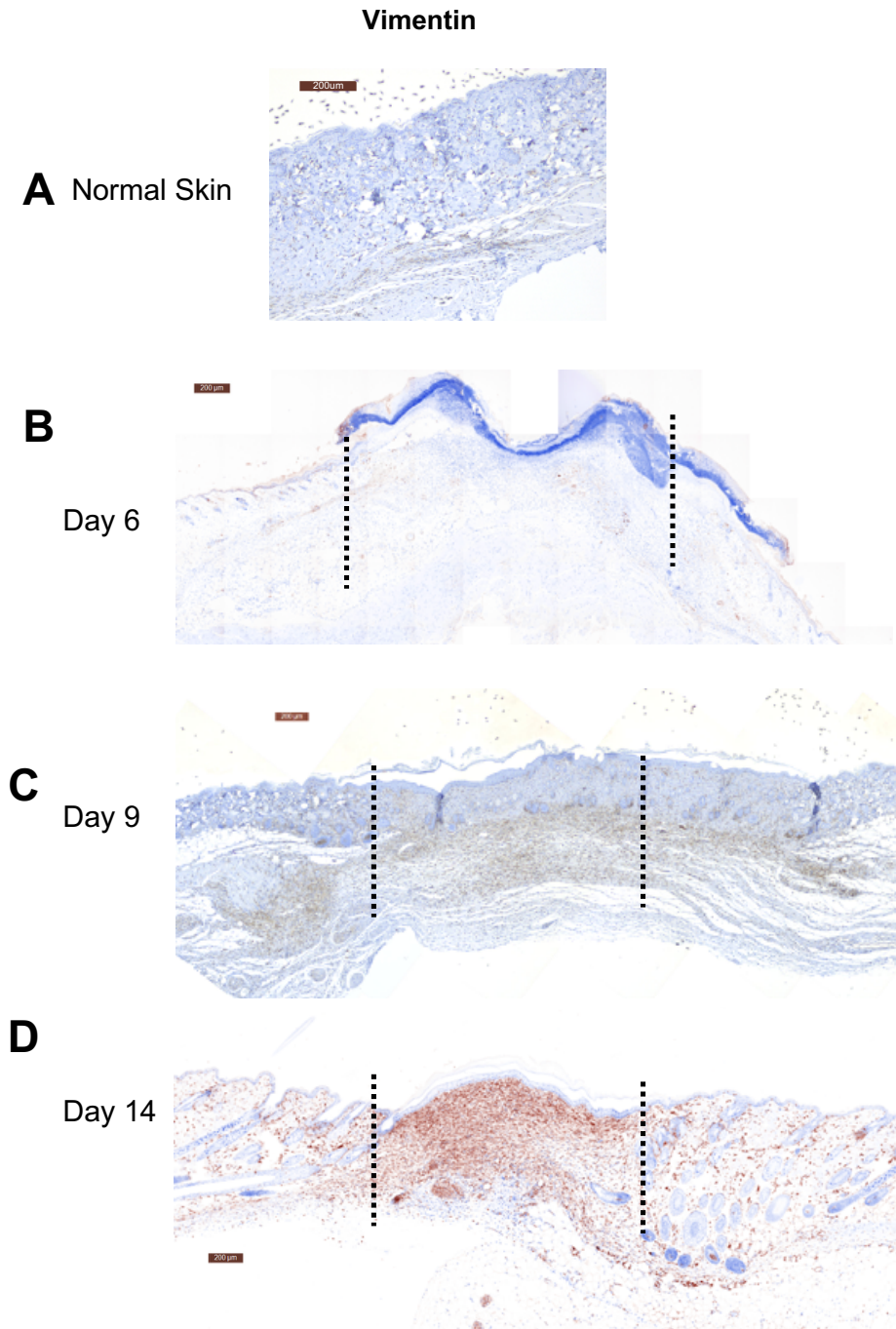


Figure 6. Vimentin expression during cutaneous wound repair
 Representative immunohistological sections of normal skin and wounds at days 6 through 14 post-wounding (Vimentin). Dashed black lines indicate wound margins.

- (A) Representative image of Vimentin immunolabeling in normal skin
- (B) Representative image of FSP1/S100A4 immunolabeling in Day 6 wounds
- (C) Representative image of FSP1/S100A4 immunolabeling in Day 9 wounds
- (D) Representative image of FSP1/S100A4 immunolabeling in Day 14 wounds

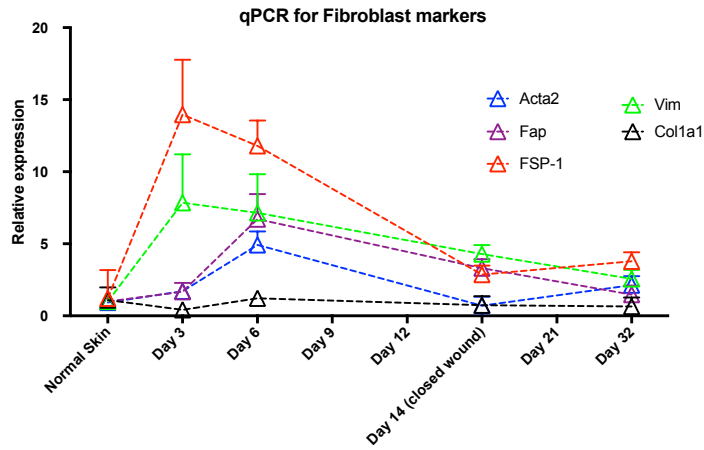


Figure 7. Differential expression of genes associated with fibroblasts and fibroblast activation during cutaneous wound repair
 The fold change in Acta2 (α SMA), Fap, FSP-1, Vimentin, and Collagen1 α 1 gene expression in wounded skin between days 3 and 32 post-wounding compared to normal skin controls (n= 4 mice per group)

fibroblasts in dermal wound repair and suggest distinct functional contribution to the wound healing process.

2. B. Spatial distribution and dynamic changes in fibroblasts population in dermal wound repair

In order to accurately quantify the dynamic expression of putative fibroblast markers during wound healing, a multiplex immunolabeling protocol based on tyramide signal amplification combined with multispectral imaging was developed. Briefly, this process occurs through three sequential steps. First, as in immunohistochemistry, sections from paraffin embedded tissues are probed with HRP-labeled antibodies against the protein of interest. Next, the HRP catalyzes the conversion of tyramide derivatives to activated fluorescent tyramide residues which become covalently bound to the targeted protein. Antigen retrieval strips the tissue section of the HRP-antibody but not the bound fluorescent residues (**Figure 8A**). The method was proven useful to capture cell identity, in a tissue section, on the basis of immunolabeling multiple markers (89). This approach offered a number of advantages for the study of fibroblast heterogeneity in dermal wound repair. Unlike traditional immunostaining methods, this procedure allows the visualization of up to eight markers within a single slide without loss of spatial resolution, enabling the analysis of yet additional markers while also enabling analyses of markers co-expression in dermal fibroblasts and distinction from other, non-fibroblast, cell types (**Figure 8B-C**). For example, endothelial cells that express the fibroblasts markers of interest (FSP-

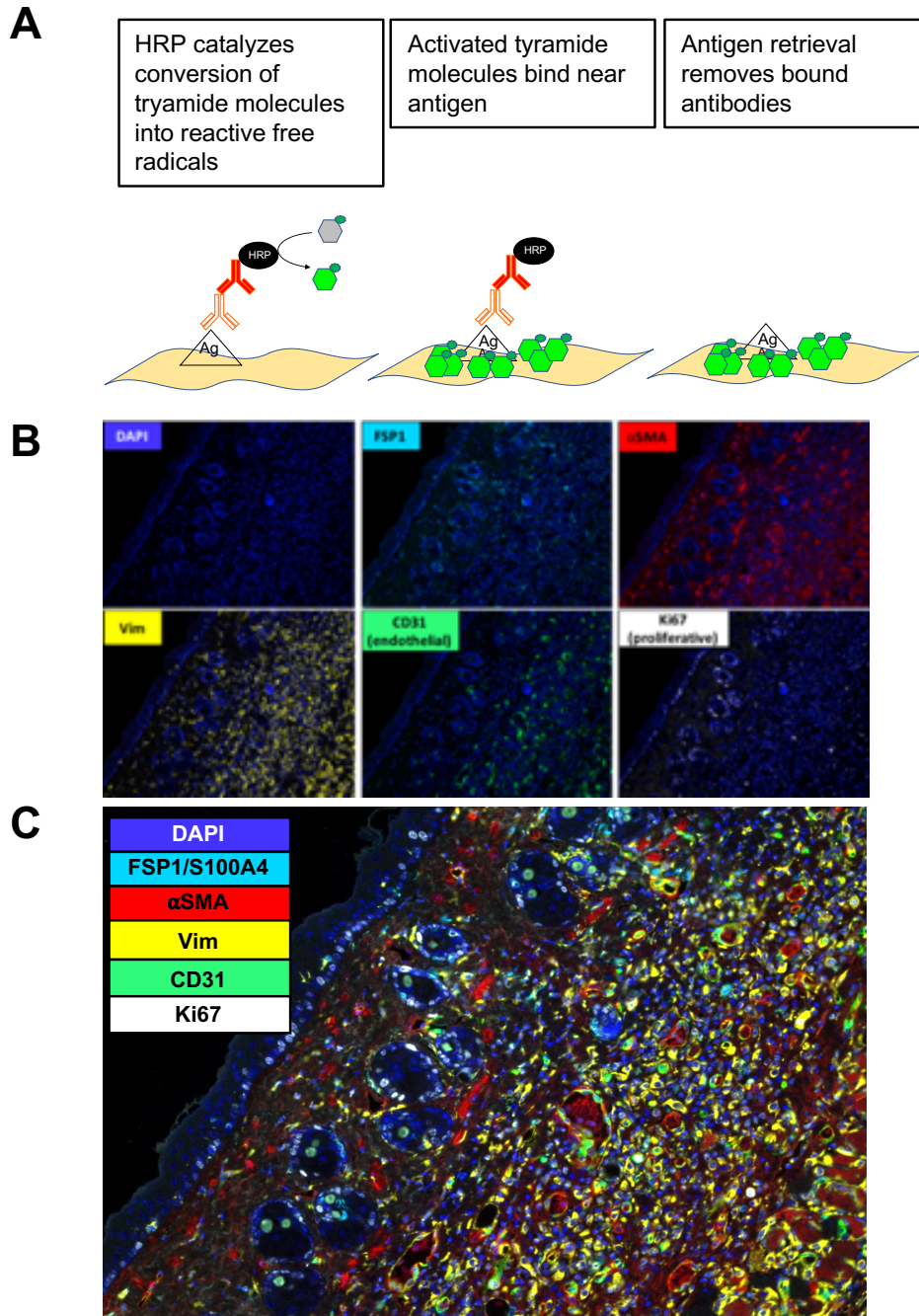


Figure 8. Schematic of multispectral imaging platform procedure
 (A) Schematic cartoon of tyramide signal amplification procedure
 (B) Representative images displaying the same section of tissue with each individual marker after spectral un-mixing
 (C) Composite false-color image generated from (B)

1/S100A4, α SMA or Vimentin), via acquisition of an endothelial to mesenchymal (EndMT) program realized in tissue damage (90), can be excluded from subsequent analysis based on their expression of CD31 (PECAM-1), a protein involved in endothelial cell junctions (**Figure 8B-C**). Multispectral imaging and scanning of the tissue section also permits the use of image analysis software and pattern recognition algorithms. These refine the spatial distribution analyses as it enables tissue segmentation based on morphological features and enables definition of distinct skin layers, including dermis, epidermis, and muscle and adipose tissue layers (**Figure 9A-C**). Finally, using cell segmentation algorithms, the signal intensity from each marker can be ascertained on a per cell basis, enabling the precise measure of the number of positive cells within the analyzed area rather than total and relative image fluorescent intensity.

To investigate the contribution of cells expressing different fibroblast markers to the wound healing process, a multiplex panel consisting of α SMA, FSP-1/S100A4, Vimentin, CD31, Ki67 and DAPI was established (**Figure 8C**). Nuclear labeling (DAPI) was used for cell phenotyping and, together with Ki67, define proliferating cells. CD31, as detailed above, was used as an endothelial cell exclusion marker. Wound tissue was collected at time-points between 3 and 32 days post-wounding, as well as healthy, unwounded skin as control tissue. Analysis was carried out exclusively on cells identified as being part of the dermal layer of the skin. In the normal skin, nearly no vimentin positive cells were detected (**Figure 10A**), corroborating observations made using immunohistochemistry (**Figure 6**). The normal skin displayed approximately 14% α SMA⁺ cells (out of all cells in the section),

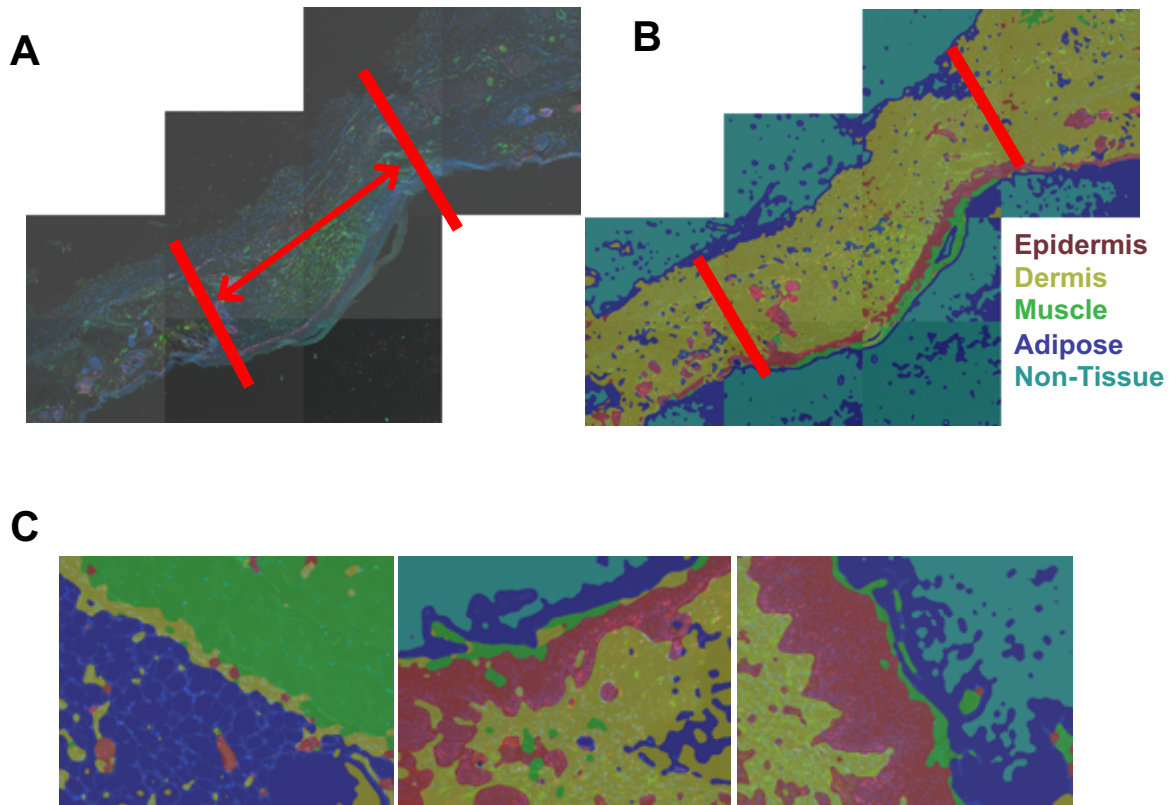


Figure 9. Definition of tissue segmentation of cutaneous wounds to restrict analysis to defined areas

- (A) Representative image demonstrating the demarcation of wound margins (red lines) and region used for analysis (red arrow)
- (B) Representative image demonstrating tissue segmentation of skin regions into epidermis (red), dermis (yellow), muscle (green), adipose tissue (blue), and non-tissue (cyan)
- (C) Representative 200x images of segmented skin regions

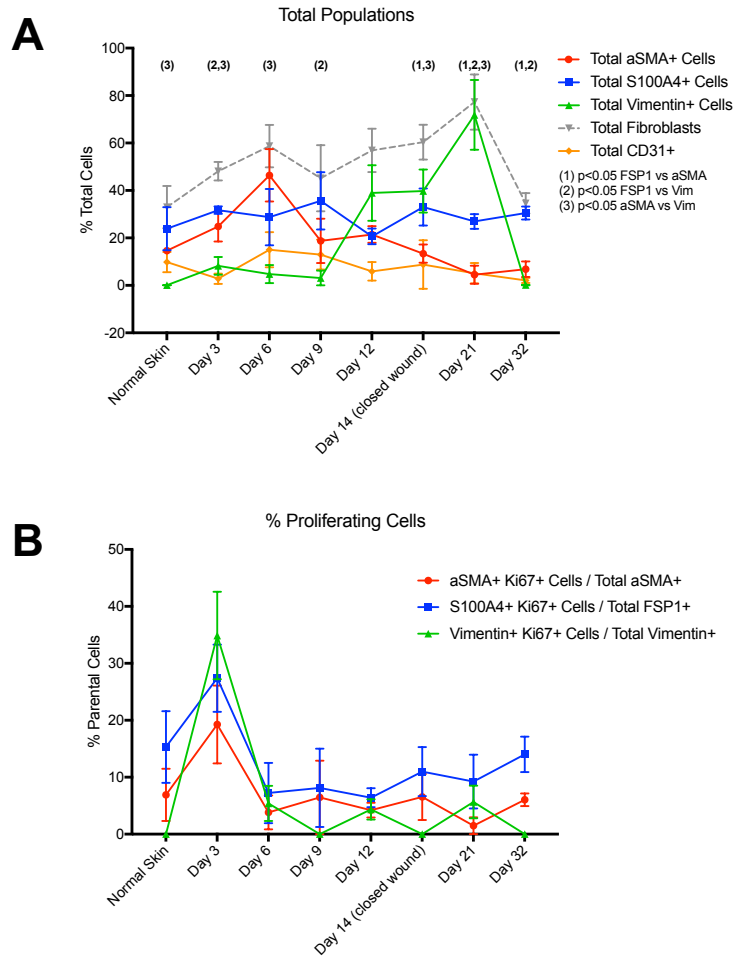


Figure 10. Dynamic changes in expression of putative fibroblast markers during cutaneous wound repair. N=6 mice per group
 (A) Percentage of α SMA⁺, FSP-1⁺, and Vimentin⁺ cells within the normal dermis and wound beds from day 3 through 32 post-wounding
 (B) Relative proliferation of fibroblast populations

and 24% FSP-1/S100A4⁺ and 0.1% Vimentin⁺ cells (**Figure 10A**). During wound repair, these cell populations changed in frequencies and showed distinct frequencies relative to one another. Although α SMA, FSP-1/S100A4, and Vimentin are often utilized interchangeably as markers of fibroblasts during tissue regeneration, each displayed unique dynamics (**Figure 10A**). In agreement with previous immunohistochemical analyses (**Figure 4**) and our gene expression results (**Figure 7**), the percent α SMA⁺ cells increased at Days 3 and 6 following wounding, and steadily declined thereafter (**Figure 10A**). By Day 6 post wounding, α SMA-positive cells emerged as the dominant fibroblast population, making up roughly 75% of fibroblast marker positive cells. This accumulation is coordinated with an increase in the frequency of α SMA⁺/Ki67⁺ cells (increasing from 14% in normal skin to 24% at Day 3 following wounding, **Figure 10A-B**), suggesting that increased proliferation of α SMA⁺ fibroblasts, at least in part, contributed to the increase in percent α SMA⁺ cells early in the wound repair (Day 3 post wounding). This increase in the percent α SMA⁺ fibroblasts is also in line with the reported increase in TGF β secreted by several cell types at this time-point during wound repair (91, 92). TGF β is a potent stimulator of differentiation of quiescent fibroblasts to the “activated fibroblast” or myofibroblast phenotype (46, 93). The decrease in the percent α SMA⁺ fibroblasts at the conclusion of re-epithelialization (Day 14-32 post wounding, **Figure 10A**) similarly coincides with the decrease in the stimulatory TGF β signaling (46). In contrast, the percent Vimentin⁺ cells showed a dramatic increase in number by day 12 post wounding, reaching 90% of all fibroblast marker positive cells by Day 21 (**Figure 10A**). Interestingly, although a peak in the proliferating Vimentin⁺ cells is noted at day 3 post wounding (**Figure**

10B), the accumulation of these cells in the wound was only obvious at day 12, suggesting that Vimentin⁺ cells accumulation may not result from increased proliferation. Interestingly, although FSP-1/S100A4 is prominently detected in the normal skin (**Figure 10A**), there was very little variation in the % FSP-1/S100A4⁺ cells during wound healing, and despite a peak in the proliferating FSP-1/S100A4⁺ cells also noted at day 3 post wounding. Since the percent of FSP-1/S100A4⁺ Ki67⁺ cells were the highest amongst the fibroblasts population studied (α SMA⁺ and Vimentin⁺ fibroblasts, respectively) (**Figure 10B**), these results suggest a rapid turnover of the FSP-1/S100A4⁺ cells during wound repair. The overall frequency of fibroblast marker positive cells that increased during wound healing were returned to baseline levels at Day 32. The lack of fully restored α SMA⁺ cell populations by Day 32 may reflect the loss in overall fibroblast number which occurs after wound healing, without the complete regeneration of endothelial cells (**Figure 10A**). While normal skin contained roughly 10% CD31⁺ cells and increased to 15% at day 6 post wounding, the number of CD31⁺ cells made up only 5% of total cells at day 21 and 2% at day 32.

We next examined the degree of overlap between expression of these fibroblast markers on a per cell basis. A weakness in traditional immunostaining methods has been the difficulty in evaluating heterogeneity of marker expression without loss of spatial information, limiting analysis to only two or three markers simultaneously. Using a newly developed analysis platform, the marker phenotype was determined and a truth table was generated in order to identify the degree of overlap between marker positive populations. In normal and fully healed skin (**Figure 11**), the cells of the dermis were primarily made up of α SMA⁺ and FSP-1/S100A4⁺

cells, with between 5-15% of cells expressing both markers. However, by Day 6 post wounding, when the number of α SMA⁺ cells had increased to 45% of all cells in the dermis, the majority population was α SMA single expressing cells with the bulk of FSP-1/S100A4⁺ cells also expressing α SMA (**Figure 11**). Interestingly, by Day 14 post wounding, when wound re-epithelialization is complete, not only did the frequency of cells singly positive for Vimentin increased, but up to 23% of Vimentin⁺ cells also expressed α SMA (**Figure 11**). By Day 32 post wounding, 18 days following re-epithelialization, the wound tissue had largely normalized and the relative overall of fibroblasts marker expression was similar to that of normal skin (**Figure 11**). These results indicate a dynamic overlap of fibroblasts marker expression during dermal wound repair, and the changes in the shared fibroblast marker expression over time raise the possibility of a common fibroblast progenitor cell giving rise to fibroblasts that subsequently narrow their fibroblast marker expression. Alternatively, the overlap in fibroblast marker expression, although unlikely, may simply reflect a promiscuous expression pattern that challenge a functional resolution of fibroblast functional heterogeneity. Subsequent functional studies below and in Chapter 3 however support the former hypothesis.

To define if the overlap in fibroblast marker expression reflects a possible differentiation of α SMA⁺ fibroblasts at Day 3 post wounding from a putative FSP-1/S100A4⁺ progenitor population found in the normal skin (**Figure 10**), we utilized genetically engineered mice that enabled the lineage tracing of FSP-1/S100A4 expressing cells. The FSP-1/S100A4-Cre mice were bred to mT/mG indicator mice. In these mice, all cells constitutively express a tdTomato transgene that converts to

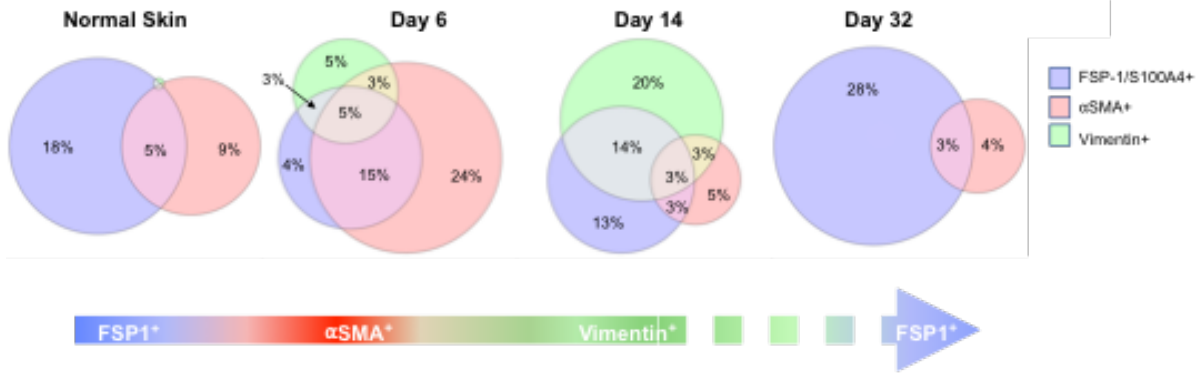


Figure 11. Co-expression of markers during wound repair
 Venn diagrams showing extent of co-expression between cells expressing FSP-1 (blue), αSMA (red), and Vimentin (green) in normal dermis and wound beds from days 6, 14, and 32 post-wounding, n=5 mice per group..

green fluorescent protein (GFP) expression following expression Cre recombinase, which in this model is under the control the FSP1-promoter. These mice were wounded as described above and wound tissue was collected at Day 6 post wounding, as this was the time-point with the greatest overlap in FSP1/S100A4 and α SMA expression. Immunolabeling of these tissues for α SMA allowed quantitative analysis of the degree to which α SMA⁺ cells are derived from FSP1/S100A4⁺ progenitors. In normal skin areas, FSP1/S100A4 lineage positive cells were localized to the epidermis and hair follicles (**Figure 12A**) with minimal α SMA⁺ cells present. Interestingly, within the granulation tissue 38% of all α SMA⁺ cells were found to be GFP⁺ (**Figure 12B-C**). These results suggest that although some α SMA⁺ cells arise from FSP1/S100A4⁺ progenitors, there exists a distinct population of α SMA⁺ cells that do not (**Figure 12C**).

As indicated above, another advantage to the multiplex imaging lies in its unique capacity to inform on spatial distribution. An understudied area of questioning in the field of dermal wound healing has been the degree to which position within a wound may influence the proliferation and abundance of fibroblast populations during the wound healing process. Despite a position in the field that fibroblast proliferation occurs at the wound margins, it remains unclear whether cells within the wound center are phenotypically distinct from those at the edge of the wound. In order to determine whether changes in fibroblast composition may be related to their position within the healing wound, each fibroblast population was 'binned' based on distance from the wound center (**Figure 13A**). Five 'bins' or areas were arbitrarily defined between the center of the wound and its edge. Two such spatial fragmentations of the wound, mirroring one another, could be defined from the center of the wound and either its

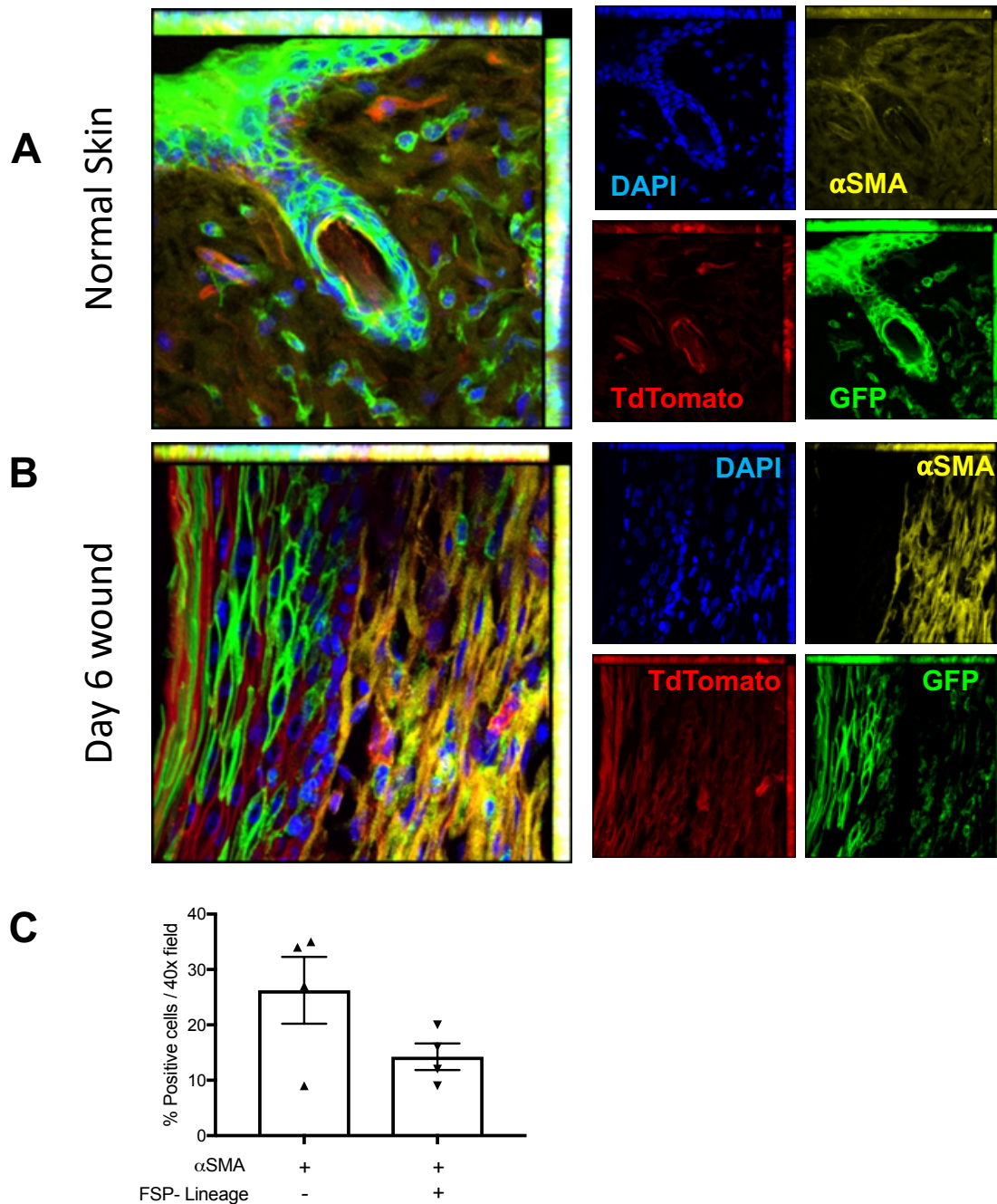


Figure 12 Lineage tracing of FSP1/S100A4⁺ cells immunolabeled with α SMA

- (A) FSP-Cre mTmG mice immunolabeled with α SMA in normal skin presented a clear distinction between FSP1/S100A4-lineage⁺ cells and α SMA⁺ cells
- (B) FSP-Cre mTmG day 6 wounds immunolabeled with α SMA
- (C) Quantification of the degree of FSP-Lineage positive and negative cells in day 6 wounds which express α SMA (n=4 wounds)

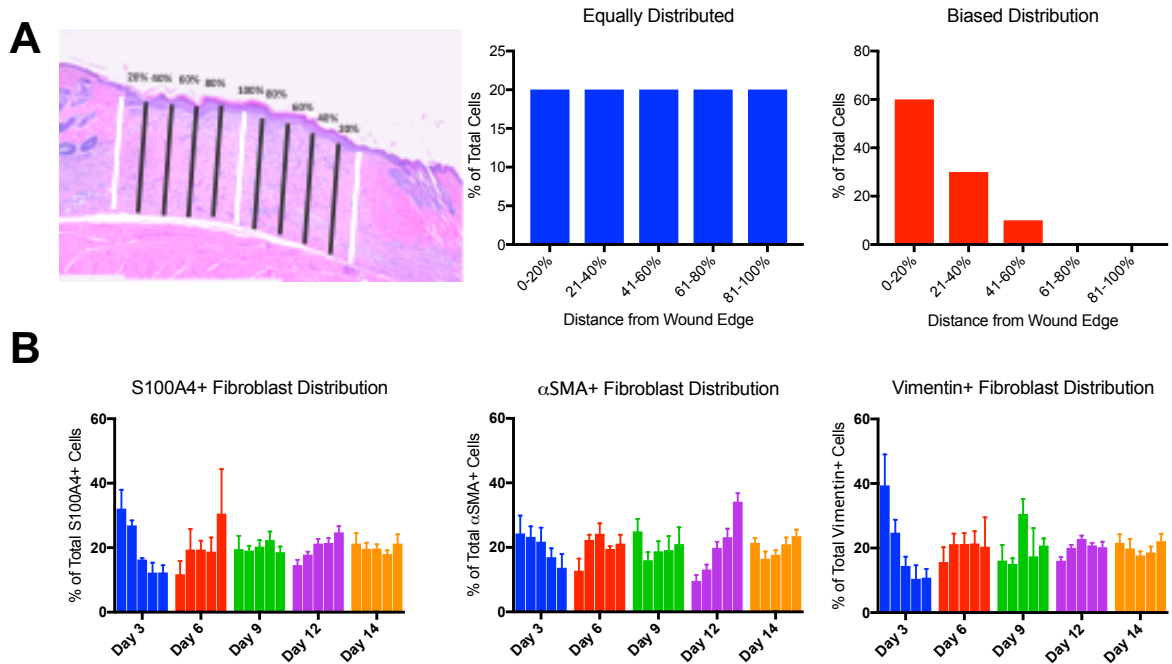


Figure 13. Spatial distribution of fibroblast subpopulations in cutaneous wounds
 (A) Left: Subdivision of wounds based on distance from wound edge with 0% indicating wound edge and 100% indicating wound center. Examples of histogram distribution for cells equally dispersed within the wound area (center) or showing biased distribution (right)
 (B) Distribution of FSP-1⁺ (left), α SMA⁺ (center), and Vimentin⁺ (right) cells within the wound at days 3 through 14 post-wounding. n=4 mice per group.

left or right edge (**Figure 13A**). The mirrored bins were then combined for subsequent analyses. Two scenarios were drawn based on a predicted equal or biased distribution of the fibroblasts population in the wound (**Figure 13A**). The results showed that α SMA⁺ cells appear to be present primarily at the leading edge of wounds at each time-point during the wound healing process (**Figure 13B**). In contrast, FSP-1/S100A4⁺ cells were generally found in the areas ahead of the leading edge. Interestingly, despite the noted increase in vimentin⁺ cells during wound healing, the cells appear equally distributed in the wound bed. These distinct patterns of fibroblasts distribution in the wound bed during wound healing suggest distinct functions for these cells in dermal wound repair.

Chapter 3. Functional role of fibroblasts in dermal wound healing

3.A. Genetic approach to deplete fibroblasts population in dermal wound injury repair

To define the rate-limiting, functional contribution of distinct fibroblast populations in dermal wound repair, we utilized an established conditional suicide gene system in mice to deplete genetically-tagged cells (41, 94-96). Specifically, mice were engineered to express the HSV-TK transgene under the control of a defined gene promoter element (**Figure 14**). In our studies, we employed gene promoter elements for the defined fibroblasts gene products detailed in Chapter 1 and 2. This approach allows for the selective depletion of defined fibroblast populations. Expression of the selected fibroblast promoter element in turn drives the expression of viral thymidine kinase (TK). This does not impact the endogenous fibroblast gene expression and has no impact on the mice viability (41, 94, 95). Notably, we engineered mice with truncated or full-length TK transgene, the latter yielding male infertility due to leaky TK expression in testes (97-99). Both forms of the transgenes however show efficient conditional suicide gene expression and cell targeting (*vide infra*).

In cells expressing the TK transgene, administration of Ganciclovir (GCV, a synthetic analog of 2'-deoxy-guanosine) results in conversion of the prodrug to ganciclovir triphosphate, a competitive inhibitor of dGTP incorporation into DNA, leading to cell cycle arrest and cell death (100). This approach, in contrast with systemic gene knockout mice, antibody depletion, or ectopic treatments, uniquely enables the dynamic functional characterization of proliferating fibroblasts that accumulate during dermal wound repair. The efficacy of the distinct constructs

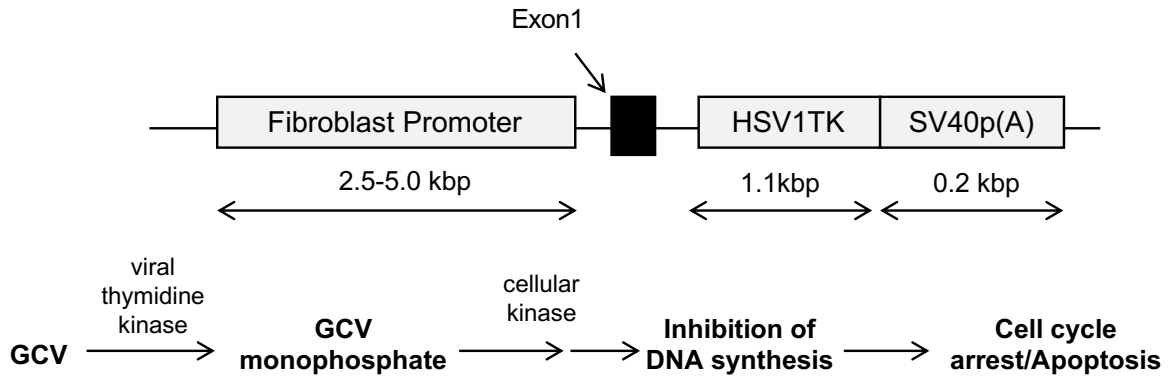


Figure 14. Schematic of thymidine-kinase mediated cell depletion in transgenic mice
 Top: Construct map of transgenes injected into C57 zygotes for the production of transgenic mice

Bottom: Mechanism of thymidine kinase mediated cell ablation. Thymidine kinase converts ganciclovir (GCV) into a nucleotide analog which becomes incorporated into DNA during replication, causing chain termination and inability to proliferate

generated was tested using primary cultures of mouse ear fibroblasts. Mouse ear fibroblasts, from TK+ and TK- mice, were expanded *in vitro*. After collagenase dissociation and a culture period of no more than two weeks, ear fibroblasts were seeded to 96 well plates at 1×10^4 cells per well and treated with GCV at concentrations of 0, 5, and 50uM. After a treatment period of three days, cell viability was measured using trypan blue exclusion. Previously studies reported on the efficacy of the α SMA-TK and FSP1 -TK transgenes using a similar procedure (41, 95). The results from these experiments indicated a specific, dose-dependent reduction of in cell viability for Col1a1-TK and FAP-TK expressing cells in comparison to wild-type (WT) control cells (**Figure 15A-B**). The reduction in Col1a1 expressing ear fibroblasts, evaluated by immunolabeling, was also evident in cultures of cells from Col1a1-TK mice subjected to GCV, when compared to untreated Col1a1-TK expressing ear fibroblasts (**Figure 15C**). Interestingly, the *in vitro* targeting of Col1a1 expressing ear fibroblasts also resulted in a decrease in α SMA expressing fibroblasts (**Figure 15C**).

Phenotypic characterization of wound closure rate and evaluation of fibroblast depletion using the conditional suicide gene construct was evaluated using FTS in α SMA-TK (**Figure 16**), FSP1-TK (**Figure 17**), FAP-TK (**Figure 18**), Col1a1-TK (**Figure 19**), and DDR2-TK (**Figure 20**) transgenic mice. These transgenes represent the complex fibroblast heterogeneity observed during dermal wound repair (**Table 1, Chapter 2**). On the day of wounding (Post Wounding Day 0), mice were treated with GCV daily and wound area was measured until the day of wound closure in TK- (WT) mice. Depletion of targeted cell populations were confirmed by immunohistochemistry or *in situ* RNA hybridization. Targeted depletion of α SMA⁺ fibroblasts resulted in a

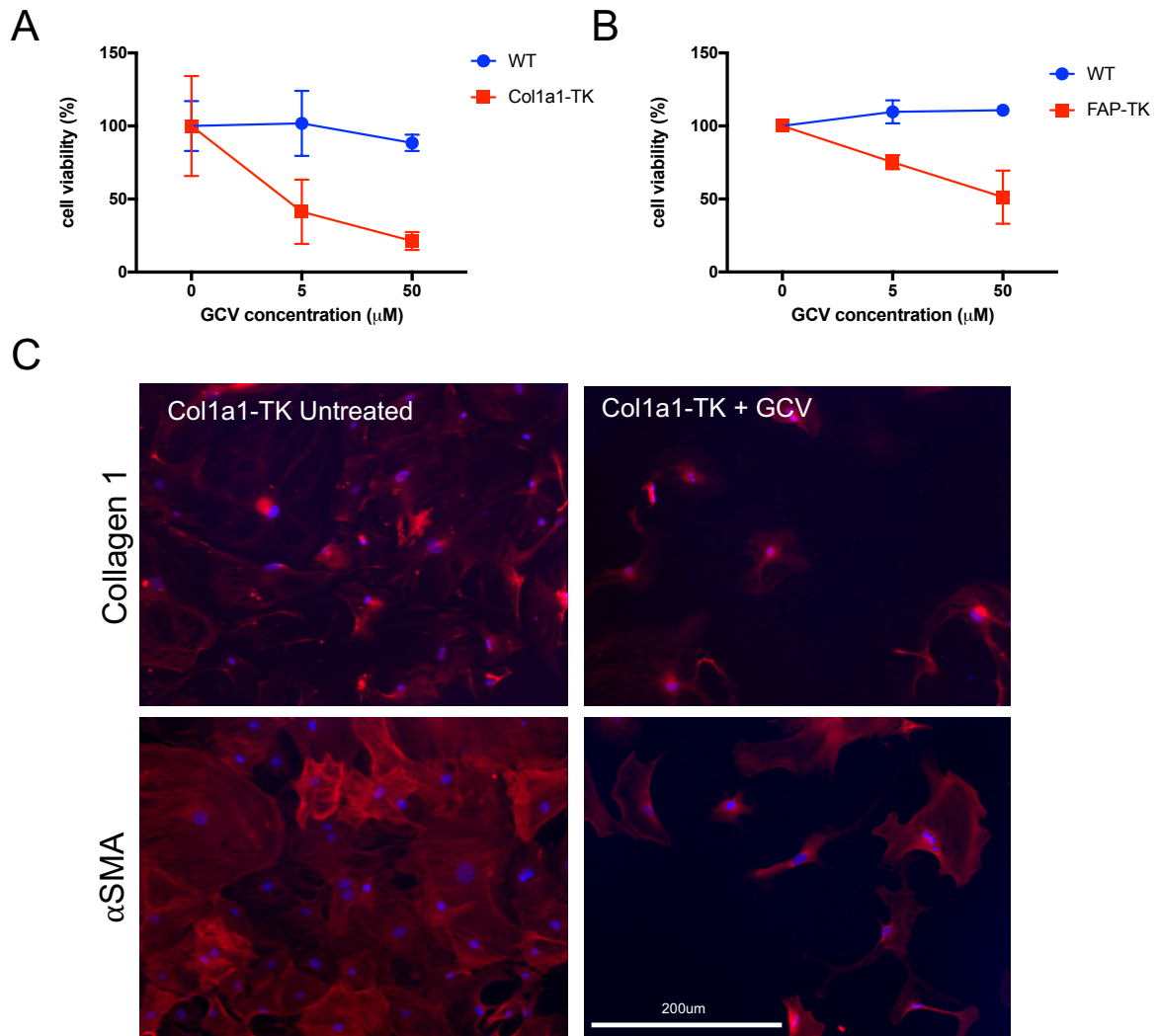


Figure 15. *In vitro* confirmation of cellular ablation of ear fibroblasts in generated mouse models

(A and B) *In vitro* ganciclovir treatment of ear fibroblasts from Col1a1-TK or FAP-TK mice demonstrates a dose-dependent ablation of viable cells compared to wild-type littermates (WT). n=3

(C) Cultured ear fibroblasts without GCV treatment (left) or with GCV treatment (right) immunostained with Collagen 1 (top) or α SMA (bottom)

defined interruption in the wound closure process, starting at roughly six days post-wounding (**Figure 16A**). Whereas control (WT) mice showed complete wound closure (0% wound area) at day 17 following wounding, α SMA-TK mice present with an open wound (32% wound area), showing a stalling in wound closure starting at day 6 of wound repair (**Figure 16A**). Immunostaining for α SMA in the wound bed, specifically focusing on the dermis, indicated a significant reduction in α SMA⁺ fibroblasts (approximately 75% reduction, **Figure 16B-C**) when comparing WT mice at day 6 post wounding (36% wound area) and α SMA-TK mice at day 17 (32% wound area).

Targeted depletion of FSP-1/S100A4⁺ fibroblasts did not result in a significant decrease in wound closure rate, with both FSP1-TK and WT mice showing complete wound closure at day 17 following wounding (**Figure 17A**). Immunostaining for FSP-1/S100A4 within the dermal layer of the wounds (**Figure 17B**) showed a significant decrease in the FSP-1/S100A4⁺ cell population of approximately 25% (**Figure 17C**).

Targeted depletion of FAP⁺ fibroblasts resulted in a significant decrease in wound closure rate presenting at Day 10 post wounding (**Figure 18A**). While WT mice reached complete wound closure by Day 14 post wounding, FAP-TK mice presented an open wound (12% wound area) up to day 16 (**Figure 18A**). Immunostaining for FAP within the wound bed (**Figure 18B**) showed a significant decrease in the number of FAP⁺ cells (approximately 35% less than WT mice, **Figure 18C**).

Targeted depletion of Col1a1⁺ fibroblasts in wounded mice presented with a significantly impaired wound closure rate starting at Day 8 post wounding (**Figure 19A**). At Day 14 following wounding, when WT mice had reached full wound closure,

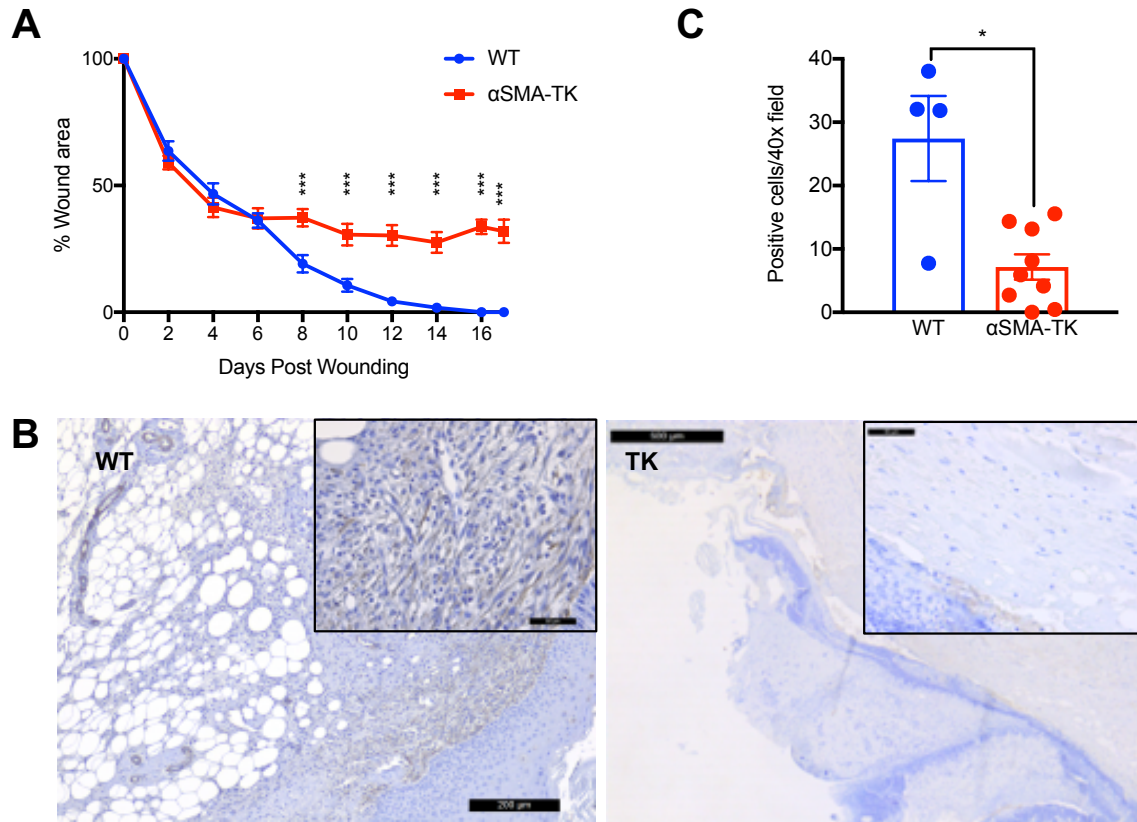


Figure 16. Functional contribution of α SMA⁺ fibroblasts in cutaneous wound closure
 (A) Wound measurements following wounding in α SMA-TK at Day 17 and wild-type mice at Day 6 post wound induction
 (B) Representative histological staining of α SMA⁺ cells within the wound area
 (C) Quantification of α SMA⁺ cell number in WT and α SMA-TK wounds on Day 6 based on immunohistological staining

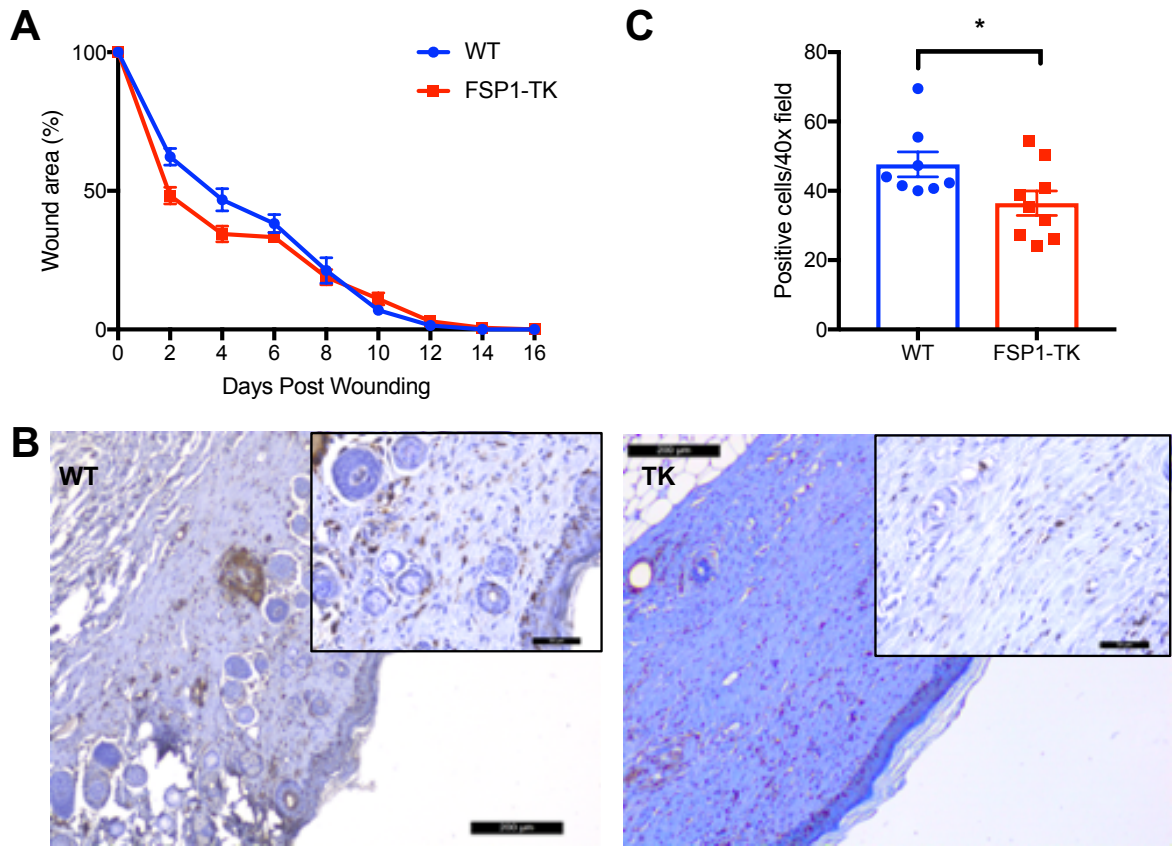


Figure 17. Functional contribution of FSP1/S100A4⁺ fibroblasts in cutaneous wound closure
 (A) Wound measurements following wounding in FSP1-TK and wild-type mice
 (B) Representative histological staining of FSP1⁺ cells within the wound area comparing wounds from WT and FSP-TK mice at Day 17
 (C) Quantification of FSP1/S100A4⁺ cell number in day 17 wounds from WT and FSP1-TK mice based on immunohistological staining

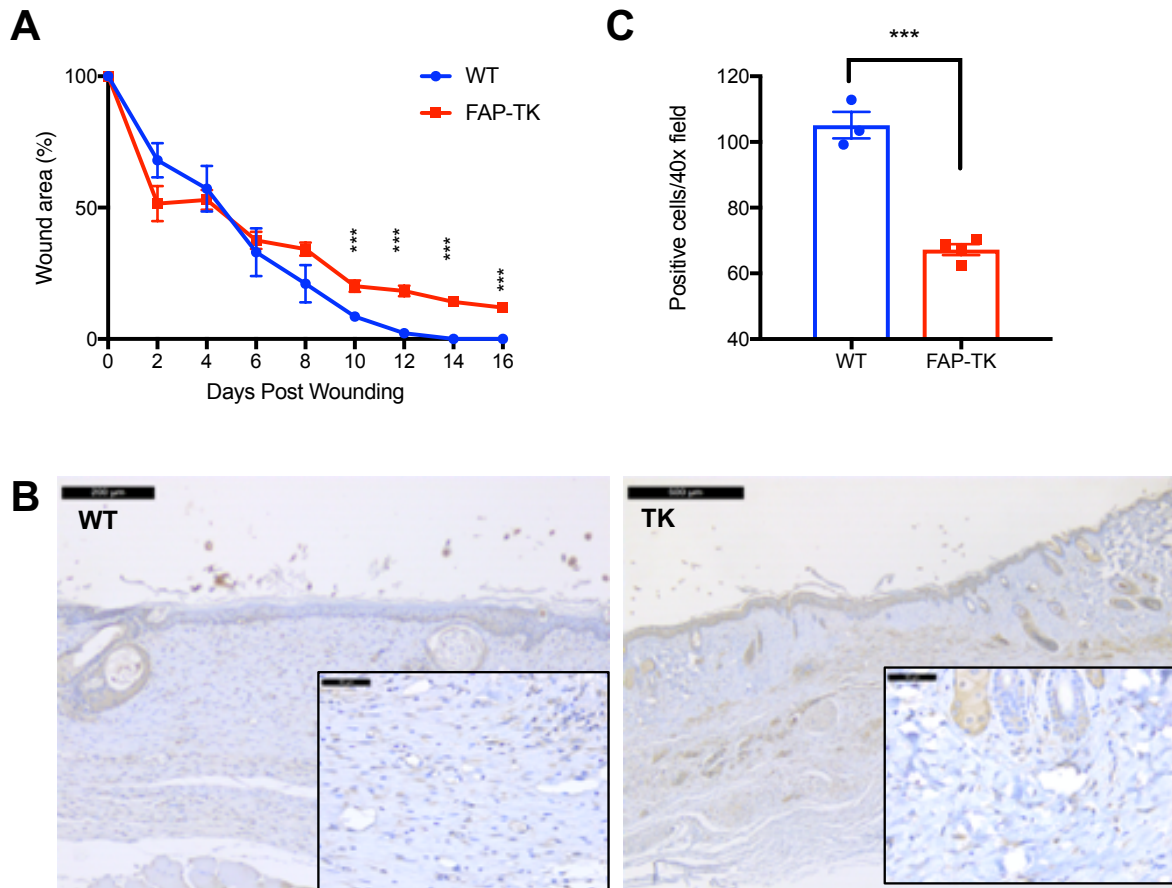


Figure 18. Functional contribution of FAP⁺ fibroblasts in cutaneous wound closure

- (A) Wound measurements following wounding in FAP-TK and wild-type mice
 (B) Representative histological staining of FAP⁺ cells within the wound area at day 17 post wounding
 (C) Quantification of FAP⁺ cell number in day 17 wounds from WT and FAP-TK mice based on immunohistological staining

Col1a1-TK still presented with open wounds (7% of initial wound area, **Figure 19A**). *In situ* RNA hybridization for expression of the Collagen1a1 gene suggested a decrease in collagen production (**Figure 19B-C**).

Targeted depletion of DDR2⁺ fibroblasts did not result in a change in wound closure rate, with both DDR2-TK and WT mice reaching full wound closure at Day 14 post wounding (**Figure 20A**). Immunostaining for DDR2⁺ cells within the repairing dermis did not indicate any decrease in DDR2-TK mice (**Figure 20B-C**). As a control for our staining procedure, heart and subdermal muscle sections were additionally stained (**Figure 20D**) as these organs have been demonstrated to express high levels of DDR2 (101).

Collectively, these results showcased a rate limiting functions for proliferating α SMA⁺, Col1a1⁺ and FAP⁺ fibroblasts in dermal wound closure, in contrast with proliferating FSP-1/S100A4⁺ fibroblasts. Despite a 25% depletion in FSP-1/S100A4⁺ fibroblasts, no impact was noted on wound closure. The lack of phenotypic changes in DDR2-tk mice, compared to WT control, is explained by the scarcity of the DDR2⁺ fibroblasts; these mice effectively controlling for any potential GCV side effects. GCV side effects were not observed.

3.B. Distinct roles of fibroblasts subpopulations in dermal wound closure

In addition to an inability to re-epithelialize, delayed or incomplete wound repair often presents with two major deficiencies: 1) An inability to replace the lost basement membrane at the wound site through production of collagen, and 2) A decreased capacity to perform neo-angiogenesis to supply oxygen and nutrients to

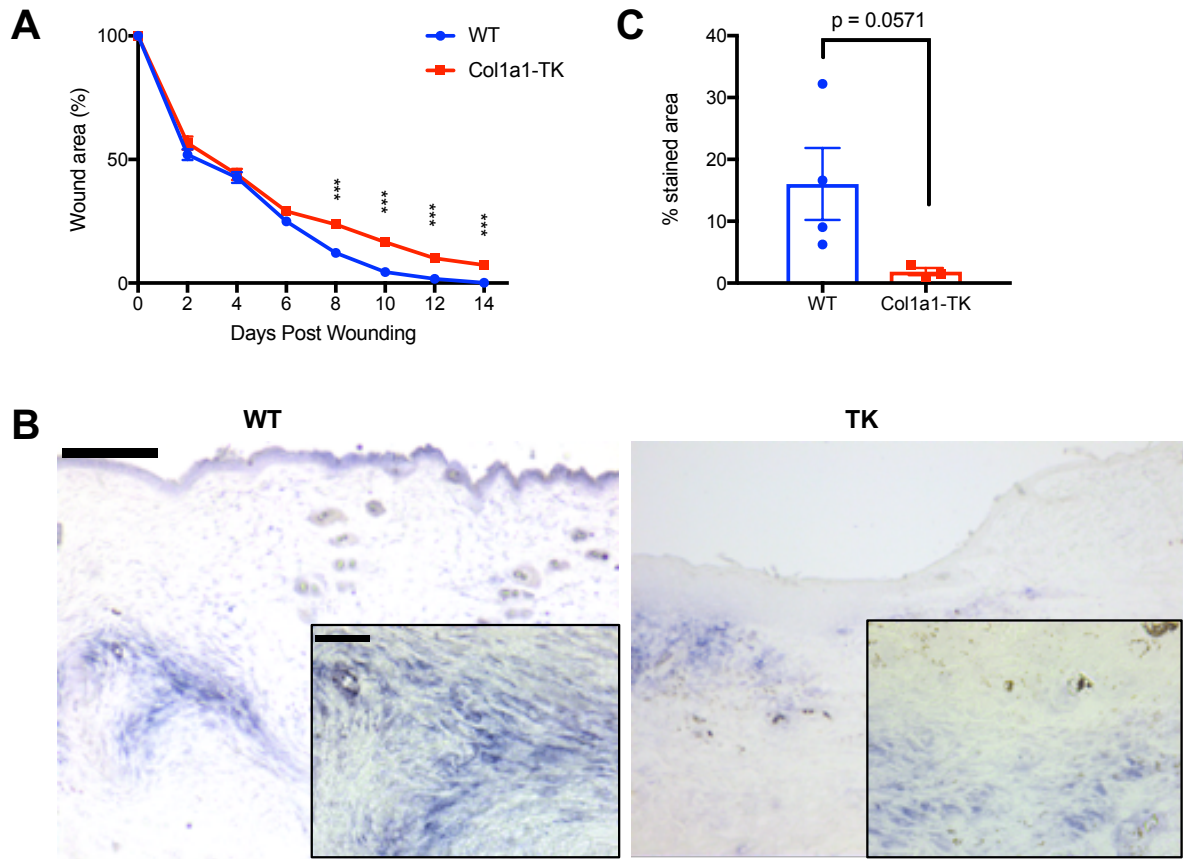


Figure 19. Functional contribution of Col1 α 1⁺ fibroblasts in cutaneous wound closure
 (A) Wound measurements following wounding in Col1 α 1-TK and wild-type mice
 (B) Representative histological *in situ* staining of Col1 α 1⁺ cells within the wound area
 (C) Quantification of Collagen1 α 1⁺ stained area in WT and Col1 α 1-TK mice based on *in situ* hybridization

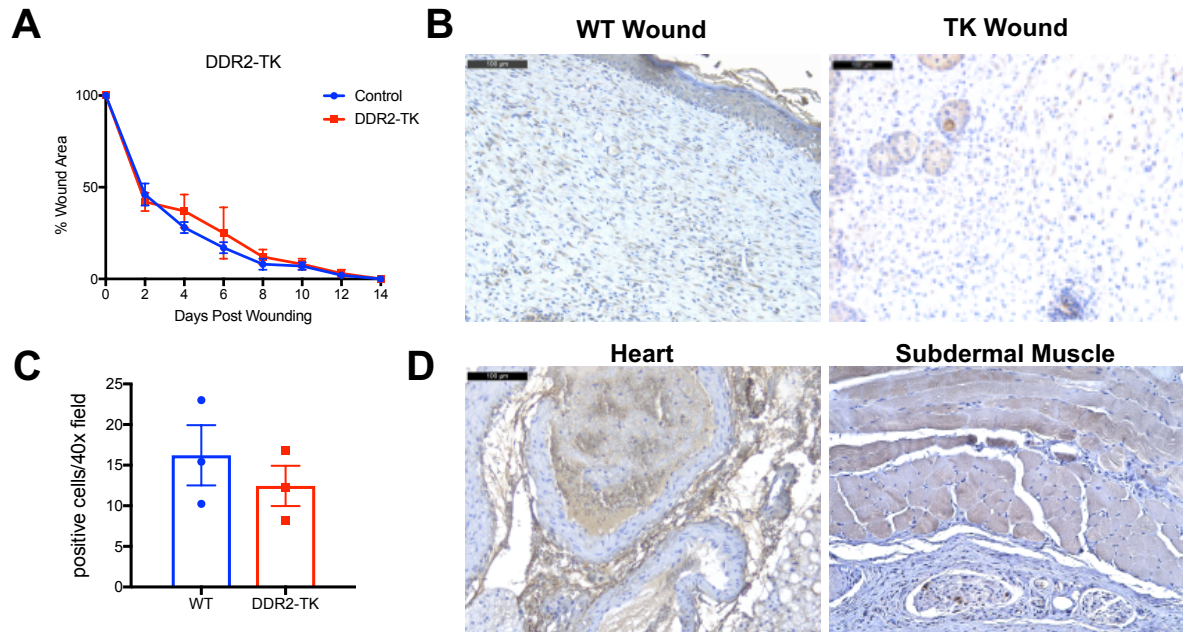


Figure 20. Functional contribution of DDR2⁺ fibroblasts in cutaneous wound closure
 (A) Wound measurements following wounding in DDR2-TK and wild-type mice
 (B) Representative histological staining of DDR2⁺ cells within the wound area at day 14
 (C) Quantification of DDR2⁺ cell number in Day 14 wounds based on immunohistological staining
 (D) Representative histological staining of DDR2⁺ cells in heart and subdermal muscle sections

the new tissue. These characteristics of the wound repair process were evaluated in each transgenic system described above (**Figures 16 to 20**). As anticipated with the observed impairment in closure rate (**Figure 16**), depletion of proliferating α SMA⁺ cells was associated with an inability to establish a granulation area or epithelial barrier (**Figure 21B, F**). Depletion of proliferating FAP⁺ (**Figure 21C**) or Col1a1⁺ (**Figure 21D**) fibroblasts also impaired granulation thickness (**Figure 21F**), whereas depletion of FSP-1/S100A4⁺ fibroblasts did not significantly impair granulation thickness (**Figure 21E-F**) compared to WT controls. Although wounds from α SMA-TK and Col1a1-TK mice, compared to control mice, showed a predictably lower type 1 collagen deposition, a marked increase in type I collagen was observed in FAP⁺ fibroblasts depleted wounds, and no changes were observed in FSP-1/S100A4⁺ fibroblasts depleted wounds (**Figure 22**).

A feature of a properly healed wound is the formation of new blood vessels via neo-angiogenesis, allowing effective tissue perfusion of oxygen, metabolites and cytokines. In alignment with the wound vessel density, a marked increase in wound tissue hypoxia was noted in α SMA⁺ fibroblasts depleted wounds compared to control wounds (**Figure 23B and 24B**), and depletion of FSP-1/S100A4⁺ fibroblasts had no impact on tissue hypoxia (**Figure 23E and 24E**). In contrast, whereas depletion of FAP⁺ resulted in a mild decrease in CD31⁺ vasculature in the wound bed (**Figure 23C**), this did not translate in measurable increase in tissue hypoxia (**Figure 24C**). In Col1a1⁺ fibroblasts depleted wounds, though CD31⁺ vessel density is markedly higher when compared to control wounds (**Figure 23D**), tissue hypoxia was elevated (**Figure 24D**).

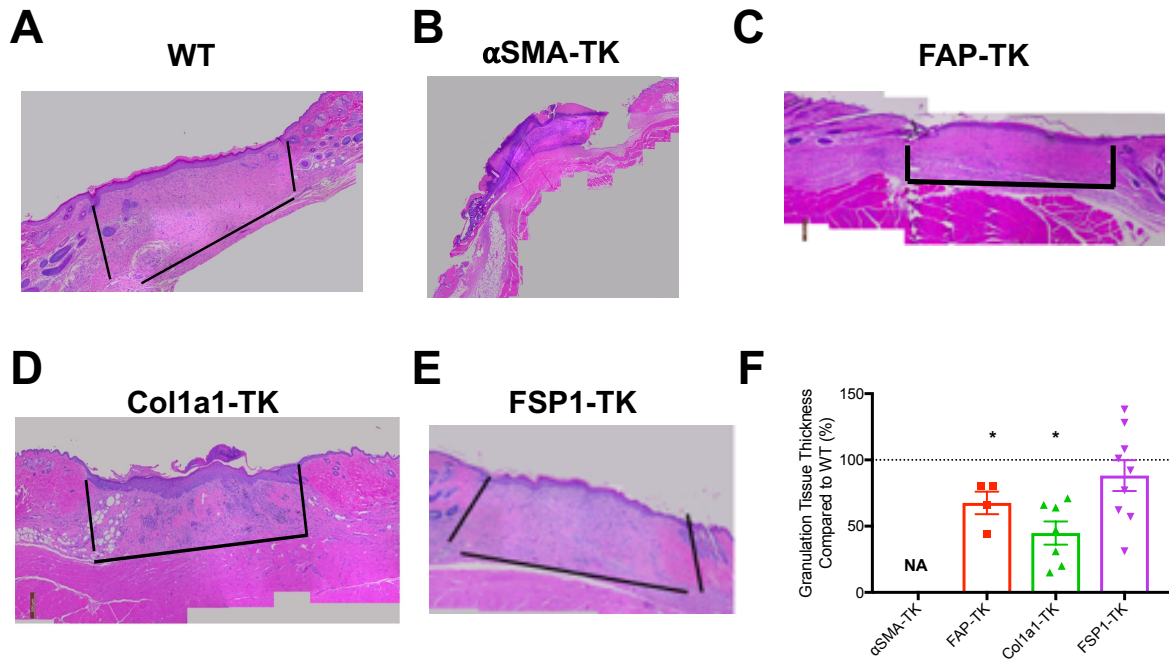


Figure 21. Col1 α ⁺ fibroblasts contribute to granulation tissue thickness in cutaneous wound healing

(A-E) H&E staining of wound sections from (A) wildtype, (B) α SMA-TK, (C) FAP-TK, (D) Col1 α 1-TK, and (E) FSP1-TK mice at day of full wound closure in wild-type mice. Black bars demarcate granulation tissue area.

(F) Quantification of granulation tissue area in transgenic mice from (B-E), compared to wild-type controls from the same experiment. n=4 per group

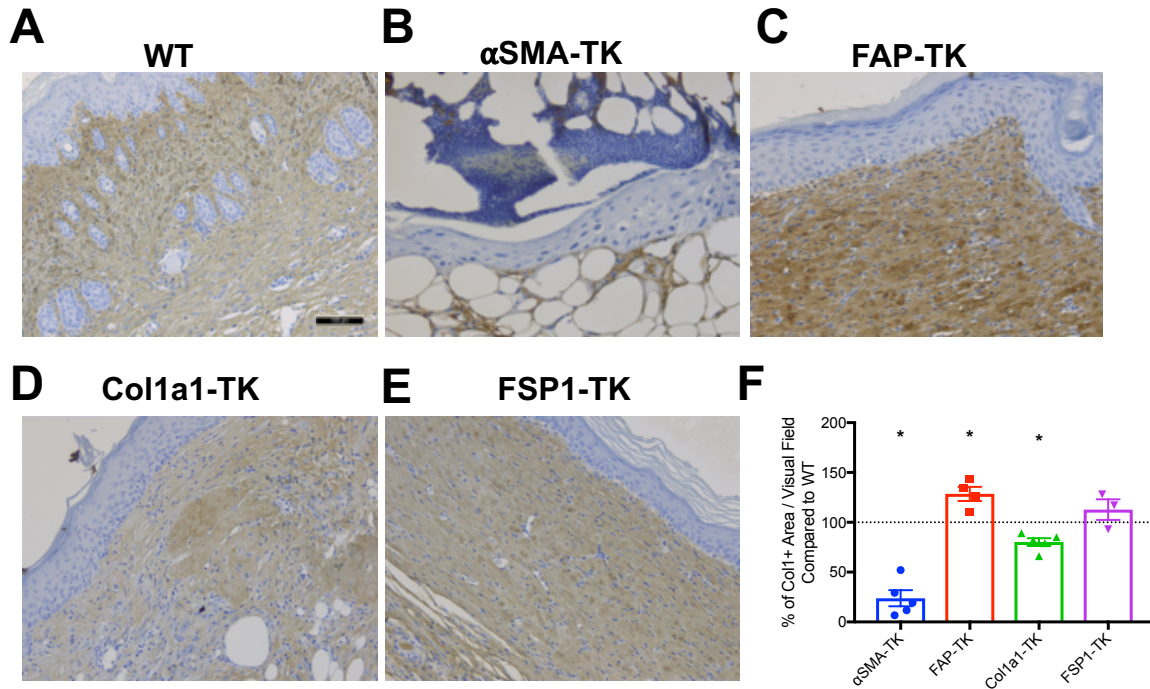


Figure 22. Differential expression of collagen-1 in wounds with distinct depletion of fibroblast subpopulations

(A-E) Collagen-1 staining of wound sections from (A) wildtype, (B) αSMA-TK, (C) FAP-TK, (D) Col1α1-TK, and (E) FSP1-TK mice at day of full wound closure in wild-type mice.

(F) Quantification of Collagen positive area in transgenic mice from (B-E), compared to wild-type controls from the same experiment.

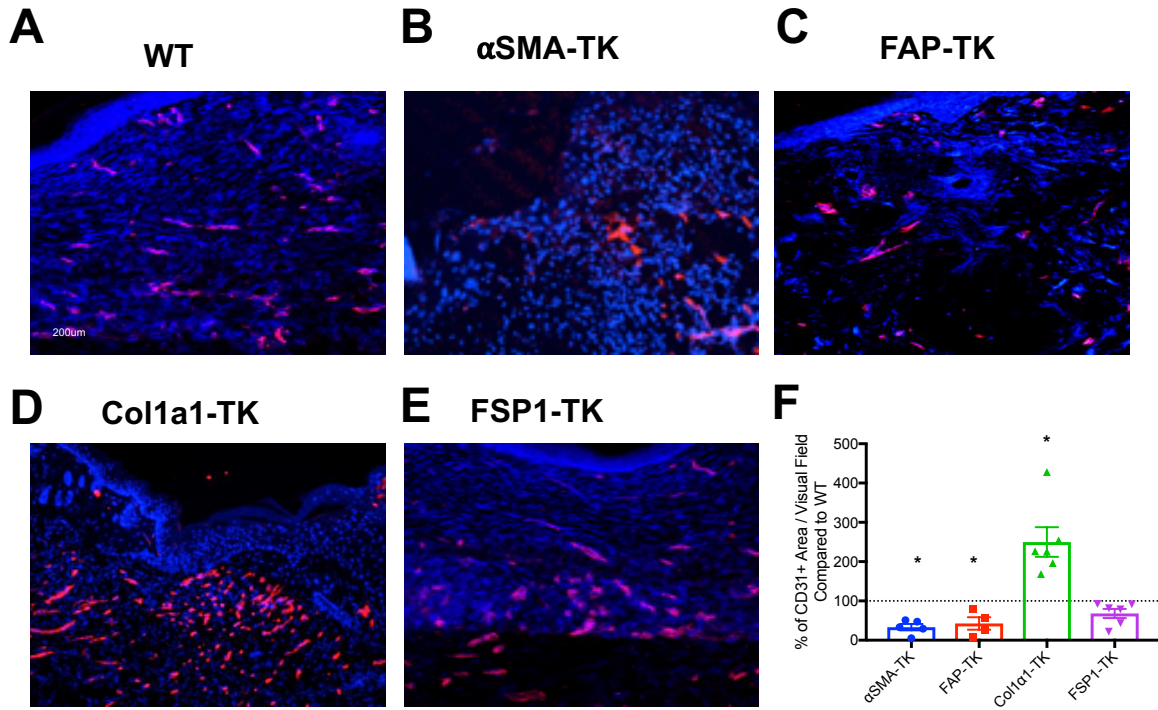


Figure 23. Differential angiogenic response in wounds with distinct depletion of fibroblast subpopulations
 (A-E) CD31 staining of wound sections from (A) wildtype, (B) α SMA-TK, (C) FAP-TK, (D) Col1 α 1-TK, and (E) FSP1-TK mice at day of full wound closure in wild-type mice.
 (F) Quantification of CD31 positive area in transgenic mice from (B-E), compared to wild-type controls from the same experiment.

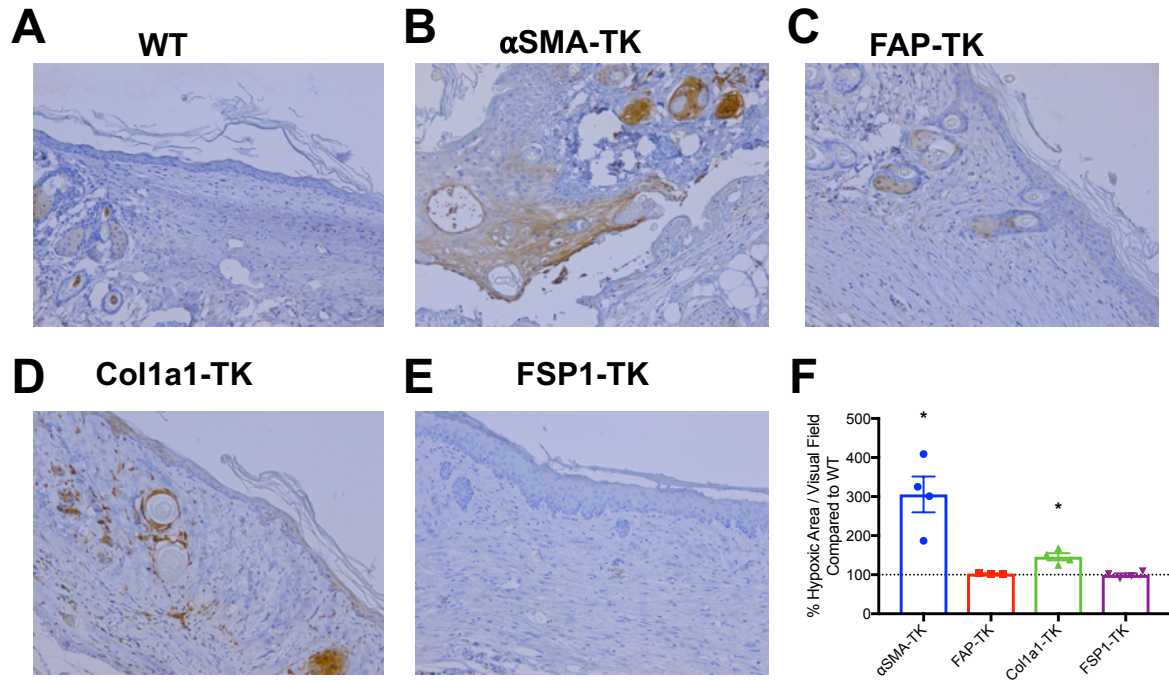


Figure 24. Depletion of α SMA⁺ fibroblasts promotes an hypoxic wound microenvironment

(A-E) Hypoxyprobe staining of wound sections from (A) wildtype, (B) α SMA-TK, (C) FAP-TK, (D) Col1a1-TK, and (E) FSP1-TK mice at day of full wound closure in wild-type mice.

(F) Quantification of hypoxic area in transgenic mice from (B-E), compared to wild-type controls from the same experiment.

Taken together, these functional depletion studies highlighted a heterogeneous response of distinctly captured fibroblast populations during dermal wound repair (**Table 2**). Our results indicate that α SMA⁺ fibroblasts play a critical role in completion of wound closure by enabling repair of the granulation tissue, ECM remodeling and angiogenesis (**Table 2**). While both FAP⁺ and FSP-1/S100A4⁺ fibroblasts exert functions in wound closure, albeit to a lesser extent than α SMA⁺ fibroblasts, their impact on type I collagen deposition and angiogenesis was opposite (**Table 2**). Interestingly, a seemingly contradictory phenotype is noted in Col1a1⁺ fibroblasts depleted wound, wherein increased vessel density was associated with increased tissue hypoxia. This raises the intriguing possibility that Col1a1⁺ fibroblasts regulate the maturation of patent blood vessels during cutaneous wound repair. Finally, our findings indicate that proliferating FSP1⁺ cells minimally act in the process of wound repair (**Table 2, Figure 17**).

	Wound Closure	Granulation Tissue Thickness	Collagen -1	Angiogenesis (CD31)	Hypoxia (Hypoxyprobe)
α SMA-TK	↓↓↓	X	↓	↓	↑
FAP-TK	↓	↓	↑	↓	-
Col1 α 1-TK	↓	↓	↓	↑	↑
FSP1-TK	↓	-	-	-	-

Table 2. Summary of findings on the functional contribution of distinct fibroblast subpopulations in cutaneous wound healing.

↑ Indicates increased closure rate, tissue thickness, or protein expression compared to control mice

↓ Indicates decreased closure rate, tissue thickness, or protein expression compared to control mice

- Indicates no change compared to control mice

X Indicates the inability to establish granulation tissue in α SMA-TK mice

Chapter 4. Origin and role of α SMA⁺ fibroblasts in dermal wound repair

4.A. Dermal α SMA⁺ fibroblasts control wound closure

The depletion of α SMA⁺ fibroblasts during wound healing resulted in a significantly impaired wound closure phenotype (**Figure 16**). This inability to complete wound healing was evidenced by both a decreased closure and decreased re-epithelialization (**Figures 25 and 26**). Because the formation of the hardened scab can sometimes obscure measurement of wound closure, we next performed H&E assessment of the migrating epithelial tongues at select time-points during wound healing of both WT and α SMA⁺ fibroblast depleted mice (**Figure 26**). While there was no measured difference in re-epithelialization at Day 3 or 6 post-wounding, wounds from α SMA-TK began to show a lower degree of re-epithelialization at Day 12 (**Figure 26**). By Day 17 post wound induction, wounds in WT mice had completely re-epithelialized. In contrast, wounds in α SMA⁺ fibroblast depleted mice had regressed, increasing from a mean epithelial tongue distance of 1.5mm at Day 12 to approximately 3mm by Day 17 (**Figure 26B**).

Informed by the decreased collagen deposition (**Figure 21B**) and re-epithelialization (**Figure 26B**) observed in wounds from α SMA-TK mice, we next investigated the nano-mechanical properties of the wound tissue (**Figure 27**). We utilized atomic force microscopy (AFM), a mechanical process based on the interaction of a very small flexible probe with the sample surface to determine the compressive stiffness at the nanometer range. Regions throughout the repairing dermis were selected for measurement of surface stiffness (**Figure 27A**) and 257

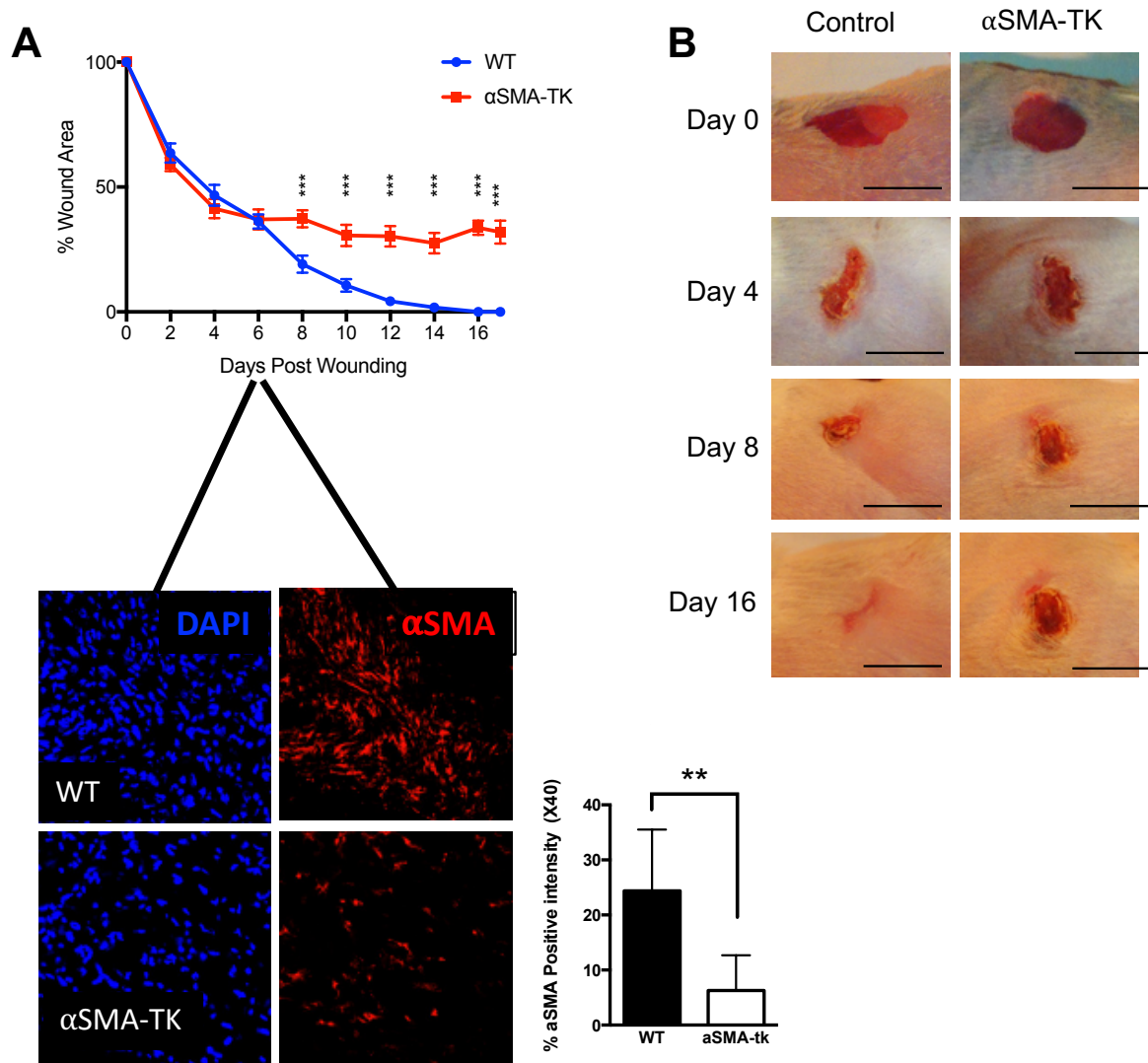


Figure 25. Depletion of α SMA⁺ fibroblasts prevents wound closure

(A) Top: Wound area measurements following wounding (day 0) in α SMA-TK and wild-type mice

Bottom: α SMA staining of wounds at Day 6 post wounding

(B) Gross view of wounds in control and α SMA-TK mice treated with GCV at days 0, 4, 8, and 16 post-wounding

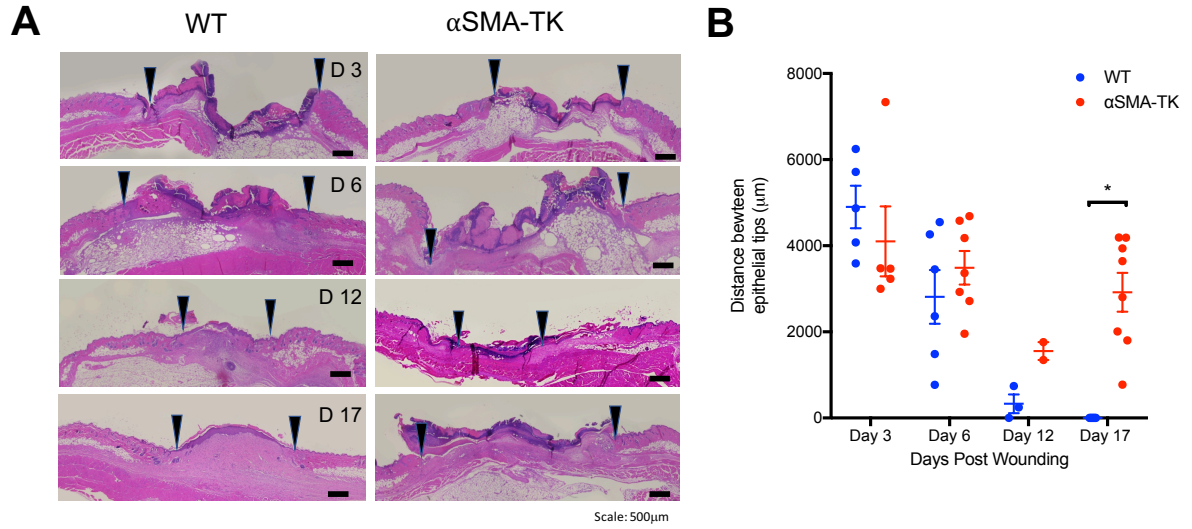


Figure 26. Impaired re-epithelialization in α SMA⁺ fibroblasts-depleted wounds

- (A) H&E staining of wounds from wild-type and α SMA-TK mice at days 3, 6, 12, and 17 post-wounding. Triangles indicate wound margins.
- (B) Quantification of distance between epithelial tips in WT compared to α SMA-TK wounds at days 3, 6, 12, and 17 post wounding

measurements were performed at each position. α SMA⁺ fibroblast depleted wounds exhibited a significantly decreased wound stiffness compared to WT mice (12.27kPa in α SMA-TK wounds compared to 13.57 kPa in WT wounds, **Figure 27D**)

Given the inability of α SMA⁺ fibroblast depleted wounds to close by Day 17 (**Figure 16**), we performed experiments extending treatment in order to determine whether the populations of α SMA-negative fibroblasts may eventually compensate for this loss (**Figure 28**). Interestingly, prolonged treatment of α SMA-TK mice with GCV completely prevented wound closure up to Day 32 (**Figure 28B**), at which point mice were sacrificed due to body weight loss and moribundancy. α SMA⁺ cell depleted wounds increased in size as treatment continued, growing from approximately 27% of initial wound area at Day 16 to 43% on Day 32 (**Figure 28B**). These results indicate that the loss of α SMA-positive cells cannot be compensated for by other cells. Conversely when GCV treatment was stopped at Day 14, wounds were eventually able to close, though complete closure did not occur until Day 42 post wounding (**Figure 28C**).

4.B. Resident α SMA⁺ fibroblasts functionally repair dermal wounds

Because transgene expression does not always correlate with the cells identified through immunostaining, we first confirmed that cells targeted in our α SMA-TK model follow a similar pattern to what was identified via our TSA panel. Due to the difficulty in staining for the TK protein directly, we instead utilized α SMA-RFP mice, which express the fluorescent protein RFP under the same α SMA promoter as our TK

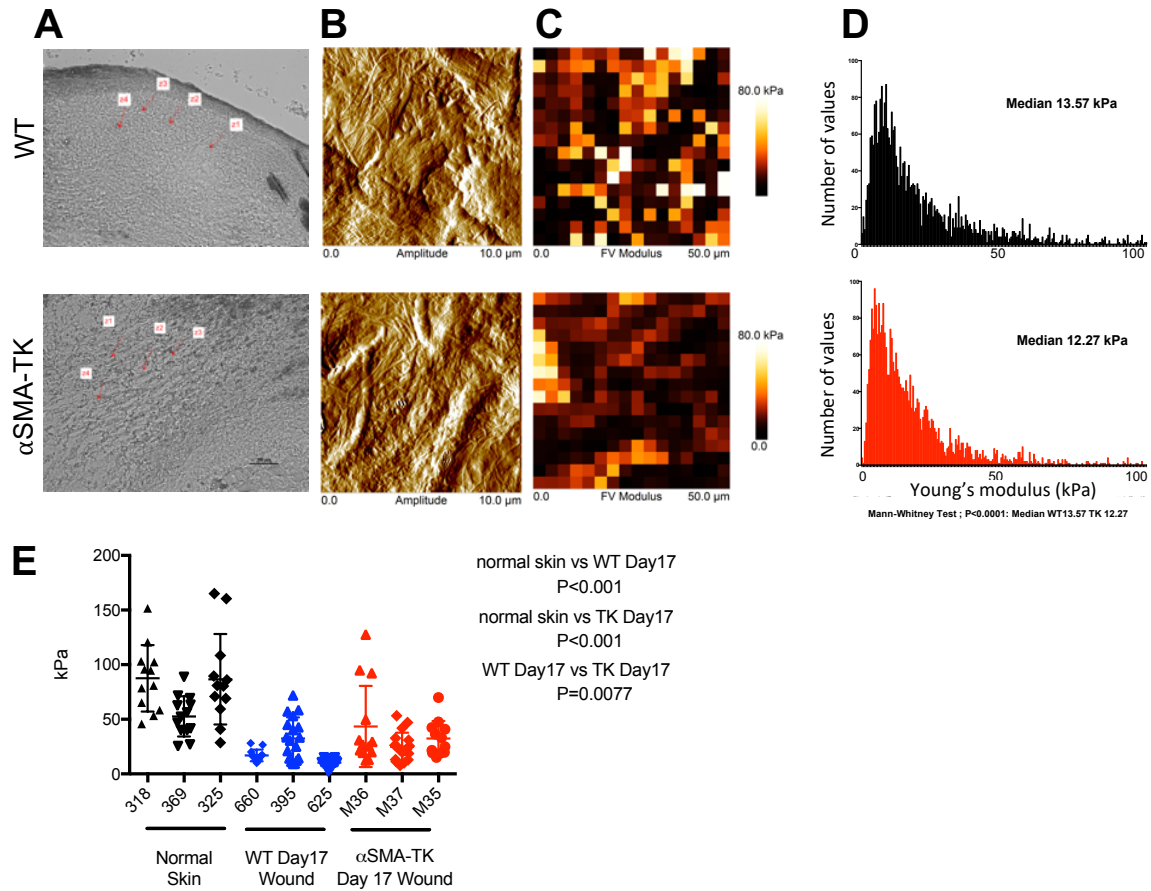


Figure 27. Reduced stiffness in α SMA⁺ fibroblasts-depleted wounds

Wound sections from wild-type (top) and α SMA-TK (bottom) mice were used for atomic force microscopy (AFM) measurements (n=3 per group, 4 positions per wound, 257 measurements per position).

- Optical microscopy images of tissue sections used for AFM, arrows indicate positions within the wound tissue used for analysis
- Representative AFM height images. Each image shows a 10.0 x 10.0 μm field.
- Representative elasticity maps. The color map indicates the modulus of elasticity (in kPa) evaluated using force curves generated at each point in the field. Each image shows a 50 x 50 μm field. This measurement does not give the absolute height but rather the height relative to the lowest contact point in the field.
- Young's elastic modulus distribution of section samples. Values were assembled in a histogram and the median was calculated.
- Plot of individual measurements of Young's elastic modulus collected from three normal skin, day 17 WT wound, and day 17 α SMA-TK wounds

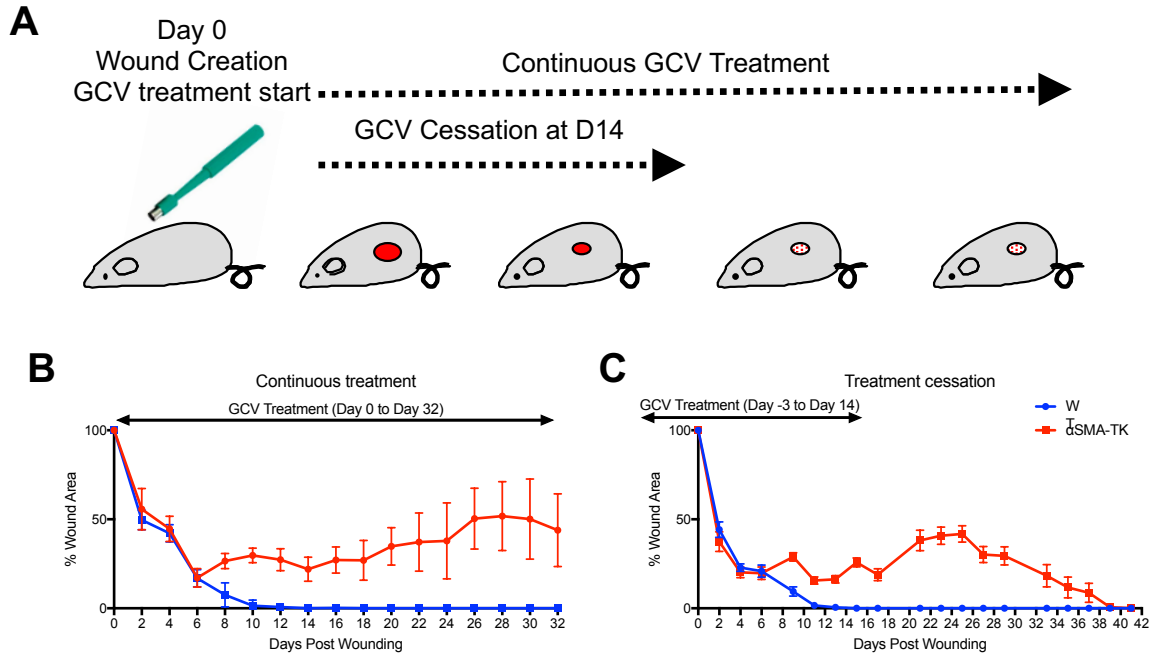


Figure 28. The impact of α SMA⁺ fibroblasts depletion on wound closure is reversible

(A) Cartoon schematic of treatment arms.

(B) Wound closure in wild-type (blue) and α SMA-TK (red) mice treated with GCV daily for 32 days.

(C) Wound closure in wild-type and α SMA-TK mice treated with GCV up to day 14.

system. These mice have been previously developed in our laboratory and have been demonstrated to show defined localization to cells identified by immunostaining in other organs (41). α SMA-RFP mice were wounded and wound tissues were harvested at Day 3, 6, 9, and 14 for analysis of RFP⁺ cell abundance by microscopy (**Figure 29A**) and flow cytometry (**Figure 29B**). As observed in our previous experiments (**Figure 10A**), uninjured skin showed a low degree of α SMA positive cells (**Figure 29C**). By Day 6 post wounding there was an accumulation of α SMA positive cells to approximately 11% of total cells, followed by a decrease to 7% on Day 14 as the wounds resolved (**Figure 29C**). Although these results are lower than what was observed in our immunolabeling experiments (**Figure 10A**), the use of flow cytometry does not allow us to limit analysis exclusively to the repairing dermis as we had previously.

We next sought to determine the relative contribution of resident fibroblasts compared to bone marrow derived mesenchymal cells to the pool of α SMA⁺ fibroblasts during wound repair. We first investigated the co-localization of α SMA with the lower-lineage dermal marker Sca-1 (**Figure 30**). The use of Sca-1 positivity to identify resident fibroblast lineages has been performed in several models (57, 102, 103). Immunolabeling for Sca-1 and examination of co-localization using flow cytometry (**Figure 30A**) and microscopy (**Figure 30B**) demonstrated the presence of α SMA⁺Sca-1⁺ cells within the Day 6 wound tissue.

We next performed bone marrow transplantation studies utilizing α SMA-RFP mice and WT mice (**Figure 31**). We confirmed high bone marrow chimerism in

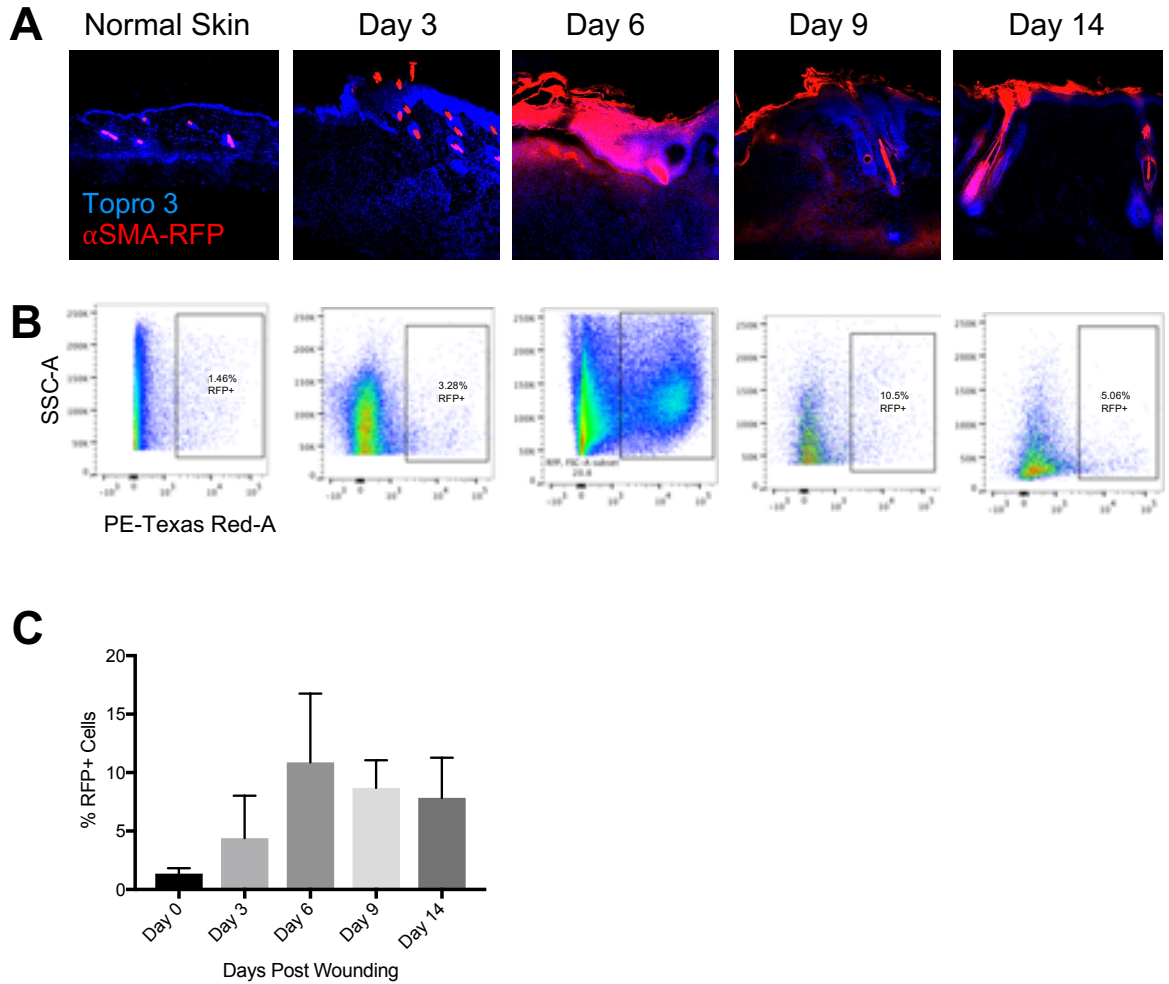


Figure 29. Visualization of α SMA-RFP⁺ fibroblasts in cutaneous wounds

Mice expressing RFP under the α SMA promoter were wounded and tissues were collected for analysis of RFP⁺ cells in normal skin and wounds from days 3, 6, 9, and 14

- (A) Assessment of α SMA⁺ fibroblasts (red) with Topro3 nuclear counterstain (blue) in normal and wounded skin from α SMA-RFP transgenic mice
- (B) Flow cytometry analysis of RFP⁺ cells (gated population) in normal and wounded skin
- (C) Quantification of α SMA-RFP⁺ cells in normal skin and 3, 6, 9, and 14 days post wound induction

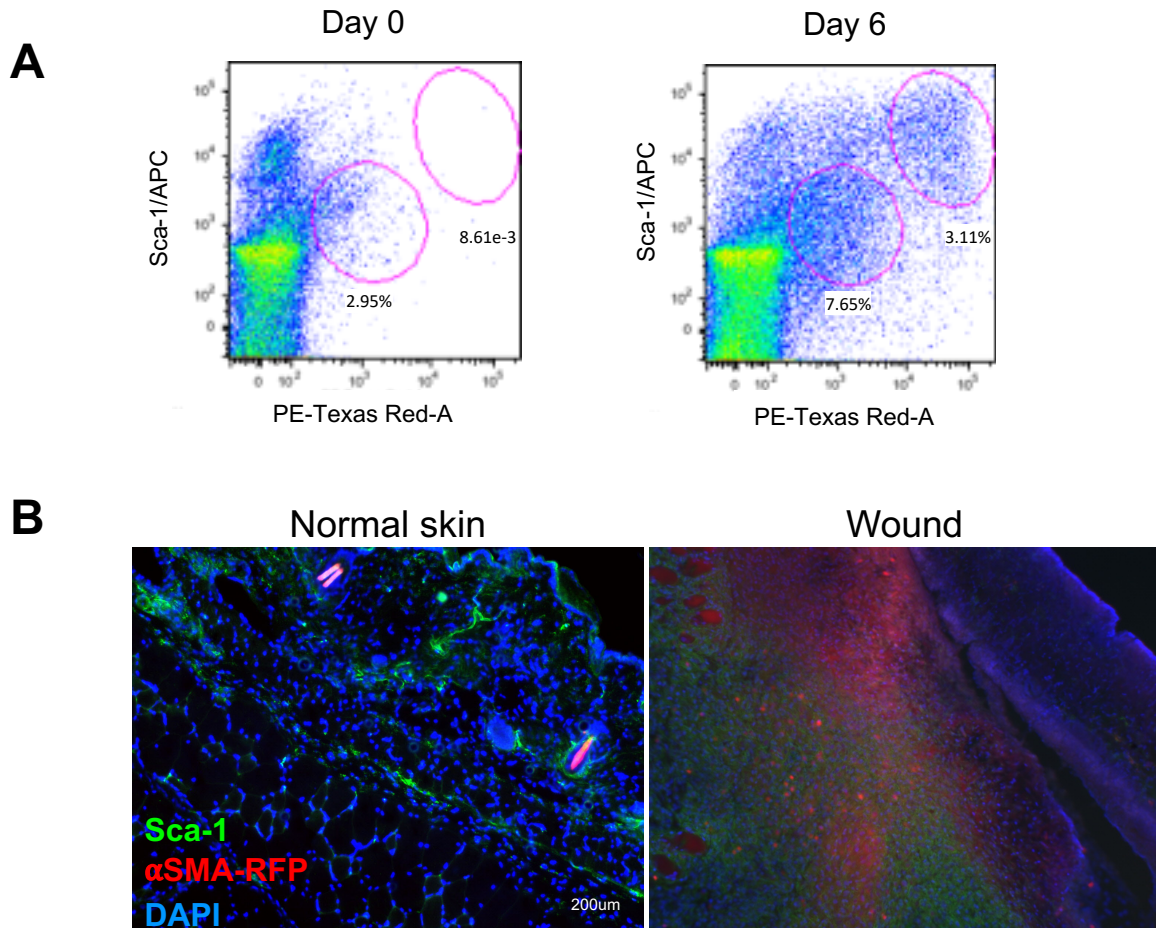


Figure 30. α SMA⁺ cells in the cutaneous wound co-express lower dermal lineage marker Sca1

Normal skin and wound tissue was collected from α SMA-RFP mice at six days post wounding

- (A) Flow cytometry analysis of wounds at day 0 (left) or day 6 (right). Cells were stained with Sca-1 and co-expression with α SMA⁺ cells was evaluated based on gated regions
- (B) Immunofluorescence staining of α SMA-RFP normal skin and day 6 wounds with Sca-1 (green) and DAPI nuclear counterstain (blue)

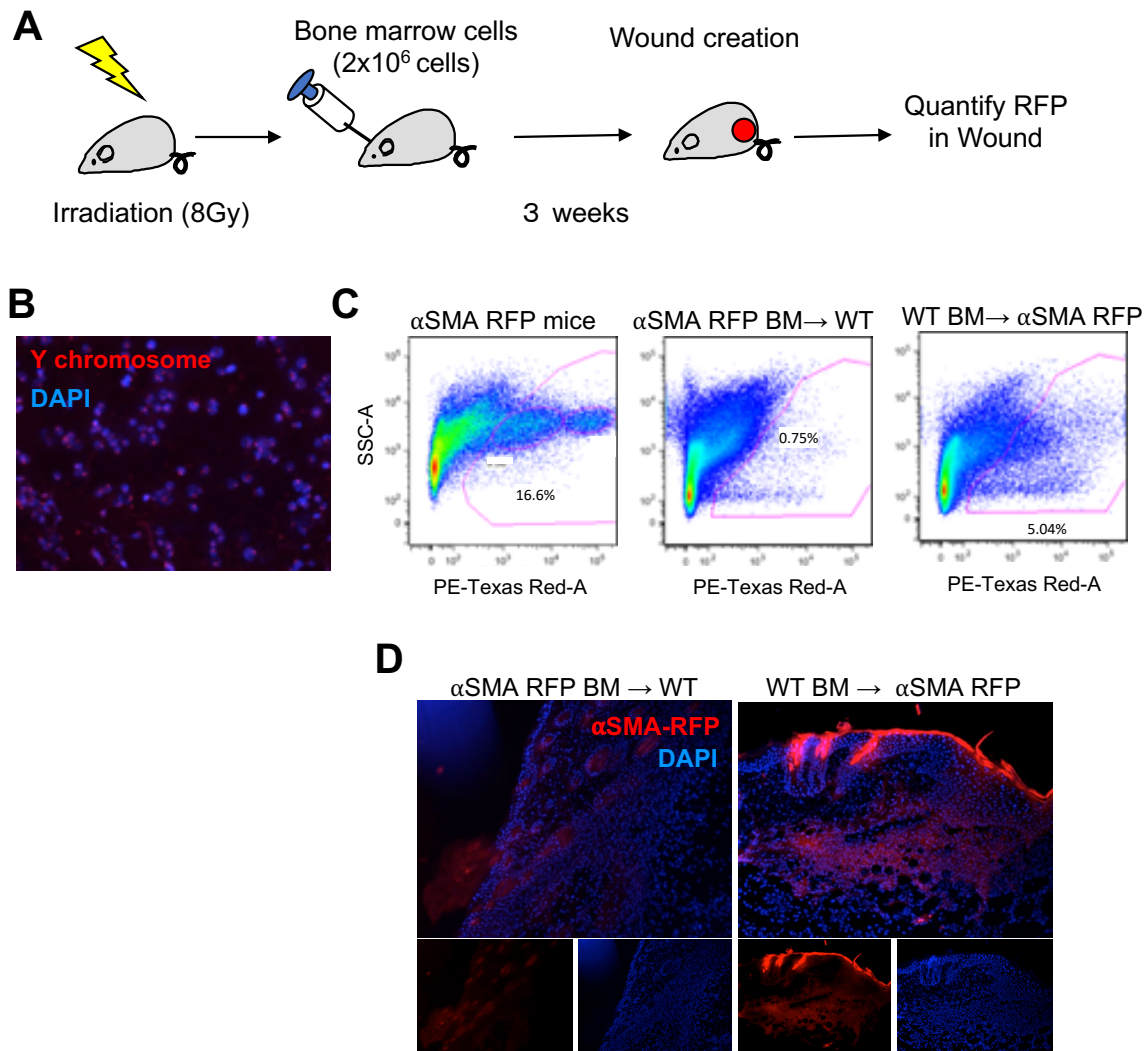


Figure 31. α SMA⁺ fibroblasts accumulating in the cutaneous wound are not recruited from the bone marrow.

Irradiated wild-type mice were transplanted with α SMA-RFP bone marrow (or vice versa) and FTS wounding was performed. Wounds were collected at six days post wounding and abundance of α SMA-RFP cells was measured

- (A) Schematic cartoon of bone marrow transplantation experiments.
 (B) Representative fluorescence in situ hybridization (FISH) for Y-chromosome in bone marrow transplantation of sex mismatched mice
 (C) Flow cytometry for RFP⁺ cells (gated population) in transplanted mice. Wounded α SMA-RFP mice without bone marrow transplantation (left) are provided for comparison
 (D) Assessment of α SMA⁺ fibroblasts (red) with DAPI nuclear counterstain (blue) in day 6 wound tissue from bone marrow transplanted mice

sex-mismatched transplants (**Figure 31B**). Wild type mice were transplanted with 2×10^6 bone marrow cells from α SMA-RFP donor mice, as well as the reverse, followed by wounding. Mice were sacrificed at Day 6 post wounding and wound tissue was evaluated for the presence of bone marrow derived α SMA-RFP⁺ cells. Bone marrow transplantation from α SMA-RFP transgenic donors to wild type recipients demonstrated that 0.75% of cells within a Day 6 wound were derived from the bone marrow (**Figure 31C**). In contrast, α SMA-RFP mice tend to show approximately 16% RFP⁺ cells at the same time-point.

To determine whether these small numbers of bone marrow-derived α SMA-positive cells nonetheless play a crucial role in the repair process, sub-lethally irradiated wild type mice were transplanted with bone marrow from α SMA-TK mice (**Figure 32**). Additionally, the reverse bone marrow transplant was also performed, transplanting α SMA-TK mice with wild-type bone marrow. In order to control for the influence of irradiation on the wound repair process, additional cohorts of WT and α SMA-TK mice were transplanted from matched donors. As in previous experiments, mice were wounded and treated with GCV and wound measurements were performed. Depletion of bone-marrow derived α SMA⁺ cells did not result in any significant change in wound closure rate compared to WT mice transplanted with WT bone marrow with both groups achieving full wound closure by day 16 (**Figure 32B**). In contrast, transplantation of wild-type bone marrow into α SMA-TK recipients did not result in a significant difference in wound closure compared to α SMA-TK mice (**Figure 32B**). These results suggest that resident, rather than bone marrow derived, fibroblasts exist as the primary source of α SMA-positive cells within the wound.

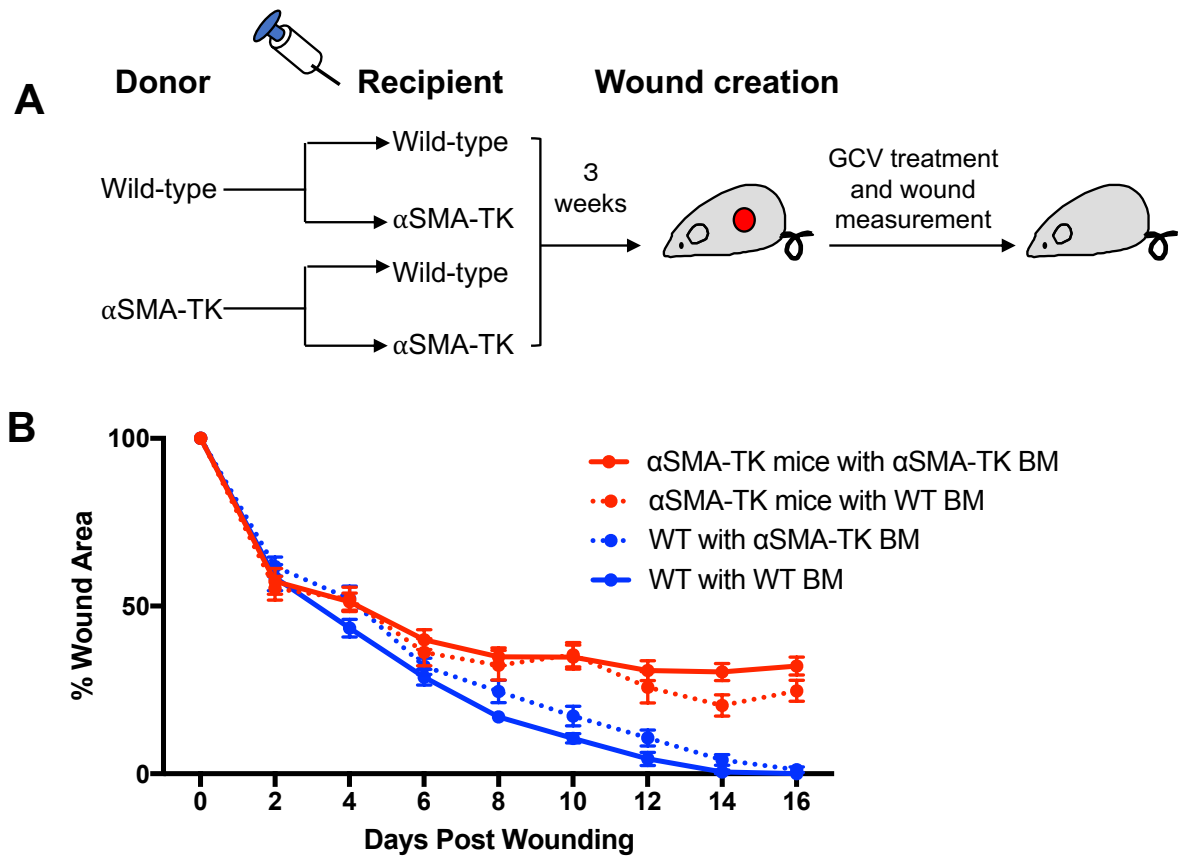


Figure 32. Wild type bone marrow transplantation in α SMA-TK mice did not rescue wound closure

- (A) Schematic diagram of experimental groups. Bone marrow from wild-type or α SMA-TK donors was transplanted into wild-type or α SMA-TK recipient mice. Three weeks after transplantation, wound healing experiments were performed, GCV treatment initiated, and wound measurements performed.
- (B) Wound area measurements in wild-type (blue) or α SMA-TK (red) mice transplanted with wild-type (dashed line) or α SMA-TK (solid line) bone marrow.

4.C. α SMA⁺ fibroblasts impair wound closure independently of Gr1⁺ myeloid inflammation and TGF β RII mediated signaling

TGF β 1 is recognized as a key cytokine in both fibroblast function and wound repair. Levels of TGF β 1 are elevated at all stages of wound healing but typically presents a biphasic pattern peaking transiently during early inflammation and persistently during later phases of the repair process (104). TGF β 's role in influencing wound healing has been considered to be rooted in its function as a promoter of the myofibroblast phenotype (46). In our model, the increase of several TGF β family cytokines and receptors were significantly upregulated at day 6 post-wounding (**Figures 33 and 34**), coinciding with the induction of α SMA expression (**Figure 10A**).

We have previously utilized α SMA-Cre mice harboring a floxed allele of TGF-beta type II receptor gene (Tgfr2^{f/f}) and demonstrated that persistent activation of α SMA⁺ cells by TGF β signaling is required to maintain α SMA⁺ cell populations in a model kidney fibrosis (41). These mice have been shown to be reproductively viable and without obvious developmental defects. In order to evaluate the role of sustained TGF β signaling on the more transient wound healing system, we utilized these mice in our full thickness wound healing model. Despite the importance of TGF β on inducing and maintaining α SMA expression in fibroblasts, we did not observe any change in closure rate between α SMA-Cre⁺ and α SMA-Cre⁻ mice (**Figure 35A**). Evaluation of wound tissue collected at Day 14 post-wounding did not reveal any changes in the quality of the repaired wound (**Figure 35B**) or collagen deposition as measured by Masson's Trichrome Stain (MTS, **Figure 35C**). These results suggest

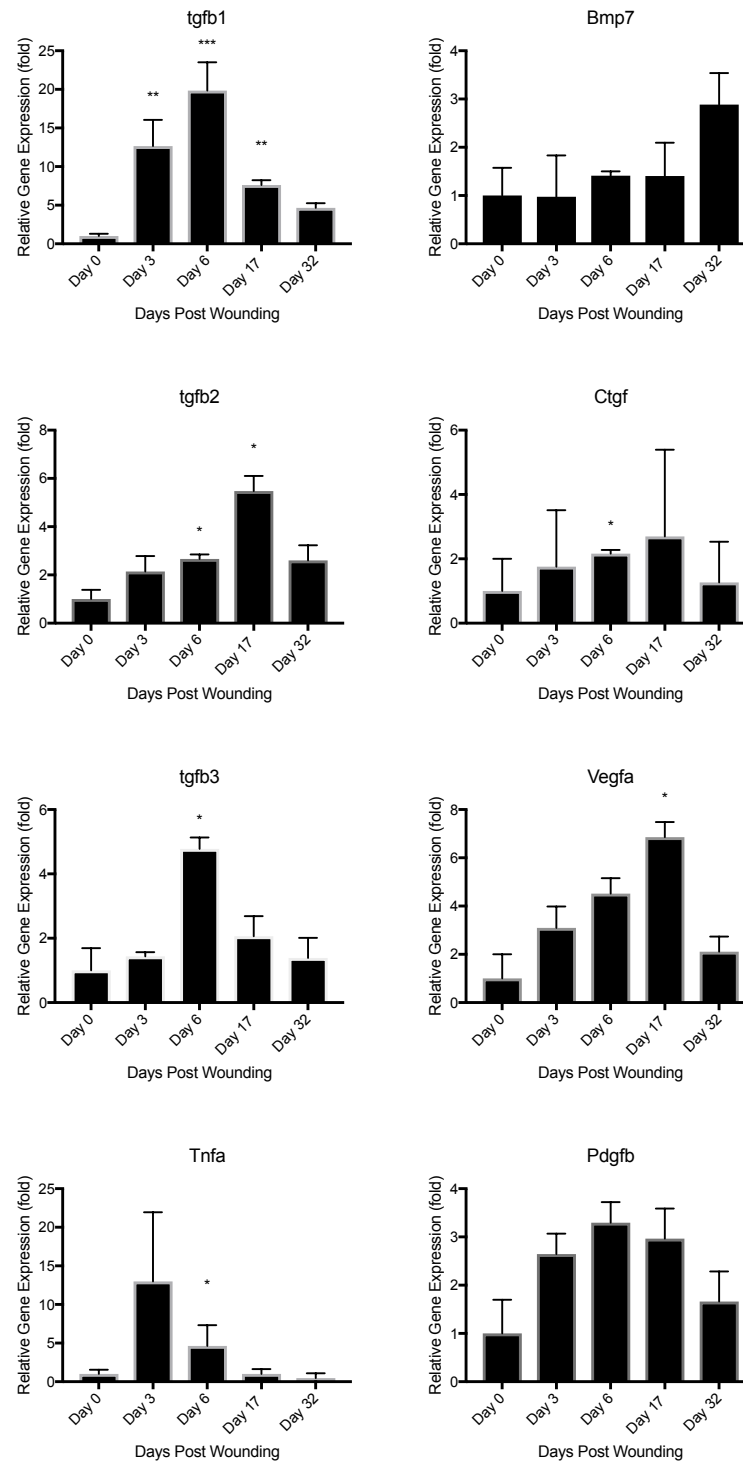


Figure 33. TGF β family cytokine gene expression in the cutaneous wound repair process.
 Dynamics of TGF β family cytokines in normal skin (day 0 post-wounding) and wound tissue from days 3 through 32 post-wounding (n=4 mice per group)

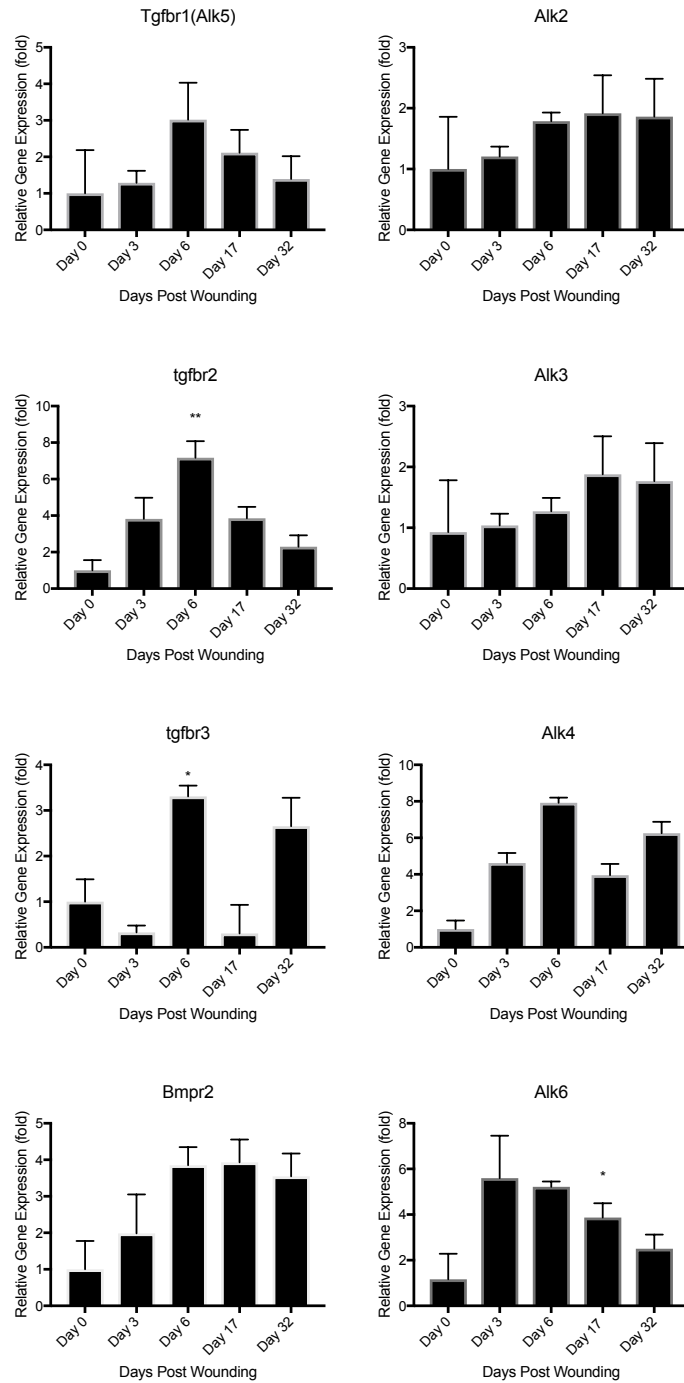


Figure 34. TGFβ family receptor gene expression in the cutaneous wound repair process.
Dynamics of TGFβ family receptor in normal skin (day 0 post-wounding) and wound tissue from days 3 though 32 post-wounding (n=4 mice per group)

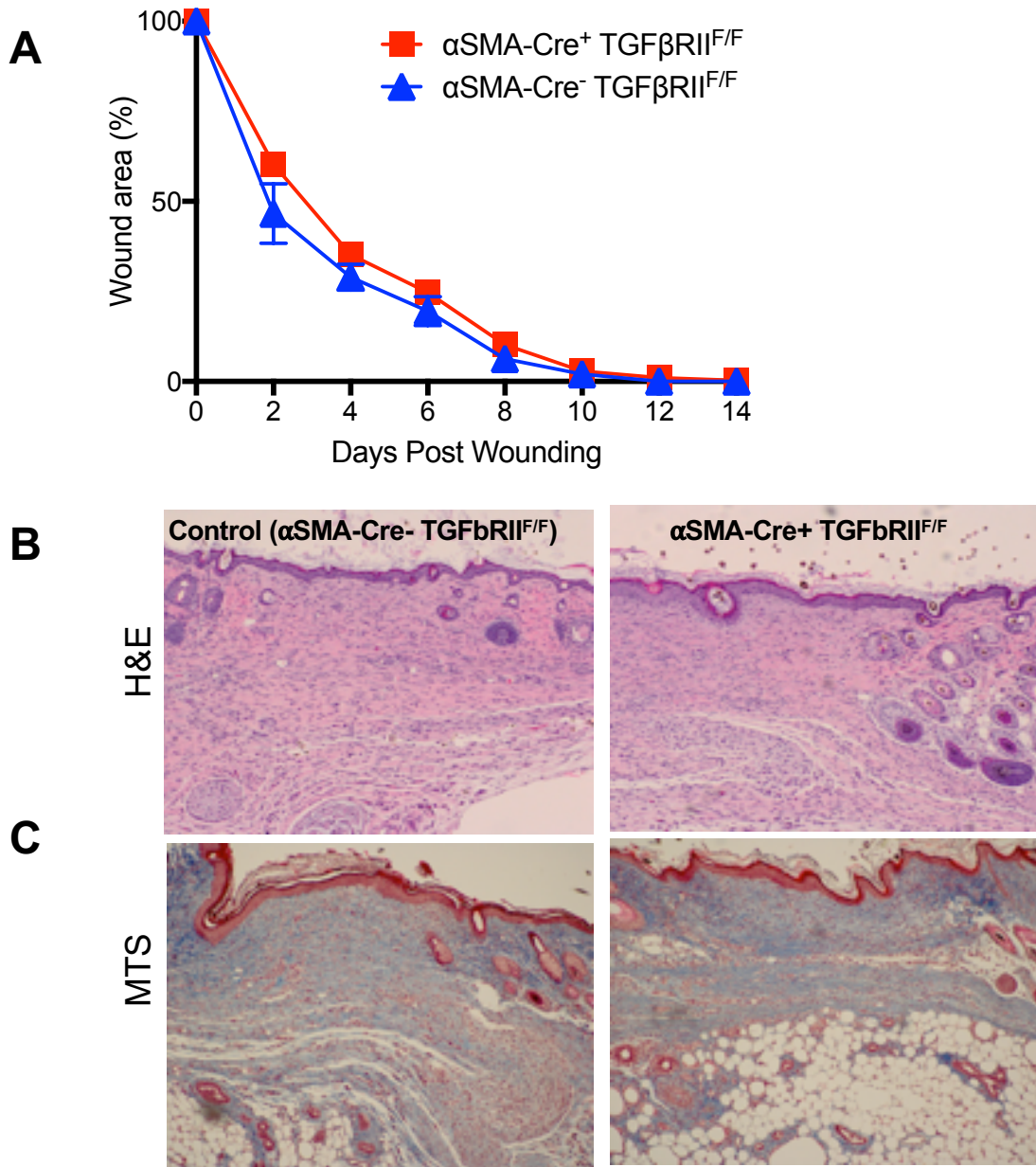


Figure 35. The functional contribution of α SMA⁺ fibroblasts in wound healing do not rely on persistent TGF β signaling

α SMA-Cre⁺ and -Cre⁻ mice were crossed with

- Wound closure rates of α SMA-Cre⁺ TGF β RII^{ff} mice compared to α SMA-Cre⁻ littermate controls, n=8 mice per group
- Representative H&E images of wounds from Cre⁺ and Cre⁻ mice at day 17 post wounding
- Representative MTS images of wounds from Cre⁺ and Cre⁻ mice at day 17 post wounding

that TGF β type II receptor signaling on α SMA⁺ fibroblasts is not required for wound repair.

In order to guide an unbiased determination of the major healing processes altered by the depletion of α SMA⁺ cells, we performed gene-expression profiling of whole wounds from α SMA-TK and WT mice. Because wound closure in α SMA-TK mice diverged from WT at six days post wounding, we compared enriched gene sets at days six and seventeen to identify pathways perturbed by the ablation of these cells (**Figure 36**). A comparison of ablated and non-ablated wounds demonstrated that gene profiles in wounds from α SMA-TK mice 17 days post-wounding clustered more closely with wounds from α SMA-TK or WT day 6 wounds than wild type wounds at day 17 (**Figure 36A**). Three gene clusters in particular were significantly altered in α SMA-TK wounds from both time-points compared to wild type mice at Day 6. As expected based on their inability to re-epithelialize, wounds from α SMA-TK mice showed a significant reduction in genes associated with hair follicle development, epidermis, and pigmentation. However, the other major gene clusters associated with α SMA⁺ cell depletion were associated with inflammation and neutrophil chemotaxis (**Figure 36A**). Additionally, gene set enrichment analysis (GSEA) was performed to identify gene sets commonly up- or down-regulated in Day 6 and Day 17 α SMA-TK wounds in comparison to Day 6 WT wounds. The most notably enriched gene sets common to the two groups were the downregulation in Hedgehog signaling pathway and the WNT signaling pathway. Interestingly, dysregulation of either pathway has been found to result in impaired wound healing and tissue repair (105-107).

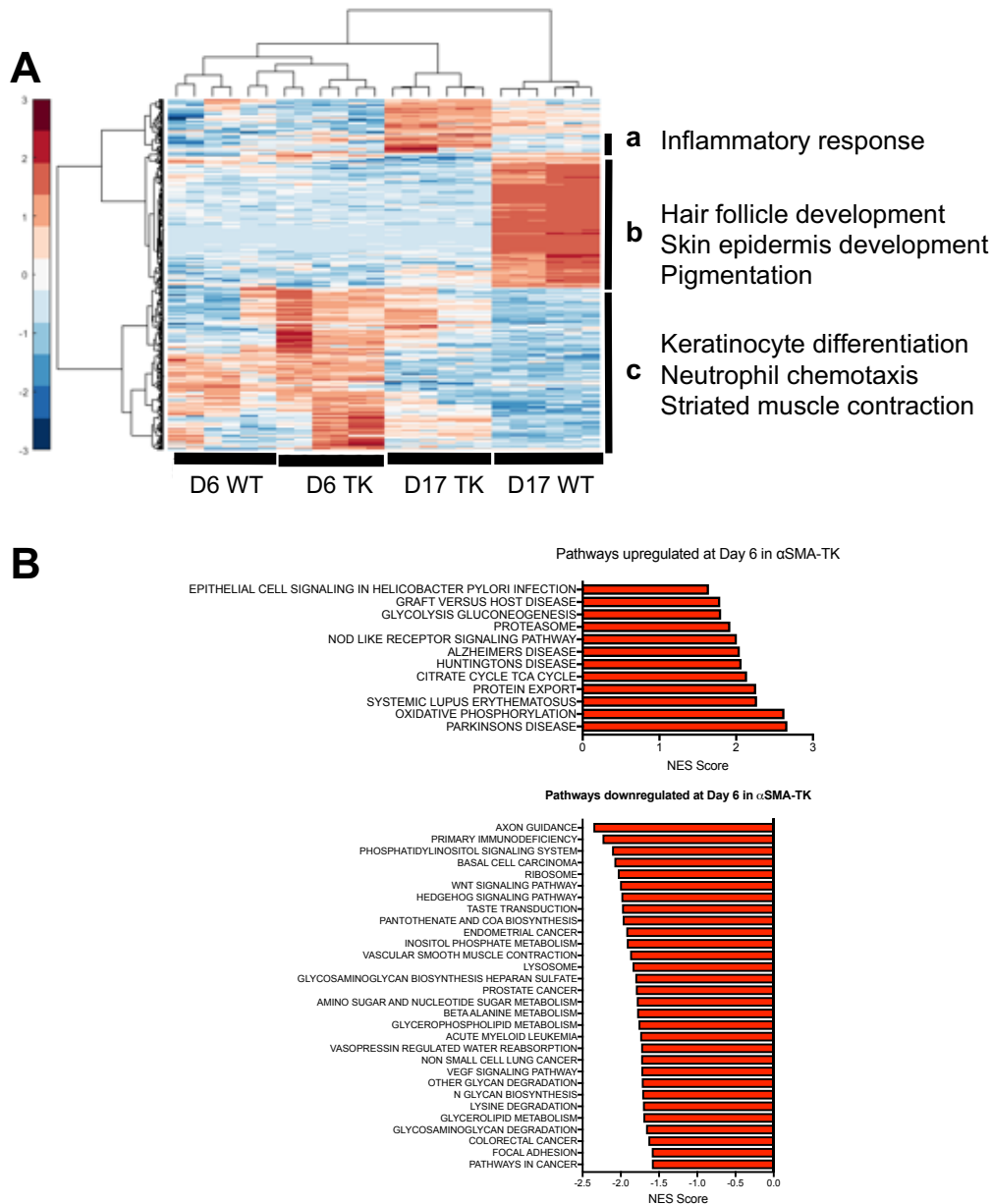


Figure 36. Global gene expression profiling of wound tissue with and without α SMA⁺ fibroblasts depletion

Wound tissue was collected from wounded wild-type (WT) and α SMA-TK mice 6 and 17 days post-wounding for gene expression profiling.

- (A) Heat map rendering and unsupervised clustering of genes differentially expressed between WT and α SMA-TK mice. n=2 mice per group.
- (B) Highly enriched gene pathways in Day 6 α SMA-TK wounds compared to WT controls based on gene set enrichment analysis (GSEA)

Based on our microarray analysis, we hypothesized that the arrest in the healing process observed in α SMA-TK mice was due to an impaired ability of fibroblasts to restrain or reverse the inflammatory stage of repair. Impaired wound repair is often associated with an increased inflammatory profile, arresting the healing process at the late inflammatory stage (108-110). We therefore performed immunotyping via flow cytometry to determine which immune populations were affected by α SMA⁺ cell ablation (**Figure 37A**). Interestingly, CD4 T-cells, CD8 T-cells, Natural Killer (NK) cells, NK T-cells, and macrophage populations were not significantly different in α SMA-TK wounds compared to WT littermates at Day 6 or Day 17 post wounding. In contrast, granulocytes numbers were significantly elevated in Day 17 wounds from α SMA-TK mice (24% of viable cells) compared to both Day 17 WT (0.8% of viable cells) and Day 6 α SMA-TK (4.6%) (**Figure 37A and B**). The increase in GR-1⁺ cells in α SMA-TK wounds was further confirmed by quantitative assessment of immunohistochemistry (**Figure 38**).

Given the preponderance of evidence for a role of neutrophils in the development of chronic wounds (111) and their persistence in fibroblast ablated wounds, we hypothesized that the chronic wound phenotype was a result of a deficiency in the fibroblast population responsible for restraining neutrophil accumulation during the repair process. Therefore, we performed antibody depletion experiments utilizing an anti-Gr-1 antibody on wounded WT and α SMA-TK mice. α SMA-TK and WT mice were wounded and split into two arms, one treated with Gr-1 depleting antibody and the other with IgG control (**Figure 39**). Both groups began treatment with GCV at day of wounding. Depletion of Gr-1⁺ cell populations was

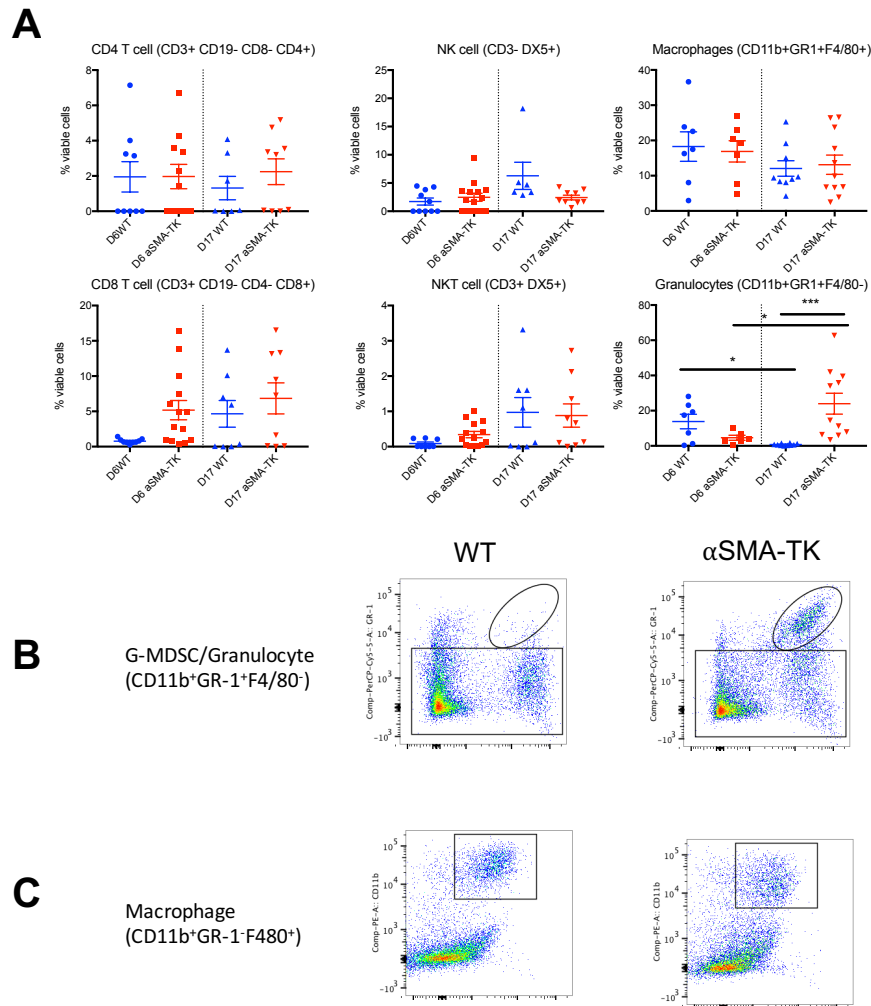


Figure 37. Immunotyping analyses of wounds with and without α SMA⁺ fibroblasts depletion
 α SMA-TK and wild-type control mice were wounded and wound tissue collected at days 6 and 17 post-wounding
 (A) Percentages of CD4 T-cell, NK cell, Granulocyte, CD8 T-cell, NKT cell, and Macrophage cells in the indicated experimental groups (n=7 per group)
 (B) Representative images of FACS analysis for CD11b⁺GR-1⁺F4/80⁻ (granulocyte) cells in wild-type and α SMA-TK mice 17 days post-wounding
 (C) Representative images of FACS analysis for CD11b⁺GR-1⁺F4/80⁺ (macrophage) cells in wild-type and α SMA-TK mice 17 days post-wounding

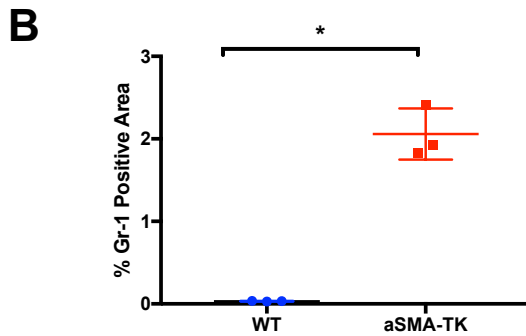
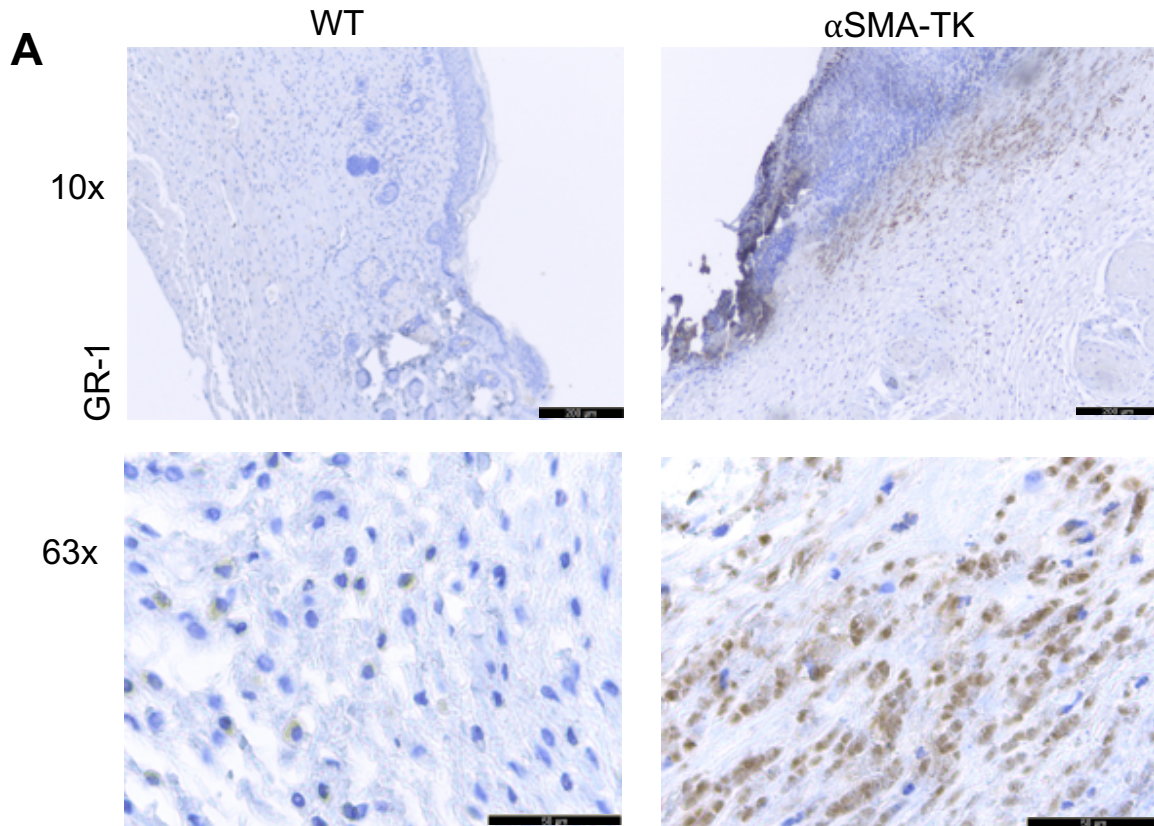


Figure 38. Gr-1⁺ cells are significantly increased in α SMA⁺ fibroblasts-depleted wounds

- (A) Immunohistochemical staining for Gr-1 expressing cells in wounds from wild-type and α SMA-TK mice at day 17 post-wounding
- (B) Quantification of Gr-1 positive stained area in day 17 wounds from WT and α SMA-TK mice

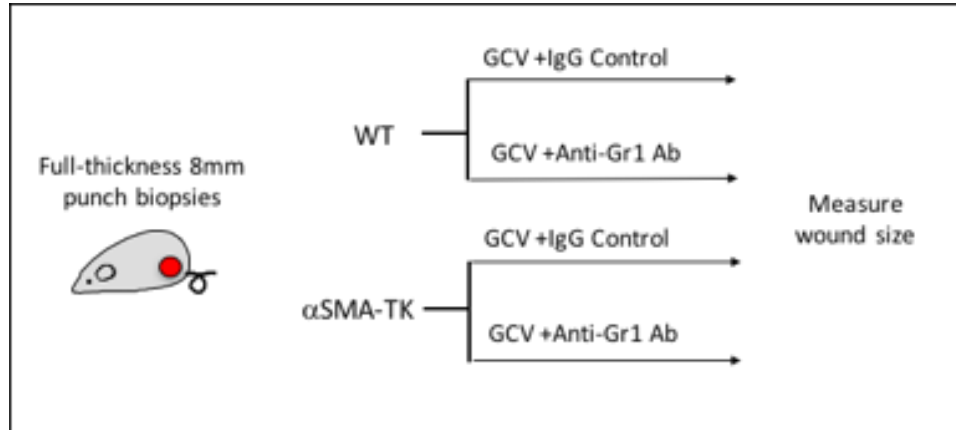
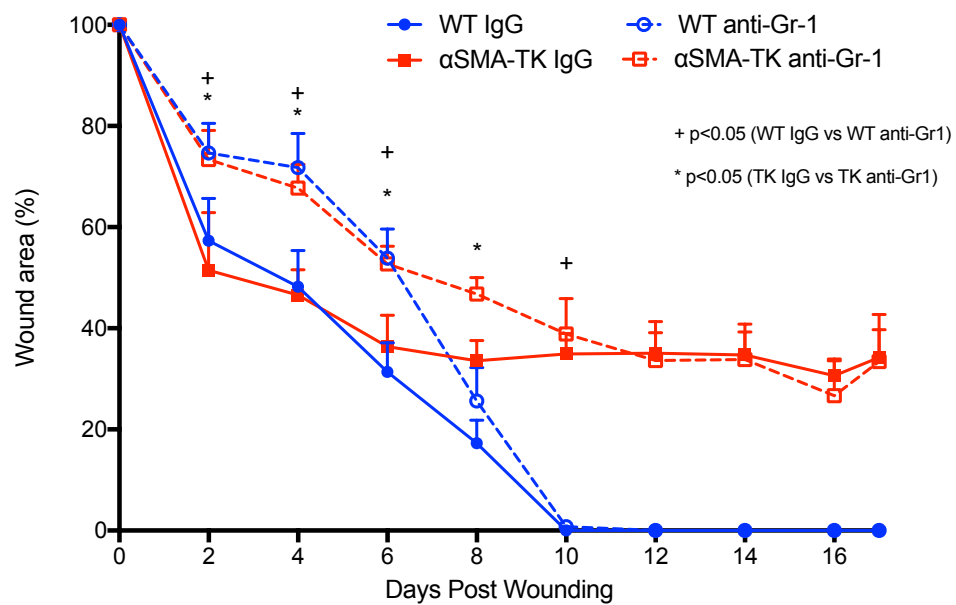
A**B**

Figure 39. Depletion of GR-1⁺ cells did not rescue the impaired wound closure in αSMA⁺ fibroblasts-depleted wounds

- (A) Schematic diagram of experimental arms. Wild-type and αSMA-TK mice were wounded and treated with GCV as described previously. Mice were additionally treated with IgG control or anti-Gr1 antibody to deplete Gr-1⁺ cells
- (B) Wound area measurements in αSMA-TK and WT mice with (dashed lines) or without (solid lines) Gr-1 depletion antibody treatment.

confirmed via immunohistochemistry (**Figure 40**). Contrary to our expectations, depletion of neutrophils did not result in an improvement of α SMA-TK wound kinetics. In fact, from Days 2 to 8 post wounding, neutrophil depleted mice showed significantly less wound closure than IgG controls in both WT and α SMA-TK mice. On day 4 post wounding, IgG treated WT mice had reduced wound size to 48% of initial wound area, while aGr1 treated WT mice remained at 67% (**Figure 39B**). However, by ten days post wounding the two treatment groups converged. These results would suggest that the accumulation of neutrophils is a consequence, rather than cause, of the impaired wound healing phenotype observed in α SMA-tk mice.

One gene which stood out in particular as part of our microarray analysis was apparent increase IL-6 in α SMA-TK wounds compared to controls. Previous studies had indicated that loss of IL6 impairs the wound repair process through delayed wound closure and re-epithelialization, as well as a blunted induction of α SMA following wounding (112, 113). We first performed rtPCR to confirm the induction of *Il6* gene expression in α SMA-TK wounds (**Figure 41A**) at days 3 and 6 post-wounding. On day 3 post wounding IL-6 was increased in wounds from both WT (3.3-fold change) and α SMA-TK (7.7-fold change) mice compared to normal, unwounded skin. On Day 6, the levels of *Il6* in α SMA-TK mice increased 20-fold higher than normal skin, in comparison to only a 6-fold induction in WT mice (**Figure 41A**). IL-6 knockout mice showed impaired, but not halted, wound healing rates (**Figure 41B**). In IL-6 KO mice, wound closure rate was reduced at day 4 post-wounding, with WT mice reducing wound sizes to 45% of initial area while IL-6 KO remained at 62%. Wounds in IL-6 KO mice did not full close until 22 days post-wounding, in contrast to 14 days in WT mice.

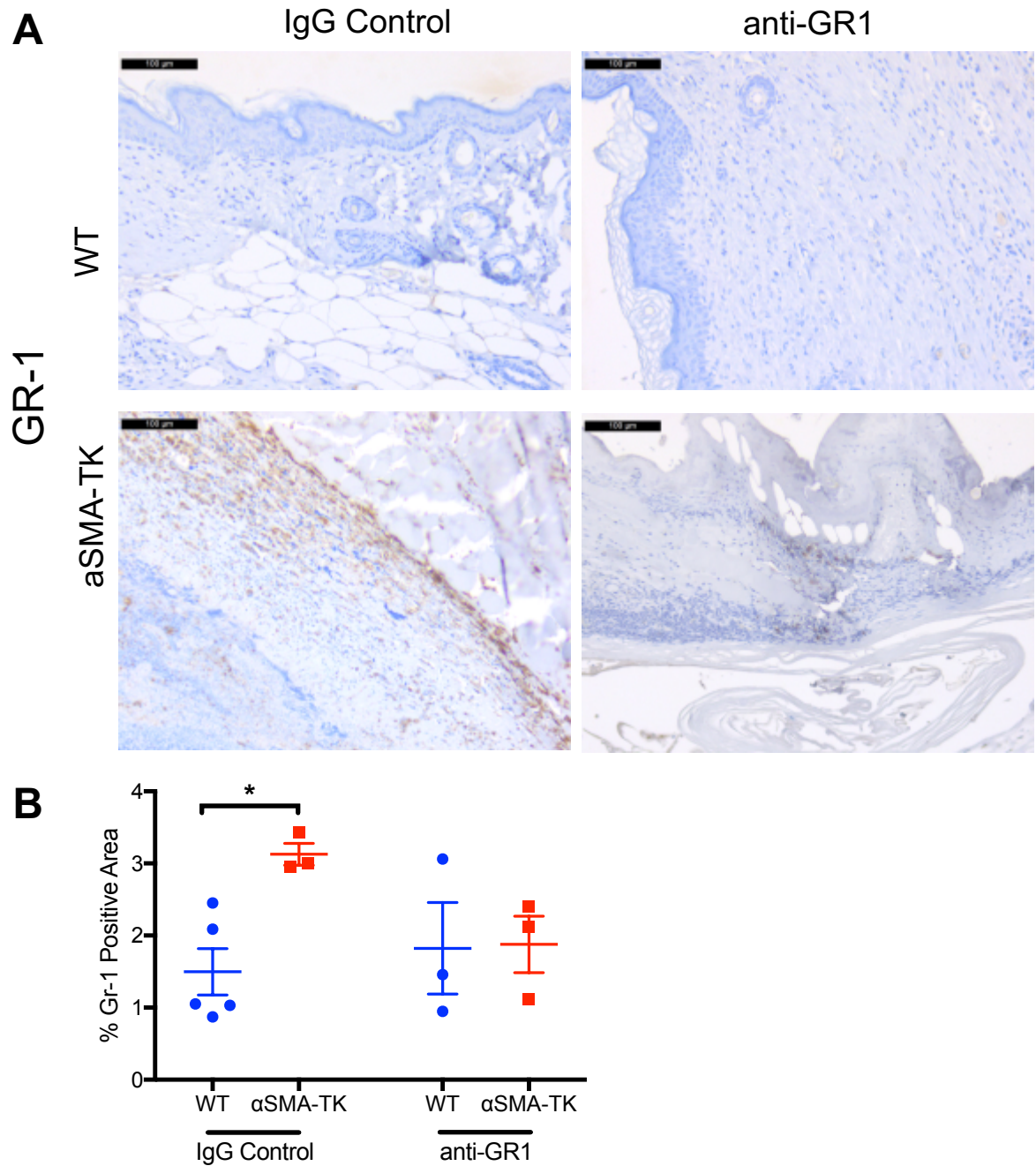


Figure 40. Confirmation of successful depletion of GR-1⁺ cells using anti-GR-1 antibody

- (A) Representative images of immunolabeling for Gr-1 in wound tissue from WT and α SMA-TK mice with or without Gr-1 depletion
- (B) Quantification of the positively stained area for Gr-1 per visual field

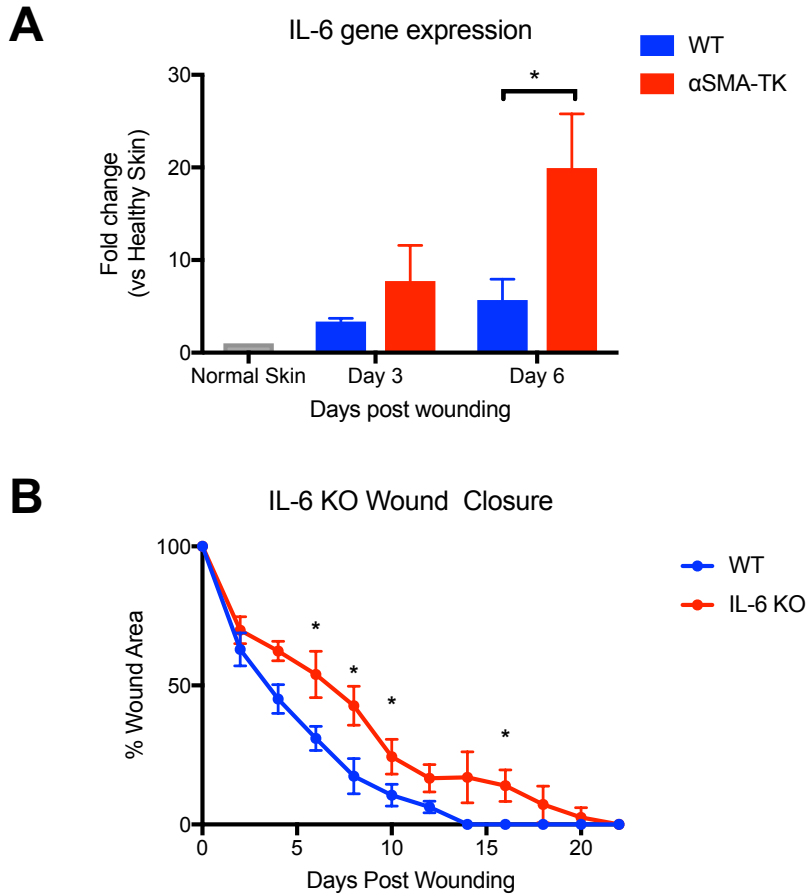


Figure 41. IL-6 production is critical for wound healing and is elevated as compensatory mechanism in α SMA⁺ fibroblasts-depleted wounds

- (A) Gene expression of IL-6 in intact (normal) skin and wound tissue from WT and α SMA-TK mice at days 3 and 6 following FTS wounding, n=5 mice per group.
- (B) Wound closure rates of IL-6 KO mice compared to wild-type controls, n=5 mice per group

These results indicate that IL-6 production is critical for wound healing and is elevated as compensatory mechanism when α SMA⁺ fibroblasts are depleted. These findings offer new insights of the regulatory elements under the control of α SMA⁺ fibroblasts in cutaneous wound healing.

Chapter 5. Materials and Methods

5.A. Mice and dermal wound healing

α SMA-TK mice, α SMA-RFP, FSP-TK, α SMA-Cre and TGF β R2-floxed mice have been described previously (41, 100). FAP-TK and Col1a1-TK transgenic mice were generated in our laboratory by Dr. Toru Miyake. All mice utilized for these experiments were 8 to 12-weeks old. All procedures were performed according to the guidelines for BIMDC and MD Anderson.

The full thickness wounding model has been previously described (57, 114). Briefly, two full-thickness wounds were created by a sterile biopsy punch with a diameter of 8 mm on the shaved bilateral flank of mice. In experiments utilizing the HSV-TK transgene system, GCV was administered daily at 50mg/kg bodyweight starting from the day of wound creation until the end of experiment unless otherwise noted. Wounds were left open and measured by caliper at the indicated time points. The wound areas (percentage of wound areas to initial) were calculated from the formula length x width x 0.7568. Skin with the wound was removed for further experiments.

For bone marrow transfer experiments, bone marrow was harvested from the tibia and femur of WT, α SMA-tk and α SMA-RFP donor mice. A single cell suspension was performed. Recipient Balb/c mice were irradiated with 800cGy Co60 source. Approximately 5×10^5 cells in PBS were injected into different sex mice via retro-orbital vein. 3 weeks after transplantation, wound healing experiments were performed. Degree of chimerism were assessed by FISH for the Y-chromosome as

previously described (41).

5.B. Fibroblasts culture

Ex vivo culture and GCV treatment of ear fibroblasts was carried out as previously described (41, 95). Briefly, ears were collected from WT and TK⁺ mice and digested using collagenase for 24 hours. Cells were then expanded in culture for no more than two weeks before being seeded to 96 well plates at 1×10^4 cells per well and treated with GCV at concentrations of 0, 5, and 50uM. After a treatment period of three days, cell viability was measured using trypan blue exclusion.

5.C. Immunolabeling and antibodies

For tissues for immunohistochemistry staining, harvested tissues were fixed in 10% formalin and embedded in paraffin. 5um sections were rehydrated and antigen retrieval was performed using 10mM citrate buffer (pH 6.0) for 15min to 1 hour. After 1 hour blocking with blocking buffer, sections were incubated with primary antibody overnight at 4°C. Following incubation with secondary antibody for 1 hour at room temperature and ABC reagent (Vector Laboratory, West Grove, PA). The sections were developed by DAB staining.

For frozen tissue sections, 8µm sections from OCT embedded tissues were fixed with 4% PFA for 20 min and incubated with 0.3% triton-X for 30 min. after blocking with blocking buffer, sections were incubated with primary antibody overnight at 4°C. This was followed by incubation with secondary antibody for 1 hour at room temperature and stained with DAPI or DRAQ5 for 30 min. Unless otherwise noted, all

analysis of positive cell number or signal intensity was limited to the wound granulation tissue. Number of positive cells identified by immunohistochemistry was quantified using the Adobe Photoshop count tool. Mean positive area was quantified using ImageJ.

Antibodies used in this study: α SMA (Dako, M0851), FSP1/S100A4 (Dako, A5114), Collagen 1 (Southern Biotech, 1310-01), DDR2 (Santa Cruz, sc-7555), FAP (Abcam, ab53066), Vimentin (Cell Signaling Technologies 5741S), Ki67 (Thermo Fisher, TM-9106-S), CD31 (Dianova, DIA310), and Sca-1 (BD Pharmingen, 557403).

5.E. Gene expression analyses

RNA was isolated from snap frozen tissue and extracted using Trizol. cDNA was synthesized using High-Capacity cDNA Reverse Transcription Kit. Real-time quantitative PCR was carried using SYBR Green Real-Time PCR Master Mixes on QuantStudio™ 7 Flex Real-Time PCR System from ThermoFisher.

5.F. *in situ* hybridization

In situ hybridization (ISH) was performed on frozen wound tissue sections using standard methods (96). Briefly, 8 μ m sections from OCT embedded tissues were post-fixed with 4% PFA, acetylated with 1% triethanolamine and 0.25% acetic anhydride, pre-hybridized, then hybridized with *Col1a1* probe overnight at 60°C. Following hybridization sections were incubated with anti-DIG antibody (1:3000, Roche) for 90 minutes. After washes, sections were incubated with BM Purple (Roche) and counterstained with Nuclear Fast Red.

5.G. Atomic Force Microscopy

Atomic Force Microscopy was conducted at the UT-Health Science Center AFM Core Facility using a BioScope IITM Controller (Bruker Corporation; Santa Barbara, CA). The image acquisition was performed with the Research NanoScope software version 7.30 and analyzed with the NanoScope Analysis software version 1.40 (copyright 2013 Bruker Corporation). This system was integrated to a Nikon TE2000-E inverted optical microscope (Nikon Instruments Inc.; Lewisville, TX) to facilitate bright field imaging of the tissue sections.

To investigate the nano-mechanical properties of the tissue surface, skin wound samples were obtained from α SMA-TK and wild type mice. Tissue cryosections of 40 μm in thickness were attached to glass microscope slides pretreated over night with poly-L-lysine (0.1% (W/V) Sigma P8920) at room temperature to enhance tissue attachment. The Elastic (Young's) Modulus was measured on hydrated tissue sections using DNP-S triangular cantilevers ($f_0=12\text{-}24$ kHz, $k=0.06$ N/m, ROC=10nm) purchased from Bruker Corporation (Santa Barbara, CA). Wound areas of the tissue sections were selected with the aid of optical microscopy. Force Volume images were captured on 50 μm^2 scan areas with 16 x 16 force measurements per line. Force curves were probed using a ramp size of 2 μm and a scan rate of 1.0 Hz, with a force load of 15 nN. The probe spring constant was determined prior to each experiment using thermal tuning. The Elastic modulus was calculated by fitting to a standard Sneddon model for a conical indenter and a Poisson's ratio of 0.5. At least, 3 areas were analyzed for every tissue sample in the skin wound. A minimum of 256 force measurements were captured for each area.

AFM topographical imaging was performed on dry tissue sections using RTESP cantilevers ($f_0=237-289$ kHz, $k=20-80$ N/m, Bruker Corporation, Santa Barbara, CA). The structure of the tissue was determined using tapping mode operated in air to a scan rate of 0.7 Hz. Images of the fibroblasts deposition were captured to a scan range of 10, 5, and $2.5 \mu\text{m}^2$.

5.O. Immunohistochemical multiplex

The process for multiplexed staining and imaging has been previously described (89). Briefly, $5\mu\text{m}$ sections of paraffin embedded tissue were deparaffinized and subjected to antigen retrieval with heated Citric Acid Buffer (pH 6.0) for 15 min (EZ Retriever microwave, BioGenex). Each section was put through sequential rounds of staining, each including a protein block with 1% BSA, primary antibody, secondary horseradish peroxidase-conjugated polymer, and a different fluorophore using tyramide signal amplification. This was followed by additional antigen retrieval in heated Citric Acid Buffer (pH 6.0) for 15 min to remove bound antibodies before the next step in the sequence. Sections were then counterstained with DAPI and mounted with Fluoroshield histology mounting medium (Sigma-Aldrich, St. Louis, MO). Stained slides were imaged using the Vectra Multispectral Imaging System version 3 (Perkin Elmer) at 200x magnification. A spectral library was then used (spectral unmixing) allowing for the colour-based identification of all six markers of interest in a single image using the inForm 2.3 image analysis software.

5.G. Multispectral imaging analyses

To quantitatively analyze changes in cell populations during wound healing,

we utilized a proprietary active learning algorithm provided by the Perkin Elmer Inform image analysis software package. This system was used to perform cell and tissue segmentation on acquired images. Tissue segmentation allows the definition of tissue compartments based on trainable features. Further, cell segmentation allowed us to identify marker-assigned fluorescent signal and coordinates for each individual cell. A threshold value of signal intensity to define marker positivity was experimentally determined for each marker investigated.

In order to perform quantitative analysis of the entire wound bed, cells and/or images acquired were merged. Cells and mosaic images were plotted on an XY coordinate plane based on identified coordinates during cell segmentation. Wound edge coordinates were defined based on morphological features (thickened epidermis, loss of hair follicles, accumulation of cells expressing myofibroblast markers). Cells in non-dermal regions or those outside the region defined by the two edges were not analyzed. Utilizing the R Statistical Computing platform, each cell within this region was defined as positive or negative based on fluorophore signal intensity above the thresholds defined above. A truth table containing the relative proportion for each identified phenotype was compiled using the R QCA package (CRAN).

The coordinates between these two experimentally defined wound edges was averaged to identify a wound center. Distance of each cell within the dermal layer of the wound bed from the closest wound edge was determined by calculating the length of a perpendicular line representing the shortest distance between the cell and wound edge line.

5.H. Statistical analyses

All statistical analyses were performed using the GraphPad Prism software unless stated otherwise. Statistical analyses of immunohistochemical quantifications were performed using a Student's t-test, Mann-Whitney test or analysis of variance as appropriate. Data are represented as the mean \pm SEM. * $p < 0.05$, ** $p < 0.01$, **** $p < 0.0001$. ns, not significant.

5.Q. Microarray analysis

For microarray analyses, total wound RNA (500 ng) was used for labeling and hybridization according to the manufacturer's protocols (Illumina, Inc, San Diego, CA) using the Illumina MouseWG-6 v2.0 expression BeadChips. The BeadChips were scanned with Illumina BeadArray Reader (Illumina, Inc). The results of microarray data were extracted with Bead Studio 3.7 (Illumina, Inc.) with background subtraction. Gene expression data were normalized using quantile normalization method in LIMMA package in R. The expression level of each gene was transformed into log₂ before further analysis. To avoid potential false-positive genes because of technical variance, all experiments were carried out in quadruplicate.

Chapter 6. Discussion

Fibroblasts in the dermis are mesenchymal cells chiefly considered to function in the maintenance of skin through to production of ECM. However, fibroblasts are now postulated to orchestrate tissue repair by interacting with and controlling other cell types, including immune cells, in the wound microenvironment. It has become increasingly clear that the generic term “fibroblast” encompasses a diverse cell population with distinct origins and heterogeneous functions. Fibroblast heterogeneity is in part exemplified by the numerous expression markers used to distinguish them. Both between and within anatomical locations, fibroblasts have been shown to present distinct marker phenotypes and gene expression profiles (51, 94, 115-117). However, the diversity of dermal fibroblasts and their dynamic contribution to the process of wound healing remain poorly understood. The overarching goal of this study was to define the heterogeneity of dermal fibroblasts and unravel their functional roles during cutaneous wound healing process.

Despite the numerous markers utilized to identify fibroblasts, few studies have worked to characterize the fibroblast composition identified using these markers. As fibroblasts, especially in repairing tissue, are not amenable to flow cytometry or *ex vivo* culture without introducing a selective pressure (118), research has relied on the laborious use of histological examination of serial tissue sections (51, 57). In this study, we have made use of Tyramine Signal Amplification (TSA)-based immunolabeling and multispectral imaging in order to evaluate the abundance and distribution of three commonly utilized fibroblast markers during wound repair. This technique offered several benefits over previous techniques: (A) By performing

multiplexed labeling on a single section, we avoided the loss of cells and morphological features which can occur even with serial sectioning. (B) Histological studies have often been limited by the potential bias introduced by examining cells only within a representative region of the tissue. In the work presented here, evaluation of fibroblast heterogeneity was carried out throughout the entirety of the repairing dermis. (C) Using computational tissue segmentation, we were able to limit our study to evaluation of the repairing dermis without the influence of putative fibroblast marker expression in non-fibroblast populations. We made use of these computational tissue and cell segmentation techniques in order to provide a more complete picture of acquisition of fibroblast markers during repair. The use of computational algorithms not only provides an unbiased quantification method, but also one that can readily scale up to the tens of thousands of individual cells within a single tissue, or millions of cells within an experimental cohort. Using this system, we were able to systematically probe the abundance and distribution of fibroblasts within the repairing dermis to a higher degree than was previously possible.

Interestingly, this approach unraveled a significant progression of marker expression, from FSP-1⁺ fibroblasts found dominantly in the intact skin, to principally α SMA⁺ fibroblasts by Day 6 following wounding, followed by an increase in Vimentin⁺ cells during the final stages of wound re-epithelialization and maturation. The changes in fibroblast marker composition we observed during wound repair did not appear to be exclusively due to proliferation of existing populations. Instead, when co-localization of multiple markers was taken into account, it suggested that the observed changes in fibroblast markers rather represent an evolution in the marker expression

of fibroblasts. Of particular note was the expansion in the FSP-1/S100A4 and α SMA double positive population observed at day 6 post-wounding, leading us to hypothesize that α SMA⁺ fibroblasts arise from FSP1/S100A4⁺ progenitors. Using FSP-Cre reporter mice, we found that at this time-point 35% of α SMA⁺ fibroblasts had at some point expressed FSP-1/S100A4. Although FSP-1/S100A4 was originally considered a pan-fibroblast marker (54), more recent work has suggested that FSP-1/S100A4 may identify a distinct population from α SMA⁺ fibroblasts in some models (51, 119-121). In 2006, Sugimoto et al. investigated the co-localization of α SMA and FSP-1/S100A4 expression in the 4T1 model of breast cancer and the Rip1-Tag2 model of pancreatic cancer. In the 4T1 model only 10.9% of α SMA⁺ cells also expressed FSP-1/S100A4. In contrast, 43.5% of α SMA⁺ cells in the Rip1-Tag2 model co-expressed FSP-1/S100A4. In a study using a murine lung fibrosis model, it was found that although FSP-1/S100A4 had no overlap with α SMA expressing cells, they did sometimes co-localize with Vimentin and CD45 (119). Together, these results suggest that a portion of α SMA⁺ fibroblasts, but not all, arise from FSP-1/S100A4 positive cells.

The markers used to identify fibroblasts in this study do not cover the entirety of proposed markers in the literature, particularly given their heterogeneous origins. New techniques employing imaging mass cytometry allow examination of over 100 markers in a single slide (122, 123). Combining these new imaging technologies with the analysis method developed as part of the presented study will not only allow even more comprehensive analysis of fibroblast evolution during tissue repair as well as exclusion of non-fibroblast populations that have acquired fibroblast phenotypes.

In our work, we controlled for the expression of mesenchymal markers in endothelial cells by removing all CD31⁺ cells from our analysis of fibroblast heterogeneity. However, immune cells, in particular macrophages, have been found to express putative fibroblast markers such as FSP-1/S100A4 and FAP (124-126). Expanding the number of markers evaluated to include populations such as immune cells, hair follicle stem cells, and epithelial cells will further allow us to probe the association between fibroblasts and these different cell types (89).

The importance of analyzing the dermis apart from other parts of the skin is highlighted by findings demonstrating the expression of commonly regarded fibroblast markers by other cell populations. Within the epidermis, there is existing evidence that during wound repair keratinocytes may acquire expression of FSP-1/S100A4 and Vimentin, presumably through TGF β induced EMT signaling (127). Our own histological examination and lineage-tracing of FSP-1/S100A4⁺ cells agrees with this. Further, lineage tracing experiments have suggested that subdermal pre-adipocytes may contribute to the pool of α SMA⁺ fibroblasts during wound repair (63), and that conversely myofibroblasts may differentiate into adipocytes following wounding (128). In the latter study, the conversion of myofibroblasts into adipocytes relied on BMP signaling by regenerated hair follicles. Although we did not observe a loss of adipose tissue in our α SMA-TK experiments, this is reasonable given the wounds inability to re-epithelialize. Additionally, hair follicle regeneration in murine models has only been described following repair of very large wounds (1.5-2cm²), roughly three to six times the surface area of the wounds generated in our experiments (129).

The question remained whether identification of fibroblasts by marker composition is reflective of their biological role in normal and disease states. This is a question explored not only in the realm of wound repair, where the division between papillary and reticular fibroblasts has been heavily studied, but also studies investigating fibrosis (41) or the tumor microenvironment (94, 95). Many studies attempting to characterize the functional role of fibroblast subpopulations on wound healing have relied on *in vitro* expansion and measurement of cytokine or gene expression measurements from cultured cells. These studies are necessarily limited by ignoring the complex interactions between fibroblast cells with other cells of the wound microenvironment (immune, epidermal, adipose, etc) as well as the potential for alterations in gene expression resulting from *in vitro* culture. To address the functional contribution of fibroblast populations on wound healing, we targeted fibroblasts using mice expressing viral thymidine kinase (HSV-TK) under fibroblast-specific promoters. In contrast to diphtheria toxin receptor-mediated targeted ablation (130), this model allows the selective depletion of proliferating fibroblasts as found in the repairing wound. Due to the ubiquity of fibroblasts throughout the body, targeting only proliferating cells is likely to result in fewer unintended side-effects. In the work presented here, utilization of the HSV-TK model targeting four specific markers (α SMA-TK, FSP1-TK, FAP-TK, Col1a1-TK) presented four distinct phenotypes.

Depletion of α SMA⁺ fibroblasts during the wound closure process resulted in a complete inability for wounds to re-epithelialize by six days post wounding, producing wounds with significantly lower collagen and re-vascularization than wild-type controls. α SMA⁺ cells were depleted to a comparable degree as what our

laboratory has previously observed in the unilateral ureteral obstruction (UUO) renal interstitial fibrosis model (41). Also, in contrast to the studies in renal fibrosis models, few of the α SMA⁺ fibroblasts within the wound were derived from the bone marrow, in comparison to 35% in the UUO model. Most interestingly, genetic deletion of TGF β receptor 2 in α SMA expressing cells did not result in an observable phenotype with respect to wound closure or collagen deposition. In contrast, studies deleting the TGFBR2 gene locus in Collagen1a2 expressing cells resulted in faster re-epithelialization and reduced collagen deposition (131, 132). TGF β is known to be a potent inducer of α SMA and collagen, and this has led research into modulation of TGF β as potential method to reduce scarring (71, 87, 133-135). It is possible that while TGF β is necessary for the initial activation of the myofibroblast phenotype, it is not required for the maintenance of that state in the timeframe of our studies. Future studies investigating the role of TGF β signaling on wound healing fibroblasts may benefit from the use of a population which exists before stimulation with TGF β . Although FSP-1/S100A4 would be an attractive option given our described results in Chapter 2, interpretation of results would require the caveat that FSP-1/S100A4 was also found to be expressed in the epidermis.

In contrast, targeted depletion of FSP-1/S100A4⁺ cells using the FSP1-TK mouse model resulted in a statistically significant but less pronounced depletion of the targeted cell population. These FSP1-TK mice showed no phenotypic difference compared to wild-type controls with regards to wound closure rates or histological assessments. In comparison, depletion using these mice in the UUO setting resulted in a 75% decrease in FSP-1/S100A4⁺ cells with a resulting significant decrease in

both fibrotic area and collagen deposition within the fibrotic kidney (100). These results are counterintuitive given our finding that FSP-1/S100A4⁺ cells in wounds displayed a higher proliferation rate than α SMA⁺ cells at all time-points examined. These data suggest that fibroblasts identified by FSP-1/S100A4 may either rapidly transition to α SMA⁺ myofibroblasts during early phases of healing, or represent a transition of fibroblasts expressing other markers to FSP-1/S100A4⁺ following re-epithelialization. Targeted depletion of FAP⁺ or Collagen1 producing cells resulted in a significant decrease in the targeted cell population but did not impair wound closure to the degree identified in α SMA-TK mice. Despite a significantly decreased wound closure rate, FAP-TK mice demonstrated an increased collagen within their granulation tissue. Although not evaluated in this study, previous work in fibrosis models have implicated FAP mediated signaling in collagen degradative pathways (136, 137). Depletion of Collagen1 producing cells resulted in a significant increase in vascularization, measured by CD31⁺ cell number, as well as an increased hypoxic area compared to control mice. These results appear at first contradictory, but it is possible that Collagen1a1⁺ cells are responsible in part for the maturation of the vasculature during wound repair, as has been suggested in the case of bone marrow derived MSCs (138). One potential weakness in the use of the thymidine kinase cell depletion model is that only proliferating cells are targeted. Despite the significant depletion quantified in our studies a portion of each population remained, and a direct link between expression of a fibroblast population and its function within the repairing dermis is thus hampered by our inability to fully deplete specific populations at arbitrary time-points. Although some studies have attempted to employ genetic deletion of fibroblast markers, as has

been performed with Vimentin knockout (139), DDR2 knockout (140), and α SMA knockout mice (141), these studies are limited by the fact that deletion of a gene does not necessarily result in loss of the underlying phenotype. Further, genetic knockout may not aid the questions asked in this study due to intracellular signaling pathways altered by deletion of these genes (139, 140) and compensation by functionally related genes (141).

A caveat in translating our findings to actionable treatments in human patients lies in the differences in human and murine wounds. Although mice are by far the most commonly used for biologic research, there exist differences between the skin of mice and humans (21, 142). In particular, murine skin has a thin muscle layer lying beneath the dermis which produces the rapid wound contraction seen during the initial days of the repair process. Experimental approaches to counter this initial contraction include the splinted wound model (143) and sponge implantation model (144). These models however come with their own caveats, primarily due to the immune response generated by implantation of foreign objects. As a result, the use of the full thickness excisional wounding model remains the most commonly utilized model in the study wound healing.

In summary, the findings presented in this study present evidence for both the heterogeneity of fibroblast marker expression during the wound repair process but also heterogeneous functional roles. Investigation of fibroblast marker expression at multiple time points during repair indicated that while in normal skin FSP-1/S100A4⁺ fibroblasts are the predominant population, there is a transition of at least part of these cells to acquire the myofibroblast phenotype characterized by expression of α SMA.

When fibroblast populations were depleted based on marker expression, distinct phenotypes could be observed in terms of wound closure rate and quality of the healed wound bed. In particular, depletion of α SMA⁺ fibroblasts resulted in a complete inability to re-epithelialize. Interestingly, despite an increased number of granulocytes found in α SMA depleted wounds, depleting these cells using antibody depletion did not reverse the α SMA-TK phenotype. As a result, these findings suggest that the primary function of α SMA⁺ fibroblasts is in supporting wound re-epithelialization.

Bibliography

1. Escandon, J., A. C. Vivas, J. Tang, K. J. Rowland, and R. S. Kirsner. 2011. High mortality in patients with chronic wounds. *Wound Repair Regen* 19: 526-528.
2. Sen, C. K., G. M. Gordillo, S. Roy, R. Kirsner, L. Lambert, T. K. Hunt, F. Gottrup, G. C. Gurtner, and M. T. Longaker. 2009. Human skin wounds: a major and snowballing threat to public health and the economy. *Wound Repair Regen* 17: 763-771.
3. Frykberg, R. G., and J. Banks. 2015. Challenges in the Treatment of Chronic Wounds. *Adv Wound Care (New Rochelle)* 4: 560-582.
4. Goldberg, S. R., and R. F. Diegelmann. 2010. Wound healing primer. *Surg Clin North Am* 90: 1133-1146.
5. Tejiram, S., S. L. Kavalukas, J. W. Shupp, and A. Barbul. 2016. Wound healing. In *Wound Healing Biomaterials*. M. S. Ågren, ed. Woodhead Publishing. 3-39.
6. Nwomeh, B. C., D. R. Yager, and I. K. Cohen. 1998. Physiology of the chronic wound. *Clinics in plastic surgery* 25: 341-356.
7. Nunan, R., K. G. Harding, and P. Martin. 2014. Clinical challenges of chronic wounds: searching for an optimal animal model to recapitulate their complexity. *Disease models & mechanisms* 7: 1205-1213.
8. Falanga, V. 2005. Wound healing and its impairment in the diabetic foot. *Lancet (London, England)* 366: 1736-1743.
9. Woo, K., E. A. Ayello, and R. G. Sibbald. 2007. The edge effect: current therapeutic options to advance the wound edge. *Advances in skin & wound care* 20: 99-117; quiz 118-119.
10. Eming, S. A., P. Martin, and M. Tomic-Canic. 2014. Wound repair and regeneration:

- mechanisms, signaling, and translation. *Science translational medicine* 6: 265sr266.
11. Sriram, G., P. L. Bigliardi, and M. Bigliardi-Qi. 2015. Fibroblast heterogeneity and its implications for engineering organotypic skin models in vitro. *Eur J Cell Biol* 94: 483-512.
 12. Clark, R. A., K. Ghosh, and M. G. Tonnesen. 2007. Tissue engineering for cutaneous wounds. *J Invest Dermatol* 127: 1018-1029.
 13. Rennert, R. C., M. Rodrigues, V. W. Wong, D. Duscher, M. Hu, Z. Maan, M. Sorkin, G. C. Gurtner, and M. T. Longaker. 2013. Biological therapies for the treatment of cutaneous wounds: phase III and launched therapies. *Expert Opin Biol Ther* 13: 1523-1541.
 14. Metcalfe, A. D., and M. W. Ferguson. 2007. Tissue engineering of replacement skin: the crossroads of biomaterials, wound healing, embryonic development, stem cells and regeneration. *Journal of the Royal Society, Interface* 4: 413-437.
 15. Singer, A. J., and R. A. Clark. 1999. Cutaneous wound healing. *N Engl J Med* 341: 738-746.
 16. Kim, M. H., W. Liu, D. L. Borjesson, F. R. Curry, L. S. Miller, A. L. Cheung, F. T. Liu, R. R. Isseroff, and S. I. Simon. 2008. Dynamics of neutrophil infiltration during cutaneous wound healing and infection using fluorescence imaging. *J Invest Dermatol* 128: 1812-1820.
 17. Diegelmann, R. F., and M. C. Evans. 2004. Wound healing: an overview of acute, fibrotic and delayed healing. *Frontiers in bioscience : a journal and virtual library* 9: 283-289.
 18. Werner, S., and R. Grose. 2003. Regulation of wound healing by growth factors and cytokines. *Physiol Rev* 83: 835-870.
 19. DiPietro, L. A. 1995. Wound healing: the role of the macrophage and other immune cells. *Shock (Augusta, Ga.)* 4: 233-240.

20. Hinz, B., and G. Gabbiani. 2003. Cell-matrix and cell-cell contacts of myofibroblasts: role in connective tissue remodeling. *Thrombosis and haemostasis* 90: 993-1002.
21. Lynch, M. D., and F. M. Watt. 2018. Fibroblast heterogeneity: implications for human disease. *J Clin Invest* 128: 26-35.
22. Dulmovits, B. M., and I. M. Herman. 2012. Microvascular remodeling and wound healing: a role for pericytes. *Int J Biochem Cell Biol* 44: 1800-1812.
23. Eming, S. A., B. Brachvogel, T. Odorisio, and M. Koch. 2007. Regulation of angiogenesis: wound healing as a model. *Prog Histochem Cytochem* 42: 115-170.
24. Li, J., Y. P. Zhang, and R. S. Kirsner. 2003. Angiogenesis in wound repair: angiogenic growth factors and the extracellular matrix. *Microsc Res Tech* 60: 107-114.
25. Wietecha, M. S., and L. A. DiPietro. 2013. Therapeutic Approaches to the Regulation of Wound Angiogenesis. *Adv Wound Care (New Rochelle)* 2: 81-86.
26. Welch, M. P., G. F. Odland, and R. A. Clark. 1990. Temporal relationships of F-actin bundle formation, collagen and fibronectin matrix assembly, and fibronectin receptor expression to wound contraction. *J Cell Biol* 110: 133-145.
27. Levenson, S. M., E. F. Geever, L. V. Crowley, J. F. Oates, 3rd, C. W. Berard, and H. Rosen. 1965. The Healing of Rat Skin Wounds. *Ann Surg* 161: 293-308.
28. Desmouliere, A., M. Redard, I. Darby, and G. Gabbiani. 1995. Apoptosis Mediates the Decrease in Cellularity during the Transition between Granulation-Tissue and Scar. *American Journal of Pathology* 146: 56-66.
29. Kalluri, R. 2016. The biology and function of fibroblasts in cancer. *Nat Rev Cancer* 16: 582-598.
30. Garrett, D. M., and G. W. Conrad. 1979. Fibroblast-like cells from embryonic chick cornea, heart, and skin are antigenically distinct. *Dev Biol* 70: 50-70.
31. Sorrell, J. M., and A. I. Caplan. 2009. Chapter 4 Fibroblasts—A Diverse Population at the Center of It All. 161-214.

32. Ishii, G., A. Ochiai, and S. Neri. 2016. Phenotypic and functional heterogeneity of cancer-associated fibroblast within the tumor microenvironment. *Adv Drug Deliv Rev* 99: 186-196.
33. Bochaton-Piallat, M. L., G. Gabbiani, and B. Hinz. 2016. The myofibroblast in wound healing and fibrosis: answered and unanswered questions. *F1000Res* 5.
34. Darby, I. A., B. Laverdet, F. Bonte, and A. Desmouliere. 2014. Fibroblasts and myofibroblasts in wound healing. *Clin Cosmet Investig Dermatol* 7: 301-311.
35. Desmouliere, A., C. Chaponnier, and G. Gabbiani. 2005. Tissue repair, contraction, and the myofibroblast. *Wound Repair Regen* 13: 7-12.
36. Gabbiani, G., G. B. Ryan, and G. Majno. 1971. Presence of Modified Fibroblasts in Granulation Tissue and Their Possible Role in Wound Contraction. *Experientia* 27: 549-&.
37. Eyden, B. 2005. The myofibroblast: a study of normal, reactive and neoplastic tissues, with an emphasis on ultrastructure. Part 1--normal and reactive cells. *Journal of submicroscopic cytology and pathology* 37: 109-204.
38. Kuhn, C., and J. A. McDonald. 1991. The roles of the myofibroblast in idiopathic pulmonary fibrosis. Ultrastructural and immunohistochemical features of sites of active extracellular matrix synthesis. *Am J Pathol* 138: 1257-1265.
39. Vyalov, S. L., G. Gabbiani, and Y. Kapanci. 1993. Rat alveolar myofibroblasts acquire alpha-smooth muscle actin expression during bleomycin-induced pulmonary fibrosis. *Am J Pathol* 143: 1754-1765.
40. Leslie, K. O., D. J. Taatjes, J. Schwarz, M. vonTurkovich, and R. B. Low. 1991. Cardiac myofibroblasts express alpha smooth muscle actin during right ventricular pressure overload in the rabbit. *Am J Pathol* 139: 207-216.
41. LeBleu, V. S., G. Taduri, J. O'Connell, Y. Teng, V. G. Cooke, C. Woda, H. Sugimoto, and R. Kalluri. 2013. Origin and function of myofibroblasts in kidney fibrosis. *Nat Med*

- 19: 1047-1053.
42. Darby, I. A., and T. D. Hewitson. 2007. Fibroblast Differentiation in Wound Healing and Fibrosis. 143-179.
 43. Desmouliere, A., C. Guyot, and G. Gabbiani. 2004. The stroma reaction myofibroblast: a key player in the control of tumor cell behavior. *The International journal of developmental biology* 48: 509-517.
 44. Kalluri, R., and M. Zeisberg. 2006. Fibroblasts in cancer. *Nat Rev Cancer* 6: 392-401.
 45. Carthy, J. M. 2017. TGF β Signalling and the Control of Myofibroblast Differentiation: Implications for Chronic Inflammatory Disorders. *Journal of Cellular Physiology*.
 46. Desmouliere, A., A. Geinoz, F. Gabbiani, and G. Gabbiani. 1993. Transforming growth factor-beta 1 induces alpha-smooth muscle actin expression in granulation tissue myofibroblasts and in quiescent and growing cultured fibroblasts. *J Cell Biol* 122: 103-111.
 47. Lichtman, M. K., M. Otero-Vinas, and V. Falanga. 2016. Transforming growth factor beta (TGF-beta) isoforms in wound healing and fibrosis. *Wound Repair Regen* 24: 215-222.
 48. Margadant, C., and A. Sonnenberg. 2010. Integrin-TGF-beta crosstalk in fibrosis, cancer and wound healing. *EMBO Rep* 11: 97-105.
 49. Driskell, R. R., and F. M. Watt. 2015. Understanding fibroblast heterogeneity in the skin. *Trends Cell Biol* 25: 92-99.
 50. Juniantito, V., T. Izawa, T. Yuasa, C. Ichikawa, E. Yamamoto, M. Kuwamura, and J. Yamate. 2012. Immunophenotypical analyses of myofibroblasts in rat excisional wound healing: possible transdifferentiation of blood vessel pericytes and perifollicular dermal sheath cells into myofibroblasts. *Histology and Histopathology* 27: 515-527.
 51. Sugimoto, H., T. M. Mundel, M. W. Kieran, and R. Kalluri. 2014. Identification of fibroblast heterogeneity in the tumor microenvironment. *Cancer Biology & Therapy* 5:

- 1640-1646.
52. Ohlund, D., E. Elyada, and D. Tuveson. 2014. Fibroblast heterogeneity in the cancer wound. *J Exp Med* 211: 1503-1523.
 53. Tomasek, J. J., G. Gabbiani, B. Hinz, C. Chaponnier, and R. A. Brown. 2002. Myofibroblasts and mechano-regulation of connective tissue remodelling. *Nat Rev Mol Cell Biol* 3: 349-363.
 54. Strutz, F., H. Okada, C. W. Lo, T. Danoff, R. L. Carone, J. E. Tomaszewski, and E. G. Neilson. 1995. Identification and characterization of a fibroblast marker: FSP1. *J Cell Biol* 130: 393-405.
 55. Jacob, M., L. Chang, and E. Pure. 2012. Fibroblast activation protein in remodeling tissues. *Curr Mol Med* 12: 1220-1243.
 56. Castillo-Briceno, P., D. Bihan, M. Nilges, S. Hamaia, J. Meseguer, A. Garcia-Ayala, R. W. Farndale, and V. Mulero. 2011. A role for specific collagen motifs during wound healing and inflammatory response of fibroblasts in the teleost fish gilthead seabream. *Mol Immunol* 48: 826-834.
 57. Driskell, R. R., B. M. Lichtenberger, E. Hoste, K. Kretzschmar, B. D. Simons, M. Charalambous, S. R. Ferron, Y. Herault, G. Pavlovic, A. C. Ferguson-Smith, and F. M. Watt. 2013. Distinct fibroblast lineages determine dermal architecture in skin development and repair. *Nature* 504: 277-281.
 58. Olaso, E., J. P. Labrador, L. Wang, K. Ikeda, F. J. Eng, R. Klein, D. H. Lovett, H. C. Lin, and S. L. Friedman. 2002. Discoidin domain receptor 2 regulates fibroblast proliferation and migration through the extracellular matrix in association with transcriptional activation of matrix metalloproteinase-2. *J Biol Chem* 277: 3606-3613.
 59. Parsonage, G., A. D. Filer, O. Haworth, G. B. Nash, G. E. Rainger, M. Salmon, and C. D. Buckley. 2005. A stromal address code defined by fibroblasts. *Trends Immunol* 26: 150-156.

60. Werner, S., T. Krieg, and H. Smola. 2007. Keratinocyte-fibroblast interactions in wound healing. *J Invest Dermatol* 127: 998-1008.
61. Marangoni, R. G., B. D. Korman, J. Wei, T. A. Wood, L. V. Graham, M. L. Whitfield, P. E. Scherer, W. G. Tourtellotte, and J. Varga. 2015. Myofibroblasts in murine cutaneous fibrosis originate from adiponectin-positive intradermal progenitors. *Arthritis Rheumatol* 67: 1062-1073.
62. Plikus, M. V., C. F. Guerrero-Juarez, M. Ito, Y. R. Li, P. H. Dedhia, Y. Zheng, M. Shao, D. L. Gay, R. Ramos, T.-C. His, J. W. Oh, X. Wang, A. Ramirez, S. E. Konopelski, A. Elzein, A. Wang, R. J. Supapannachart, H.-L. Lee, C. H. Lim, A. Nace, A. Guo, E. Treffeisen, T. Andl, R. N. Ramirez, R. Murad, S. Offermanns, D. Metzger, P. Chambon, A. D. Widgerow, T.-L. Tuan, A. Mortazavi, R. K. Gupta, B. A. Hamilton, S. E. Millar, P. Seale, W. S. Pear, M. A. Lazar, and G. Cotsarelis. 2017. Regeneration of fat cells from myofibroblasts during wound healing. *Science*: aai8792.
63. Schmidt, B. A., and V. Horsley. 2013. Intra dermal adipocytes mediate fibroblast recruitment during skin wound healing. *Development* 140: 1517-1527.
64. Gilchrest, B. A., R. L. Karassik, L. M. Wilkins, M. A. Vrabel, and T. Maciag. 1983. Autocrine and paracrine growth stimulation of cells derived from human skin. *J Cell Physiol* 117: 235-240.
65. Boxman, I., C. Lowik, L. Aarden, and M. Ponc. 1993. Modulation of IL-6 production and IL-1 activity by keratinocyte-fibroblast interaction. *J Invest Dermatol* 101: 316-324.
66. Smola, H., G. Thiekotter, and N. E. Fusenig. 1993. Mutual induction of growth factor gene expression by epidermal-dermal cell interaction. *J Cell Biol* 122: 417-429.
67. Kupper, T. S., and R. W. Groves. 1995. The interleukin-1 axis and cutaneous inflammation. *J Invest Dermatol* 105: 62S-66S.
68. Werner, S., and H. Smola. 2001. Paracrine regulation of keratinocyte proliferation and differentiation. *Trends Cell Biol* 11: 143-146.

69. Grinnell, F., M. Zhu, M. A. Carlson, and J. M. Abrams. 1999. Release of mechanical tension triggers apoptosis of human fibroblasts in a model of regressing granulation tissue. *Exp Cell Res* 248: 608-619.
70. Gallit. 1994. Wound repair in the context of extracellular matrix. *Current Opinion in Cell Biology*.
71. Shah, M. 1995. Neutralisation of TGF- β 1 and TGF- β 2 or exogenous addition of TGF- β 3 to cutaneous rat wounds reduces scarring. *J Cell Sci*.
72. Harper, R. A., and G. Grove. 1979. Human skin fibroblasts derived from papillary and reticular dermis: differences in growth potential in vitro. *Science* 204: 526-527.
73. Janson, D. G., G. Saintigny, A. van Adrichem, C. Mahe, and A. El Ghalbzouri. 2012. Different gene expression patterns in human papillary and reticular fibroblasts. *J Invest Dermatol* 132: 2565-2572.
74. Mine, S., N. O. Fortunel, H. Pigeon, and D. Asselineau. 2008. Aging alters functionally human dermal papillary fibroblasts but not reticular fibroblasts: a new view of skin morphogenesis and aging. *PLoS One* 3: e4066.
75. Woodley, D. T. 2017. Distinct Fibroblasts in the Papillary and Reticular Dermis: Implications for Wound Healing. *Dermatol Clin* 35: 95-100.
76. Azzarone, B., and A. Macieiracoelho. 1982. Heterogeneity of the Kinetics of Proliferation within Human-Skin Fibroblastic Cell-Populations. *Journal of Cell Science* 57: 177-187.
77. Sorrell, J. M., and A. I. Caplan. 2004. Fibroblast heterogeneity: more than skin deep. *J Cell Sci* 117: 667-675.
78. Jahoda, C. A., and A. J. Reynolds. 2001. Hair follicle dermal sheath cells: unsung participants in wound healing. *Lancet (London, England)* 358: 1445-1448.
79. Garcin, C. L., and D. M. Ansell. 2017. The battle of the bulge: re-evaluating hair follicle stem cells in wound repair. *Exp Dermatol* 26: 101-104.

80. Reynolds, A. J., C. Chaponnier, C. A. Jahoda, and G. Gabbiani. 1993. A quantitative study of the differential expression of alpha-smooth muscle actin in cell populations of follicular and non-follicular origin. *J Invest Dermatol* 101: 577-583.
81. Abe, R., S. C. Donnelly, T. Peng, R. Bucala, and C. N. Metz. 2001. Peripheral blood fibrocytes: differentiation pathway and migration to wound sites. *Journal of immunology (Baltimore, Md. : 1950)* 166: 7556-7562.
82. Mori, L., A. Bellini, M. A. Stacey, M. Schmidt, and S. Mattoli. 2005. Fibrocytes contribute to the myofibroblast population in wounded skin and originate from the bone marrow. *Exp Cell Res* 304: 81-90.
83. Suga, H., R. C. Rennert, M. Rodrigues, M. Sorkin, J. P. Glotzbach, M. Januszyk, T. Fujiwara, M. T. Longaker, and G. C. Gurtner. 2014. Tracking the elusive fibrocyte: identification and characterization of collagen-producing hematopoietic lineage cells during murine wound healing. *Stem Cells* 32: 1347-1360.
84. Meigel, W. N., S. Gay, and L. Weber. 1977. Dermal architecture and collagen type distribution. *Archives for dermatological research = Archiv fur dermatologische Forschung* 259: 1-10.
85. Schafer, I. A., M. Pandey, R. Ferguson, and B. R. Davis. 1985. Comparative observation of fibroblasts derived from the papillary and reticular dermis of infants and adults: growth kinetics, packing density at confluence and surface morphology. *Mechanisms of ageing and development* 31: 275-293.
86. Sorrell, J. M., M. A. Baber, and A. I. Caplan. 1996. Construction of a bilayered dermal equivalent containing human papillary and reticular dermal fibroblasts: use of fluorescent vital dyes. *Tissue engineering* 2: 39-49.
87. Hinz, B. 2016. Targeting the myofibroblast to improve wound healing. In *Wound Healing Biomaterials*. M. S. Ågren, ed. Woodhead Publishing. 69-100.
88. Martin, Y. H., F. V. Lali, and A. D. Metcalfe. 2016. Modelling wound healing. In *Wound*

- Healing Biomaterials*. 151-173.
89. Carstens, J. L., P. Correa de Sampaio, D. Yang, S. Barua, H. Wang, A. Rao, J. P. Allison, V. S. LeBleu, and R. Kalluri. 2017. Spatial computation of intratumoral T cells correlates with survival of patients with pancreatic cancer. *Nat Commun* 8: 15095.
 90. Charytan, D. M., R. Padera, A. M. Helfand, M. Zeisberg, X. Xu, X. Liu, J. Himmelfarb, A. Cinelli, R. Kalluri, and E. M. Zeisberg. 2014. Increased concentration of circulating angiogenesis and nitric oxide inhibitors induces endothelial to mesenchymal transition and myocardial fibrosis in patients with chronic kidney disease. *Int J Cardiol* 176: 99-109.
 91. Bryan, D., K. B. Walker, M. Ferguson, and R. Thorpe. 2005. Cytokine gene expression in a murine wound healing model. *Cytokine* 31: 429-438.
 92. Ishida, Y., T. Kondo, T. Takayasu, Y. Iwakura, and N. Mukaida. 2004. The Essential Involvement of Cross-Talk between IFN- and TGF- in the Skin Wound-Healing Process. *The Journal of Immunology* 172: 1848-1855.
 93. Clark, R. A., G. A. McCoy, J. M. Folkvord, and J. M. McPherson. 1997. TGF-beta 1 stimulates cultured human fibroblasts to proliferate and produce tissue-like fibroplasia: a fibronectin matrix-dependent event. *J Cell Physiol* 170: 69-80.
 94. Ozdemir, B. C., T. Pentcheva-Hoang, J. L. Carstens, X. Zheng, C. C. Wu, T. R. Simpson, H. Laklai, H. Sugimoto, C. Kahlert, S. V. Novitskiy, A. De Jesus-Acosta, P. Sharma, P. Heidari, U. Mahmood, L. Chin, H. L. Moses, V. M. Weaver, A. Maitra, J. P. Allison, V. S. LeBleu, and R. Kalluri. 2014. Depletion of carcinoma-associated fibroblasts and fibrosis induces immunosuppression and accelerates pancreas cancer with reduced survival. *Cancer Cell* 25: 719-734.
 95. O'Connell, J. T., H. Sugimoto, V. G. Cooke, B. A. MacDonald, A. I. Mehta, V. S. LeBleu, R. Dewar, R. M. Rocha, R. R. Brentani, M. B. Resnick, E. G. Neilson, M. Zeisberg, and R. Kalluri. 2011. VEGF-A and Tenascin-C produced by

- S100A4⁺ stromal cells are important for metastatic colonization. *Proceedings of the National Academy of Sciences* 108: 16002-16007.
96. Keskin, D., J. Kim, Vesselina G. Cooke, C.-C. Wu, H. Sugimoto, C. Gu, M. De Palma, R. Kalluri, and Valerie S. LeBleu. 2015. Targeting Vascular Pericytes in Hypoxic Tumors Increases Lung Metastasis via Angiopoietin-2. *Cell Reports* 10: 1066-1081.
 97. Cohen, J. L., O. Boyer, B. Salomon, R. Onclercq, D. Depetris, L. Lejeune, V. Dubus-Bonnet, S. Bruel, F. Charlotte, M. G. Mattei, and D. Klatzmann. 1998. Fertile homozygous transgenic mice expressing a functional truncated herpes simplex thymidine kinase delta TK gene. *Transgenic research* 7: 321-330.
 98. Salomon, B., S. Maury, L. Loubière, M. Caruso, R. Onclercq, and D. Klatzmann. 1995. A truncated herpes simplex virus thymidine kinase phosphorylates thymidine and nucleoside analogs and does not cause sterility in transgenic mice. *Molecular and cellular biology* 15: 5322–5328.
 99. al-Shawi, R., J. Burke, H. Wallace, C. Jones, S. Harrison, D. Buxton, S. Maley, A. Chandley, and J. O. Bishop. 1991. The herpes simplex virus type 1 thymidine kinase is expressed in the testes of transgenic mice under the control of a cryptic promoter. *Mol Cell Biol* 11: 4207-4216.
 100. Iwano, M., A. Fischer, H. Okada, D. Plieth, C. Xue, T. M. Danoff, and E. G. Neilson. 2001. Conditional abatement of tissue fibrosis using nucleoside analogs to selectively corrupt DNA replication in transgenic fibroblasts. *Mol Ther* 3: 149-159.
 101. Morales, M. O., R. L. Price, and E. C. Goldsmith. 2005. Expression of Discoidin Domain Receptor 2 (DDR2) in the developing heart. *Microscopy and microanalysis : the official journal of Microscopy Society of America, Microbeam Analysis Society, Microscopical Society of Canada* 11: 260-267.
 102. Akamatsu, T., Y. Arai, I. Kosugi, H. Kawasaki, S. Meguro, M. Sakao, K. Shibata, T. Suda, K. Chida, and T. Iwashita. 2013. Direct isolation of myofibroblasts and

- fibroblasts from bleomycin-injured lungs reveals their functional similarities and differences. *Fibrogenesis & tissue repair* 6: 15.
103. McQualter, J. L., N. Brouard, B. Williams, B. N. Baird, S. Sims-Lucas, K. Yuen, S. K. Nilsson, P. J. Simmons, and I. Bertoncello. 2009. Endogenous fibroblastic progenitor cells in the adult mouse lung are highly enriched in the sca-1 positive cell fraction. *Stem Cells* 27: 623-633.
 104. Brunner, G., and R. Blakytyn. 2004. Extracellular regulation of TGF-beta activity in wound repair: growth factor latency as a sensor mechanism for injury. *Thrombosis and haemostasis* 92: 253-261.
 105. Le, H., R. Kleinerman, O. Z. Lerman, D. Brown, R. Galiano, G. C. Gurtner, S. M. Warren, J. P. Levine, and P. B. Saadeh. 2008. Hedgehog signaling is essential for normal wound healing. *Wound Repair Regen* 16: 768-773.
 106. Jahoda, C. A., and A. C. Gilmore. 2016. What Lies Beneath: Wnt/beta-Catenin Signaling and Cell Fate in the Lower Dermis. *J Invest Dermatol* 136: 1084-1087.
 107. Rognoni, E., C. Gomez, A. O. Pisco, E. L. Rawlins, B. D. Simons, F. M. Watt, and R. R. Driskell. 2016. Inhibition of beta-catenin signalling in dermal fibroblasts enhances hair follicle regeneration during wound healing. *Development* 143: 2522-2535.
 108. MacLeod, A. S., and J. N. Mansbridge. 2016. The Innate Immune System in Acute and Chronic Wounds. *Adv Wound Care (New Rochelle)* 5: 65-78.
 109. Clark, R. A. 1985. Cutaneous tissue repair: basic biologic considerations. I. *J Am Acad Dermatol* 13: 701-725.
 110. Yamaguchi, Y., and K. Yoshikawa. 2001. Cutaneous wound healing: an update. *The Journal of dermatology* 28: 521-534.
 111. Takagi, N., K. Kawakami, E. Kanno, H. Tanno, A. Takeda, K. Ishii, Y. Imai, Y. Iwakura, and M. Tachi. 2017. IL-17A promotes neutrophilic inflammation and disturbs acute wound healing in skin. *Exp Dermatol* 26: 137-144.

112. McFarland-Mancini, M. M., H. M. Funk, A. M. Paluch, M. Zhou, P. V. Giridhar, C. A. Mercer, S. C. Kozma, and A. F. Drew. 2010. Differences in wound healing in mice with deficiency of IL-6 versus IL-6 receptor. *Journal of immunology (Baltimore, Md. : 1950)* 184: 7219-7228.
113. Gallucci, R. M., E. G. Lee, and J. J. Tomasek. 2006. IL-6 modulates alpha-smooth muscle actin expression in dermal fibroblasts from IL-6-deficient mice. *J Invest Dermatol* 126: 561-568.
114. Shinzawa, H., A. Takeda, Y. Sone, K. Murashita, and E. Uchinuma. 2007. Wound healing process of a full-thickness skin wound model in rats. *Int Surg* 92: 63-72.
115. Fries, K. M., T. Blieden, R. J. Looney, G. D. Sempowski, M. R. Silvera, R. A. Willis, and R. P. Phipps. 1994. Evidence of fibroblast heterogeneity and the role of fibroblast subpopulations in fibrosis. *Clinical immunology and immunopathology* 72: 283-292.
116. Rinn, J. L., J. K. Wang, N. Allen, S. A. Brugmann, A. J. Mikels, H. Liu, T. W. Ridky, H. S. Stadler, R. Nusse, J. A. Helms, and H. Y. Chang. 2008. A dermal HOX transcriptional program regulates site-specific epidermal fate. *Genes Dev* 22: 303-307.
117. Rinn, J. L., C. Bondre, H. B. Gladstone, P. O. Brown, and H. Y. Chang. 2006. Anatomic demarcation by positional variation in fibroblast gene expression programs. *PLoS genetics* 2: e119.
118. Balin, A. K., A. J. Fisher, M. Anzelone, I. Leong, and R. G. Allen. 2002. Effects of establishing cell cultures and cell culture conditions on the proliferative life span of human fibroblasts isolated from different tissues and donors of different ages. *Exp Cell Res* 274: 275-287.
119. Rock, J. R., C. E. Barkauskas, M. J. Cronic, Y. Xue, J. R. Harris, J. Liang, P. W. Noble, and B. L. Hogan. 2011. Multiple stromal populations contribute to pulmonary fibrosis without evidence for epithelial to mesenchymal transition. *Proc Natl Acad Sci U S A* 108: E1475-1483.

120. Zeisberg, E. M., S. Potenta, L. Xie, M. Zeisberg, and R. Kalluri. 2007. Discovery of endothelial to mesenchymal transition as a source for carcinoma-associated fibroblasts. *Cancer Res* 67: 10123-10128.
121. Zeisberg, E. M., O. Tarnavski, M. Zeisberg, A. L. Dorfman, J. R. McMullen, E. Gustafsson, A. Chandraker, X. Yuan, W. T. Pu, A. B. Roberts, E. G. Neilson, M. H. Sayegh, S. Izumo, and R. Kalluri. 2007. Endothelial-to-mesenchymal transition contributes to cardiac fibrosis. *Nat Med* 13: 952-961.
122. Di Palma, S., and B. Bodenmiller. 2015. Unraveling cell populations in tumors by single-cell mass cytometry. *Curr Opin Biotechnol* 31: 122-129.
123. Giesen, C., H. A. Wang, D. Schapiro, N. Zivanovic, A. Jacobs, B. Hattendorf, P. J. Schuffler, D. Grolimund, J. M. Buhmann, S. Brandt, Z. Varga, P. J. Wild, D. Gunther, and B. Bodenmiller. 2014. Highly multiplexed imaging of tumor tissues with subcellular resolution by mass cytometry. *Nat Methods* 11: 417-422.
124. Cabezon, T., J. E. Celis, I. Skibshoj, J. Klingelhofer, M. Grigorian, P. Gromov, F. Rank, J. H. Myklebust, G. M. Maelandsmo, E. Lukanidin, and N. Ambartsumian. 2007. Expression of S100A4 by a variety of cell types present in the tumor microenvironment of human breast cancer. *Int J Cancer* 121: 1433-1444.
125. Tchou, J., P. J. Zhang, Y. Bi, C. Satija, R. Marjundar, T. L. Stephen, A. Lo, H. Chen, C. Mies, C. H. June, J. Conejo-Garcia, and E. Pure. 2013. Fibroblast activation protein expression by stromal cells and tumor-associated macrophages in human breast cancer. *Human pathology* 44: 2549-2557.
126. Inoue, T., D. Plieth, C. D. Venkov, C. Xu, and E. G. Neilson. 2005. Antibodies against macrophages that overlap in specificity with fibroblasts. *Kidney international* 67: 2488-2493.
127. Cheng, F., Y. Shen, P. Mohanasundaram, M. Lindstrom, J. Ivaska, T. Ny, and J. E. Eriksson. 2016. Vimentin coordinates fibroblast proliferation and keratinocyte

- differentiation in wound healing via TGF-beta-Slug signaling. *Proc Natl Acad Sci U S A* 113: E4320-4327.
128. Plikus, M. V., C. F. Guerrero-Juarez, M. Ito, Y. R. Li, P. H. Dedhia, Y. Zheng, M. Shao, D. L. Gay, R. Ramos, T. C. Hsi, J. W. Oh, X. Wang, A. Ramirez, S. E. Konopelski, A. Elzein, A. Wang, R. J. Supapannachart, H. L. Lee, C. H. Lim, A. Nace, A. Guo, E. Treffeisen, T. Andl, R. N. Ramirez, R. Murad, S. Offermanns, D. Metzger, P. Chambon, A. D. Widgerow, T. L. Tuan, A. Mortazavi, R. K. Gupta, B. A. Hamilton, S. E. Millar, P. Seale, W. S. Pear, M. A. Lazar, and G. Cotsarelis. 2017. Regeneration of fat cells from myofibroblasts during wound healing. *Science* 355: 748-752.
129. Wang, X., T.-C. Hsi, C. F. Guerrero-Juarez, K. Pham, K. Cho, C. D. McCusker, E. S. Monuki, K. W. Y. Cho, D. L. Gay, and M. V. Plikus. 2015. Principles and mechanisms of regeneration in the mouse model for wound-induced hair follicle neogenesis. *Regeneration* 2: 169-181.
130. Saito, M., T. Iwawaki, C. Taya, H. Yonekawa, M. Noda, Y. Inui, E. Mekada, Y. Kimata, A. Tsuru, and K. Kohno. 2001. Diphtheria toxin receptor-mediated conditional and targeted cell ablation in transgenic mice. *Nature biotechnology* 19: 746-750.
131. Denton, C. P., K. Khan, R. K. Hoyles, X. Shiwen, P. Leoni, Y. Chen, M. Eastwood, and D. J. Abraham. 2009. Inducible Lineage-Specific Deletion of T β RII in Fibroblasts Defines a Pivotal Regulatory Role during Adult Skin Wound Healing. *Journal of Investigative Dermatology* 129: 194-204.
132. Martinez-Ferrer, M., A. R. Afshar-Sherif, C. Uwamariya, B. de Crombrughe, J. M. Davidson, and N. A. Bhowmick. 2010. Dermal transforming growth factor-beta responsiveness mediates wound contraction and epithelial closure. *Am J Pathol* 176: 98-107.
133. Shah, M., D. M. Foreman, and M. W. Ferguson. 1992. Control of scarring in adult wounds by neutralising antibody to transforming growth factor beta. *Lancet (London,*

- England*) 339: 213-214.
134. Shah, M., D. M. Foreman, and M. W. Ferguson. 1994. Neutralising antibody to TGF-beta 1,2 reduces cutaneous scarring in adult rodents. *J Cell Sci* 107 (Pt 5): 1137-1157.
 135. Shah, M., D. M. Foreman, and M. W. Ferguson. 1995. Neutralisation of TGF-beta 1 and TGF-beta 2 or exogenous addition of TGF-beta 3 to cutaneous rat wounds reduces scarring. *J Cell Sci* 108 (Pt 3): 985-1002.
 136. Fan, M.-H., Q. Zhu, H.-H. Li, H.-J. Ra, S. Majumdar, D. L. Gulick, J. A. Jerome, D. H. Madsen, M. Christofidou-Solomidou, D. W. Speicher, W. W. Bachovchin, C. Feghali-Bostwick, Pur, and E. eacute. 2015. Fibroblast Activation Protein (FAP) Accelerates Collagen Degradation and Clearance from Lung in Mice. *Journal of Biological Chemistry*.
 137. Mazur, A., E. Holthoff, S. Vadali, T. Kelly, and S. R. Post. 2016. Cleavage of Type I Collagen by Fibroblast Activation Protein-alpha Enhances Class A Scavenger Receptor Mediated Macrophage Adhesion. *PLoS One* 11: e0150287.
 138. Au, P., J. Tam, D. Fukumura, and R. K. Jain. 2008. Bone marrow-derived mesenchymal stem cells facilitate engineering of long-lasting functional vasculature. *Blood* 111: 4551-4558.
 139. Eckes, B., E. Colucci-Guyon, H. Smola, S. Nodder, C. Babinet, T. Krieg, and P. Martin. 2000. Impaired wound healing in embryonic and adult mice lacking vimentin. *J Cell Sci* 113 (Pt 13): 2455-2462.
 140. Olaso, E., H. C. Lin, L. H. Wang, and S. L. Friedman. 2011. Impaired dermal wound healing in discoidin domain receptor 2-deficient mice associated with defective extracellular matrix remodeling. *Fibrogenesis & tissue repair* 4: 5.
 141. Tomasek, J. J., C. J. Haaksma, R. J. Schwartz, and E. W. Howard. 2013. Whole animal knockout of smooth muscle alpha-actin does not alter excisional wound healing

- or the fibroblast-to-myofibroblast transition. *Wound Repair Regen* 21: 166-176.
142. Wong, V. W., M. Sorkin, J. P. Glotzbach, M. T. Longaker, and G. C. Gurtner. 2011. Surgical approaches to create murine models of human wound healing. *J Biomed Biotechnol* 2011: 969618.
143. Galiano, R. D., J. t. Michaels, M. Dobryansky, J. P. Levine, and G. C. Gurtner. 2004. Quantitative and reproducible murine model of excisional wound healing. *Wound Repair Regen* 12: 485-492.
144. Deskins, D. L., S. Ardestani, and P. P. Young. 2012. The polyvinyl alcohol sponge model implantation. *Journal of visualized experiments : JoVE*.

Vita

Ehsan A. Ehsanipour was born in Palo Alto, California. He received the degree of Bachelor of Science with a major in Biochemistry from the University of California at Santa Barbara in Santa Barbara, California in June, 2010. In September of 2010 he entered the Master of Science program in Physiology and Biophysics at the University of Southern California, Los Angeles, California and received his degree in May, 2013. In August of 2013 he entered The University of Texas MD Anderson Cancer Center UTHHealth Graduate School of Biomedical Sciences.

Permanent address:

1885 El Paseo Road, Apt #33112

Houston, Texas

77054